

Design and fabrication of superhydrophobic membranes by electrospinning for direct contact membrane distillation

Liao, Yuan

2014

Liao, Y. (2014). Design and fabrication of superhydrophobic membranes by electrospinning for direct contact membrane distillation. Doctoral thesis, Nanyang Technological University, Singapore.

<https://hdl.handle.net/10356/62225>

<https://doi.org/10.32657/10356/62225>



**DESIGN AND FABRICATION OF
SUPERHYDROPHOBIC MEMBRANES BY
ELECTROSPINNING FOR DIRECT CONTACT
MEMBRANE DISTILLATION**

LIAO YUAN

SCHOOL OF CIVIL AND ENVIRONMENTAL ENGINEERING

2014

**DESIGN AND FABRICATION OF
SUPERHYDROPHOBIC MEMBRANES BY
ELECTROSPINNING FOR DIRECT CONTACT
MEMBRANE DISTILLATION**

LIAO YUAN

SCHOOL OF CIVIL AND ENVIRONMENTAL ENGINEERING

A thesis submitted to the Nanyang Technological University
in fulfillment of the requirement for the degree of
Doctor of Philosophy

2014

ACKNOWLEDGEMENTS

This thesis would not have been possible without the guidance and helps of many people who contributed and extended their valuable assistance in the preparation and completion of this study.

First of all, I would like to express my deep gratitude to my academic supervisor, Associate Professor Wang Rong, for her supports, guidance, encouragement, patience and advices. And it is my great pleasure showing appreciation to my co-supervisor, Professor Anthony Gordon Fane, for his supervision and contribution. Without their important suggestions, strong supports and scientific guidance, it is impossible for me to overcome difficulties during investigation. Their friendly supervision and ceaseless encouragement give me courage and confidence to finish my research.

I also sincerely thank Professor William Bill Krantz who is a visiting professor in Singapore Membrane Technology Centre (SMTC) for the helpful workshops and suggestions regarding to the communication and writing skills, and qualification exam reviewer committee, Associate Professor Sun Delai, Associate Professor Tang Chuyang and Assistant Professor Cao Bin, for their kind suggestions and comments.

This research grant is supported by the Singapore National Research Foundation under its Environmental & Water Technologies Strategic Research Programme and administered by the Environment & Water Industry Programme Office (EWI) of the PUB (EWI RFP 0901-IRIS-02-03). I also acknowledge funding support from the Singapore Economic Development Board to SMTC.

What's more, thanks to National Research Foundation (NRF) Singapore who provides Environmental and Water Technologies (EWT) PhD scholarship, I can have enough financial supports to continue my research. Meanwhile, their conference allowances offer me great opportunities to communicate with scholars and other research students in water research area in international conferences.

And I am grateful to School of Civil and Environmental Engineering (CEE) in NTU and SMTC for providing a safe and comfortable workplace equipped with necessary facilities.

Also, my sincere thanks go to Ms. Tian Miao, Ms. Loo Siewleng, Dr. Loh Chunheng, Dr. Laurentia E.K. Setiawan, Dr. Yang Xing, Dr. Shi Lei, Dr. Chou Shuren, Dr. Zhang Yuan, Dr. Li Xuesong and other research staff in SMTC laboratory for their kind helps and valuable discussion. And I also would like to thank Dr. Chong Tzyy Haur for his involvement and guidance in laboratory safety and equipment purchasing. Many thanks are also due to the FYP students: Ms. Lau Zhihui (2013) and Mr. Hengki Setiadi Siah (2014) for their diligent assistance.

I am thankful to Mrs. Lim-Tay Chew Wang for her kind supports and helps for the purchases of consumables and equipment for my investigation, Ms. Maria Chong Ai Shing and Ms. See Shen Yen Pearlyn for their assistances in equipment usage, and other staff in CEE Environment Laboratory for their kindhearted helps.

Here I also want to express my appreciation to my friends and colleagues for their companionship, supports and helps. Special thanks to my office and lab buddies as well as my group mates: Dr. Qi saren, Ms. Yao Lei, Dr. Wu Bing, Mr. Liu Chang, Ms. Li Tian, Dr. Zuo Guangzhi, Mr. Goh Kunli, Dr. Wei Jing, Ms. Li Ye, Dr. Lu Yinghong, Ms. Chen Guizi, Dr. Sunee Wongchitphimon and other friends. It is my pleasure to be part of SMTC family.

Last, but not the least, my fully gratitude is given to my parents for their love, encouragement and supports. Without their constant moral supports, perseverance and concerns, it is impossible for me to finish my PhD works.

LIAO YUAN

TABLE OF CONTENTS

ACKNOWLEDGEMENTS	i
TABLE OF CONTENTS	iii
LIST OF PUBLICATIONS	vi
LIST OF FIGURES	viii
LIST OF TABLES	xiii
LIST OF SYMBOLS	xv
SUMMARY	xix
CHAPTER 1 Introduction.....	1
1.1. Background.....	1
1.2. Challenges for Membrane Distillation (MD).....	3
1.3. Research objectives.....	5
1.4. Thesis outlines	6
CHAPTER 2 Literature review	9
2.1. Membrane Distillation (MD)	9
2.1.1. Concept and advantages of MD	9
2.1.2. MD applications and challenges.....	10
2.1.3. Requirements and current status of MD membranes	11
2.2. Development of nanofiber membranes by electrospinning	19
2.2.1. Introduction of electrospinning	19
2.2.2. Understanding the complex process of electrospinning.....	23
2.2.3. Parameters affecting electrospinning process	32
2.2.4. Current status of nanofiber membrane fabrication for MD process.....	38
CHAPTER 3 Fabrication of PVDF nanofiber membranes by electrospinning for DCMD.....	39
3.1. Introduction.....	39
3.2. Experiments	39
3.2.1. Membrane materials and chemicals	39
3.2.2. Dope preparation, dope viscosity and conductivity measurements	40
3.2.3. Electrospinning of PVDF nanofiber membranes and post-treatment.....	41
3.2.4. Characterizations of PVDF nanofiber membranes	41
3.2.5. MD performance tests	43

3.3. Results and discussion.....	44
3.3.1. Determination of appropriate polymer concentrations and solvents	44
3.3.2. Effect of polymer dope solution.....	46
3.3.3. Effect of sprayer moving speed	48
3.3.4. Effect of inorganic additives	49
3.3.5. Effect of relative humidity (RH).....	52
3.3.6. Effect of heat-press post-treatment	53
3.3.7. Preliminary evaluation of membrane performance in DCMD	55
3.3.8. Comparison with other flat-sheet PVDF MD membranes.....	59
3.4. Conclusions	61
CHAPTER 4 Engineering superhydrophobic surface on PVDF nanofiber membranes for DCMD	62
4.1. Introduction	62
4.2. Experiments.....	64
4.2.1. Membrane materials and chemicals	64
4.2.2. Electrospinning of PVDF nanofiber membranes and post-treatment	65
4.2.3. Membrane modification	65
4.2.4. Characterizations of PVDF electrospun membranes	67
4.3. Results and discussion.....	68
4.3.1. Chemical modification reactions on the PVDF nanofiber membranes ..	68
4.3.2. Membrane surface morphologies.....	72
4.3.3. Effects of surface modification conditions on membrane superhydrophobicity	74
4.3.4. Confirmation of nanostructures of modified membrane surfaces.....	77
4.3.5. DCMD performance	79
4.4. Conclusions	86
CHAPTER 5 Fabrication of bioinspired composite nanofiber membranes with robust superhydrophobicity for DCMD	87
5.1. Introduction	87
5.2. Materials and methods.....	89
5.2.1. Materials	89
5.2.2. Silica modification and dope preparation	89

5.2.3. Electrospinning of PVDF nanofiber membranes and composite superhydrophobic membranes.....	90
5.2.4. Characterizations of PVDF nanofiber and composite membranes	91
5.3. Results and discussion	93
5.4. Conclusions.....	108
CHAPTER 6 Electrospun superhydrophobic membranes with unique structures for membrane distillation.....	109
6.1. Introduction.....	109
6.2. Materials and methods	111
6.2.1. Materials	111
6.2.2. Fabrication of dual-layer superhydrophobic membranes	111
6.2.3. Characterizations of PVDF nanofiber and composite membranes	112
6.3. Results and discussion	114
6.3.1. Effects of dope concentration on stability of FS10-SiO ₂ and PVDF dispersion.....	114
6.3.2. Morphology of FS10-SiO ₂ -PVDF composite membranes	115
6.3.3. Superhydrophobicity of FS10-SiO ₂ -PVDF composite membranes	117
6.3.4. Comparison of different PVDF membranes.....	119
6.3.5. Continuous DCMD performance	124
6.3.6. Comparison of properties and DCMD performance of different electrospun PVDF membranes	127
6.4. Conclusions.....	129
CHAPTER 7 Conclusions and recommendations	130
7.1. Overall conclusions.....	130
7.2. Recommendations for future research	133
References.....	135

LIST OF PUBLICATIONS

- *Journals*

- **Y. Liao**, C. H. Loh, R. Wang, A.G. Fane, Electrospun superhydrophobic membrane with unique structures for membrane distillation, *ACS Applied Materials & Interfaces*, 6 (2014) 16035-48.
- **Y. Liao**, R. Wang, A.G. Fane, Fabrication of bioinspired composite nanofiber membranes with robust superhydrophobicity for direct contact membrane distillation, *Environmental Science & Technology*, 48 (2014) 6335-41.
- **Y. Liao**, R. Wang, A.G. Fane, Engineering superhydrophobic surface on poly(vinylidene fluoride) nanofiber membranes for direct contact membrane distillation, *Journal of Membrane Science*, 440 (2013) 77-87.
- **Y. Liao**, R. Wang, M. Tian, C. Qiu, A.G. Fane, Fabrication of polyvinylidene fluoride (PVDF) nanofiber membranes by electro-spinning for direct contact membrane distillation, *Journal of Membrane Science*, 425–426 (2013) 30-39.
- M. Tian, C. Qiu, **Y. Liao**, S. Chou, R. Wang, Preparation of polyamide thin film composite forward osmosis membranes using electrospun polyvinylidene fluoride (PVDF) nanofibers as substrates, *Separation and Purification Technology*, 118 (2013) 727-736.
- **Y. Liao**, M. Tian, C. H. Loh, R. Wang, A.G. Fane, Fabrication of electrospun composite nanofiber membrane for water applications: a review, to be submitted (2014).

- *Conference presentations*

- **Y. Liao**, R. Wang, A.G. Fane, Engineering superhydrophobic surface on poly(vinylidene fluoride) nanofiber membranes for direct contact membrane distillation, *Engineering with Membranes Towards a Sustainable*

Future, Saint-Pierre d' Oléron, France, 3-7 September 2013. (oral presentation).

- **Y. Liao**, R. Wang, A.G. Fane, Fabrication of bioinspired composite nanofiber membranes with robust superhydrophobicity for direct contact membrane distillation, The 24nd Annual Meeting North American Membrane Society (NAMS), Houston, Texas USA, May 31- June 4 2014 (Oral presentation).

- ***Patents***

- R. Wang, **Y. Liao**, A.G. Fane. “Fabrication of bioinspired composite nanofiber membranes with robust superhydrophobicity for direct contact membrane distillation”, NTU Technical Disclosure, NTU Ref. No. PAT/302/13/13/US PRV.

LIST OF FIGURES

Figure 1-1. Growth of research activities of MD presented by the number of papers included in refereed database (Science Direct) per year	4
Figure 1-2. Number of papers about MD membrane fabrications included in refereed database (Science Direct) per year	4
Figure 2-1. Schematic configuration of DCMD process. T_f , T_{fm} , T_{pm} and T_p are the temperatures of feed side, on the membrane surface in feed side, on the membrane surface in the permeate side, and of permeate side, respectively. The water vapor would transport through the hydrophobic MD membrane.....	9
Figure 2-2. Annual number of publications on the subject of electrospinning, as provided by the search engine of Science Direct Scholar	19
Figure 2-3. Schematic illustration of the basic setup for electrospinning	22
Figure 2-4. Schematic diagram illustrating the possible mechanism of nanofiber formation during electrospinning process	24
Figure 2-5. A diagram showing the prototypical instantaneous position of the pathway of an electrospinning jet [figure adopted from (Reneker Darrell and Fong 2006)]	24
Figure 2-6. Evolution of the shape of a fluid drop in electrospinning process [figure adopted from (Fong and Reneker Darrell 2000)]	26
Figure 2-7. Frame images that show the evolution of the bending instability on a jet of 15 wt% PCL in acetone [figure adopted from (Reneker, Kataphinan et al. 2002)]	28
Figure 2-8. Schematics of electrospinning systems with various spinnerets and various target electrodes, and resultant nanofiber morphologies [surface morphology images inserted in this figure are adopted from (Deitzel, Kleinmeyer et al. 2001; Theron, Zussman et al. 2001; Huang, Zhang et al. 2003; Kameoka, Orth et	

al. 2003; Larsen, Spretz et al. 2004; Li and Xia 2004; Bhattarai, Edmondson et al. 2005; Kidoaki, Kwon et al. 2005; Lin, Wang et al. 2005; Smit, Büttner et al. 2005; Subramanian, Vu et al. 2005; Teo and Ramakrishna 2005; Dosunmu, Chase et al. 2006; Teo and Ramakrishna 2006; Zhang and Chang 2008; Wang, Ding et al. 2011; Liao, Wang et al. 2013)]	31
Figure 3-1. Schematic diagram of homemade LEP test setup.....	43
Figure 3-2. Schematic diagram of direct contact membrane distillation	44
Figure 3-3. Surface morphology and water contact angle of M-4-HS (A: 500 ×; B: 3K ×) and M-5-HS (C: 500 ×; D: 3K ×) membranes.....	47
Figure 3-4. Surface morphology and water contact angle of M-6-LS (A: 500 ×), M-7-LS (B: 500 ×; C: 3K ×) and M-9-LS (D: 3K ×) membranes	50
Figure 3-5. SEM pictures of electrospun PVDF membrane M-9-LS-LM before heat press (A1: 3K ×; A2: 500 × cross section; A3: water contact angle), after 160 °C heat press (B1: 3K ×; B2: 500 × cross section; B3: water contact angle), after 170 °C heat press post-treatment (C1: 3K ×; C2: 500 × cross section; C3: water contact angle) and 180 °C heat press post-treatment (D1: 3K ×; D2: 500 × cross section; D3: water contact angle)	54
Figure 3-6. Effects of heat-press post-treatment on permeation flux and long term performance of PVDF membranes for DCMD application (3.5 wt% NaCl solution as feed, $T_f = 323$ K, $T_p = 293$ K, flow rate at feed side= 0.6 L/min, flow rate at permeate side= 0.6 L/min)	56
Figure 3-7. Illustration of water entrapment in a nanofiber membrane	58
Figure 4-1. Schematic diagram of preparing superhydrophobic PVDF nanofiber membranes by silver nanoparticle and 1-dodecanethiol hydrophobic modification.....	66
Figure 4-2. Possible reaction pathways of superhydrophobic membrane preparation	69

Figure 4-3. The XPS wide-scan and C 1s core-level spectra of (A and B) PVDF membrane and (C and D) dopamine-modified PVDF membrane (PDA-PVDF).....	70
Figure 4-4. The XPS wide scan and Ag 3d core-level spectra of silver deposited PVDF membrane (Ag-PVDF) (A and B), and XPS wide scan and C 1s core-level spectra of modified PVDF membrane (C12-PVDF) (C and D).	71
Figure 4-5. FE-SEM images of pristine PVDF (A1, A2), I-PVDF (B1, B2) and S-PVDF (C1, C2) nanofiber membranes. Cross section images of pristine PVDF (A3, A4), I-PVDF (B3, B4) and S-PVDF (C3, C4) nanofiber membranes.....	72
Figure 4-6. Effect of silver nanoparticle treatment time on the contact angle	74
Figure 4-7. Schematic illustrations of water drops on different membrane surfaces	75
Figure 4-8. Surface height maps and flat maps along with 2D profiles in a given location of PVDF nanofiber membranes: (A1, A2, A3) original PVDF nanofiber membrane; (B1, B2, B3) I-PVDF; (C1, C2, C3) S-PVDF.	78
Figure 4-9. Pore size distribution of PVDF nanofiber membranes (A): original membrane; (B): I-PVDF; (C): S-PVDF membrane and (D): commercial PVDF flat sheet membrane	82
Figure 4-10. Continuous DCMD tests of the original PVDF, modified S-PVDF and I-PVDF and commercial PVDF membranes (3.5 wt% NaCl as feed, $T_f=333$ K, $T_p=293$ K, Flow rate at feed side=0.4 L/min, Flow rate at permeate side=0.6 L/min)	84
Figure 5-1. Schematic of an ideal MD membrane with a lotus leaf-like superhydrophobic selective layer and a scaffold-like nanofiber support layer.....	88
Figure 5-2. Schematic diagram of homemade LEPw test setup.....	92
Figure 5-3. The sliding angle test configuration: (A) sliding angle calculation; (B) image of sliding angle testing.....	93

Figure 5-4. Schematic diagram of the mechanism of modification reaction on SiO ₂ nanoparticle surface (A) and chemical structure of Fluorolink FS10 (B)	94
Figure 5-5. The XPS wide-scan and O 1s core-level spectra of (A and B) original SiO ₂ nanoparticles and (C and D) modified SiO ₂ surface.	95
Figure 5-6. The XPS C 1s core-level spectra of (A) PVDF nanofiber membrane, (B) modified silica and (C) modified SiO ₂ -PVDF composite membrane.....	97
Figure 5-7. Photo images, FE-SEM surface morphologies of PVDF nanofiber membrane (A) and superhydrophobic silica-PVDF composite membrane (B) and corresponding schematic illustrations of nanofiber and superhydrophobic composite membrane (C and D).....	98
Figure 5-8. Variation of contact angle and sliding angles of composite membranes with different nano-particle sizes and various electrospinning times: (A) membrane fabricated by PVDF/ small FS10-SiO ₂ mixture; (B) membrane fabricated by PVDF/ large FS10-SiO ₂ mixture.....	100
Figure 5-9. Behavior of the water droplets on the superhydrophobic surface of S-PVDF (A) and L-PVDF (B) after ultrasonic-treatment for different times	102
Figure 5-10. Continuous DCMD tests of the original electrospun PVDF membrane (A), S-PVDF (B), L-PVDF composite membranes (C) and commercial PVDF (D) (3.5 wt% NaCl solution as feed, T _f =333 K, T _p =293K).....	104
Figure 5-11. Surface and cross-section morphologies of fabricated electrospun membranes after continuous DCMD testing: (A and B) PVDF nanofiber membrane; (C and D) S-PVDF and (E and F) L-PVDF. Inserted images are the water contact pictures of corresponding used nanofibrous membranes.....	105
Figure 5-12. Schematic illustration of PVDF nanofiber membrane surface (A) and superhydrophobic PVDF membrane surface (B) used in the DCMD configuration	106

Figure 6-1. (A) Photographs of various FS10-SiO ₂ -blended PVDF dopes after hours and schematic illustrations of (B) unstable low concentrated dope and (C) stable high concentrated dope.....	114
Figure 6-2. The diagrams and morphologies of superhydrophobic dual-layer membranes (A) #3S-N and (B) #5S-W: (1) schematic drawing; (2) enlarged cross section image of the middle layer; (3) surface morphology; (4) cross section morphology of prepared membranes.....	116
Figure 6-3. Variation of water contact angle and sliding angle as a function of different membrane fabrication dopes and structures	117
Figure 6-4. (A) Captured images of water droplet movement on the surface of superhydrophobic membrane #3S-N, (B) surface topography of superhydrophobic membrane #3S-N, (C) the liquid–membrane interface scheme on silica blended superhydrophobic membrane	119
Figure 6-5. Comparisons of (A) pore sizes and porosity, and (B) LEPw of different PVDF membranes	120
Figure 6-6. Cross section and surface morphologies of commercial PVDF membrane GVHP (A), #3S-N (B), #4S-N (C) and #5S-W (D).....	121
Figure 6-7. Tensile properties of different PVDF membranes	124
Figure 6-8. Continuous DCMD test and membrane surface morphology after the test of #3S-N (A and B) and #5S-W superhydrophobic membranes (C and D). (3.5 wt% NaCl solution as feed, T _f =333 K, T _p =293K).....	125
Figure 6-9. Possible membrane wetting processes of (A) #3S-W and (B) #5S-N superhydrophobic membranes.....	126

LIST OF TABLES

Table 2-1. Commercial membranes commonly used in DCMD (membrane selective layer thickness, δ_s , μm ; total membrane thickness, δ_t , μm ; mean pore size, d_p , μm ; porosity, ε_m , %; membrane surface water contact angle, C_a , $^\circ$; DCMD permeate flux, J , $\text{kg}/\text{m}^2\text{h}$)	14
Table 2-2. Lab-fabricated PVDF membranes for DCMD (membrane selective layer thickness, δ_s , μm ; total membrane thickness, δ_t , μm ; mean pore size, d_p , μm ; maximum pore size, d_m , μm ; porosity, ε_m , μm ; membrane surface water contact angle, C_a , $^\circ$; liquid enter pressure, LEP, Kpa; DCMD permeate flux, J , $\text{kg}/\text{m}^2\text{h}$) ...	17
Table 2-3. Advantages and disadvantages of different membrane fabrication methods.....	20
Table 2-4. Effects of different parameters on electrospun nanofibers	33
Table 3-1. Viscosity of different dope solutions.....	45
Table 3-2. Surface properties of PVDF membranes made under different conditions	48
Table 3-3. Additive effects on dope viscosity and conductivity	51
Table 3-4. Effect of heat-press post-treatment on membrane properties	55
Table 3-5. DCMD performances of flat-sheet MD membranes for desalination....	60
Table 4-1. Characteristic properties of original PVDF, modified I-PVDF and S-PVDF nanofiber membranes and commercial PVDF membrane.....	81
Table 4-2. DCMD performances of flat-sheet PVDF membranes.....	85
Table 5-1. Electrospinning conditions of PVDF nanofiber and composite membranes.....	91
Table 5-2. Characteristic properties of PVDF nanofiber, S-PVDF, L-PVDF composite and commercial PVDF membranes.....	103

Table 6-1. Operating parameters for superhydrophobic nanofiber membranes.....113

Table 6-2. Properties and DCMD performances of different electrospun PVDF membranes.....128

LIST OF SYMBOLS

3D	3-dimensional
a	Raised height of composite membrane
AFM	Atomic force microscope
AGMD	Air gap membrane distillation
Ag-PVDF	Silver-deposited PVDF membrane
b	Horizontal length of the membrane when the droplet started moving downward
B	Geometric factor
BE	Binding energy
C12	1-Dodecanethiol
C12-PVDF	1-dodecanethiol-coated PVDF membrane
C _a	Membrane surface water contact angle
CTA	Cellulose triacetate
CVD	Chemical vapour deposition
DCMD	Direct contact membrane distillation
D _i	Isopropyl alcohol density
d _m	Maximum pore size
DMAC	N, N-Dimethylacetamide
DMF	N, N-Dimethylformamide
d _p	Mean pore size
D _p	Polymer density
E	Applied electric field
E ₀	Initial applied electric field
EDX	Energy-dispersive X-ray spectroscopy
E _t	Tensile modulus
FAS	Fluoroalkylsilane
FE-SEM	Field emission scanning electron microscope
FO	Forward osmosis
FS10	Fluorolink® S10 perfluoropolyether

FSi	Fluorinated silica
f_{SL}	Fraction of the water droplet in direct contact with the surface
GS	Gas separation
H	Distance from the needle tip to the collecting screen
h	Length of the liquid column
I	Current passing through the jet
IPA	Isopropyl alcohol
J	Permeate flux
k	Dimensionless conductivity
L	Critical length of the straight jet
l	Radius of the jet
LBL	Layer-by-layer assembly
LEP	Liquid enter pressure
LEP _w	Liquid entry pressure of water
LiCl	Lithium chloride
MD	Membrane distillation
MDC	Membrane distillation crystallization
MF	Microfiltration
NF	Nanofiltration
NIPS	Non-solvent induced phase separation
PCL	Polycaprolactone
PDA	Poly-dopamine
PDA-PVDF	Poly-dopamine pre-activated PVDF membranes
PEG	Polyethylene glycol
PET	Polyethylene terephthalate
PP	Polypropylene
PRO	Pressure retarded osmosis
PTFE	Polytetrafluoroethylene
PV	Pervaporation
PVDF	Poly (vinylidene fluoride)
Q	Flow rate
R	Needle outer radius

r_0	Initial radius of the jet
R_a	Arithmetic mean of the surface roughness
R_f	Non-dimensional surface factor
RH	Relative humidity
r_{\max}	Largest pore radius
RO	Reverse osmosis
SEM	Scanning electron microscopy
SGMD	Sweeping gas membrane distillation
TEOS	Tetraethoxysilane
T_f	Temperature of feed solution
$T_{f,in}$	Temperate of feed solution when it flow into membrane cell
T_{fm}	Temperature on the membrane surface in feed side
TIPS	Thermal induce phase separation
T_p	Temperature of permeate solution
$T_{p,in}$	Temperate of permeation when it flow into membrane cell
T_{pm}	Temperature on the membrane surface in the permeate side
UF	Ultrafiltration
V_c	Critical voltage
VMD	Vacuum membrane distillation
XPS	X-ray photoelectron spectroscopy
Greek	
γ	Surface tension of the solution
γ_L	Liquid surface tension
γ_{LA}	Surface energy of liquid against air
γ_{SA}	Surface energy of solid against air
γ_{SL}	Surface energy of solid against liquid
δ	Strain at break
δ_s	Membrane selective layer thickness
δ_t	Total membrane thickness
ϵ	Dielectric constant inside of the jet
ϵ'	Dielectric constant outside of the jet
ϵ_m	Porosity

θ	Liquid-solid contact angle
θ_0	Static contact angle
θ_c	Contact angle calculated by Cassie-Baxter equation
θ_{SA}	Water sliding angle
θ_w	Contact angle of a water droplet upon a rough solid surface
v_f	Velocity of feed solution
v_p	Velocity of permeation
ρ	Liquid density
σ	Surface charge
σ_B	Tensile at break
ω_1	Weight of the wet membrane
ω_2	Weight of the dry membrane

SUMMARY

Fast global population growth, serious environmental pollution and rapid economic developments have resulted in water scarcity around the world. Membrane distillation (MD) processes were considered as an attractive technology to treat waste water, recycle polluted water and provide more freshwater resources. This thesis provides a brief review on the research and developments of MD process, commercial MD membranes and lab-fabricated MD membranes. As the electrospun composite nanofibrous membranes have great potential to be used in MD due to their unique structural features, the complex electrospinning process has also been reviewed, including the materials and operating parameters which could control nanofiber formation, and various designs of electrospun apparatus which can produce nanofiber membranes with different appearances. However, it is found that limited works have been carried out to fabricate MD membranes by electrospinning.

In this work, poly (vinylidene fluoride) (PVDF) nanofiber membranes were fabricated through electrospinning for direct contact membrane distillation (DCMD) as a first trial. The effects of PVDF dope concentration, inorganic salt additives, sprayer's moving speed, and chamber moisture on the properties of resultant membranes were investigated. It also illustrates the importance of processing parameters and heat-press post-treatment, and demonstrates that the heat-press post-treatment improved membrane integrity significantly and enhanced permeate flux in DCMD process. All the electrospun nanofiber membranes possessed high water contact angles (between 135 ° to 142 °) due to their high surface roughness. The post-treated PVDF nanofiber membranes were able to present a steady water permeation flux of 21 kg m⁻²h⁻¹ throughout the entire testing period of 15 h, using a 3.5 wt% NaCl solution as the feed under the feed and permeate inlet temperatures of 323 K and 293 K, respectively.

However, PVDF nanofiber membranes without hydrophobic additives or surface modification do not have sufficient anti-wetting performance. Further treatment of PVDF nanofiber should be carried out to impart them with better wetting resistance and long-term stability. Two types of superhydrophobic PVDF

nanofiber membranes, integrally-modified and surface-modified PVDF membranes, have been successfully fabricated by electrospinning followed by surface modification, which includes dopamine surface activation, silver nanoparticle deposition and hydrophobic treatment. The modification is convenient because of mild reactions and wide applicability. The characterizations revealed that the modifications have altered the membrane surface morphology and topology, and made the membrane superhydrophobic due to their hierarchical structures. Compared with unmodified membrane, the integrally-modified membrane (I-PVDF) can achieve a high and stable MD water flux of $31.6 \text{ kg m}^{-2}\text{h}^{-1}$ using a 3.5 wt% NaCl as the feed solution while the feed and permeate temperatures were fixed at 333 K and 293 K, respectively. To the best of our knowledge, this result is superior to all other PVDF flat sheet membranes tested under the same or similar conditions, which is believed to be attributed to the open surface pore structure and the thin thickness of the PVDF nanofiber membrane with the aid of electrospinning. The superhydrophobic nature of the membrane surface brought by the integral modification on all nanofibers renders the membrane anti-wetting property while remaining high water flux.

Moreover, inspired by the unique structure of lotus leaf, a novel strategy is developed to construct composite nanofiber membranes with robust superhydrophobicity and high porosity suitable for use in MD. The newly developed membrane consists of a superhydrophobic silica-PVDF composite selective skin formed on PVDF porous nanofiber scaffold via electrospinning. This fabrication method could be easily scaled up due to its simple preparing procedures. The effects of silica diameter on membrane contact angle, sliding angle and MD performance were investigated thoroughly. For the first time, the DCMD tests demonstrate that the newly developed membranes are able to present stable high performance over 50 h of testing time, and the superhydrophobic selective layer exhibits excellent durability in ultrasonic treatment and continuous DCMD test. It is believed that this novel design strategy has great potential for MD membrane fabrication.

Additionally, to further improve the wetting repellent property of superhydrophobic membranes, 3-dimensional (3D) superhydrophobic membranes were developed as a possible solution. Moreover, since highly porous nanofiber membranes usually suffer from insufficient mechanical property, which have adverse impact on membrane packing in the module, thus, a dual-layer membrane was fabricated by electrospinning 3D superhydrophobic composite layers on a non-woven support to improve its wetting resistance and enhance mechanical robustness. Another type of dual-layer superhydrophobic composite membranes consisting of PVDF nanofibrous support and an ultrathin 3D superhydrophobic selective layer was prepared to compare with the as-fabricated non-woven-supported superhydrophobic dual-layer membrane. All these membranes exhibit superhydrophobicity towards distilled water, salty water, oil-water mixture and beverages, which enables them to be used not only for desalination but also for other concentrating treatments. Compared with nanofiber-supported dual-layer membranes, the non-woven-supported membranes exhibit higher mechanical strength as a result of excellent combination with non-woven support and better long-term performance because of the thicker 3D superhydrophobic structure. The morphology, pore size, porosity, mechanical properties as well as liquid entry pressure of water of these superhydrophobic composite membranes and commercial PVDF membrane are measured and compared. The possible wetting procedures of the as-prepared superhydrophobic dual-layer membranes are also illustrated in this study.

Finally, this thesis provides some personal perspectives for the future developments in which the composite nanofiber membranes could be pursued for water research.

In conclusion, this thesis presents the design and development of novel superhydrophobic nanofiber membranes based on the studies of the fundamental mechanisms of electrospinning, surface modification on nanofiber membranes, fabrication of robust superhydrophobic membranes, and preparation of 3D superhydrophobic dual-layer membrane. This work contributes to the development

of membrane fabrication technology and facilitates the practical applications of membrane distillation process.

CHAPTER 1

Introduction

1.1. Background

Water is essential for all organisms in nature including human beings, animals and plants. Even though our planet is called the “Blue Planet” meaning that most part of the planet is covered by water, severe water scarcity around the world is encountered especially in recent years. The well-known explanation for it is that although three quarters of the Earth’s surface is covered by water, only 2.5% is fresh water (Oki and Kanae 2006). More than 80 countries encounter severe water shortage and about 25% of all the population has no adequate access to fresh water with satisfied quality and quantity (Karagiannis and Soldatos 2008). The construction of massive infrastructure in the forms of pipelines, aqueducts and dams dominated the water agenda in the 20th century, which offered tremendous benefits to billions of people (Gleick 2003). However, these approaches for water management and transition are not enough to solve the water crisis. More fresh water resources should be produced by treating waste water and seawater to feed the growing water demands.

The water treatment processes are carried out to remove or reduce existing contaminants in the water by physical processes such as settling and filtration, chemical processes such as disinfection and coagulation, or biological processes such as aerated lagoons and activated sludge (Hill, McIntyre et al. 1986; Li, Mahendra et al. 2008; Vahedi and Gorczyca 2012). Among these processes, membrane technologies are advanced separation processes to produce various qualities of water from surface water, brackish water and seawater used in industrial process, and offer the possibilities of managing the total water resources in a region, which is of special interest in areas where the natural water resources are scarce (Nicolaisen 2003). The membrane technologies have attracted worldwide interests since the 1970s, and can be classified into different categories based on process

principles and membrane properties, which include microfiltration (MF), ultrafiltration (UF), nanofiltration (NF), reverse osmosis (RO), forward osmosis (FO), pressure retarded osmosis (PRO), gas separation (GS), pervaporation (PV), membrane distillation (MD) and separation by liquid membranes (Marcel 1990). The benefits of membrane processes compared with other separation processes are: (1) energy consumption is relatively low; (2) separation can be carried out continuously under mild conditions without additives; (3) membrane processes can be combined with other separation processes and are easy to up-scale; (4) membrane properties are variable and can be adjusted to meet special requirements. Among various membrane processes, MD process can use low-grade waste heat or renewable energy sources to produce high quality water with high water recovery (in principle 100 %) (Khayet 2011).

In a membrane separation process, the membrane plays a significant role. A number of different techniques are available to fabricate membranes including sintering, stretching, track-etching and phase inversion (Lalia, Kochkodan et al. 2013). Most commercial membranes are obtained by the phase inversion where a polymer is transformed in a controlled manner from a liquid to a solid phase. Within the last decades, the electrospinning of polymers has become an internationally highly recognized method for the preparation of polymeric nanofiber membranes composed of nanofibers with diameters down to a few nanometers, and a broad range of complex architectures of nanofibers can be formed (Agarwal, Greiner et al. 2013). Unlike other methods, the formation of electrospun nanofiber membranes is based on the uniaxial stretching or elongation of a viscoelastic jet derived from a polymer solution or melt under a high voltage field. Compared with traditional membranes, nanofiber membranes have attractive advantages such as large surface-to-volume ratio, high porosity, and high orientations of structural elements. These key features make nanofiber membranes have great potential for a number of applications in energy storage, healthcare, biotechnology, environmental engineering, defense and security as well as MD (Agarwal, Greiner et al. 2013). Furthermore, the need for membranes with advanced functions has lead to the development of various new and modified membranes. It is relatively easy to add additives into nanofibers and modify the nanofiber surface to grant electrospun

membranes with various properties to meet requirements, which makes electrospinning highly attractive to both academia and industry. In this research, the electrospun membranes have been designed, fabricated and modified for MD application.

1.2. Challenges for Membrane Distillation (MD)

MD is a thermally driven membrane process, which is realized by means of a micro-porous hydrophobic membrane, which plays a significant role in separating the hot salt or contaminated water from a cool and clean permeation. Only water vapor and volatile molecules can transport through the membrane pores. In a MD system, simultaneous heat and mass transfer phenomena occur through the membrane. There are four different MD configurations, including direct contact membrane distillation (DCMD), vacuum membrane distillation (VMD), air gap membrane distillation (AGMD) and sweeping gas membrane distillation (SGMD) (Lawson and Lloyd 1997; Khayet, Godino et al. 2000; Phattaranawik, Jiratananon et al. 2003; Qtaishat, Matsuura et al. 2008; Charfi, Khayet et al. 2010). Each MD configuration has its own advantages and disadvantages under a certain application condition.

Research and developments about MD processes have been carried out with focuses on theoretical modelling of MD, experimental studies on the effects of operating conditions as well as MD membrane fabrications and modifications. There have been substantial literatures on MD work over last two decades. **Figure 1-1** presents the number of MD papers published from Jan. 2004 to Dec. 2013 in refereed database (Science Direct). It is worth mentioning that DCMD is the most investigated MD process. This is because in DCMD configuration, the condensation step is carried out inside of the membrane module, which makes it relatively easier to construct modules (Lawson and Lloyd 1996). VMD process has a lower heat loss and higher mass transfer efficiency than other MD processes. In contrast, SGMD configuration attracts the least interests due to the need of an external condenser, which increases the cost of the entire system. In this study, all the fabricated membranes are evaluated in DCMD process.

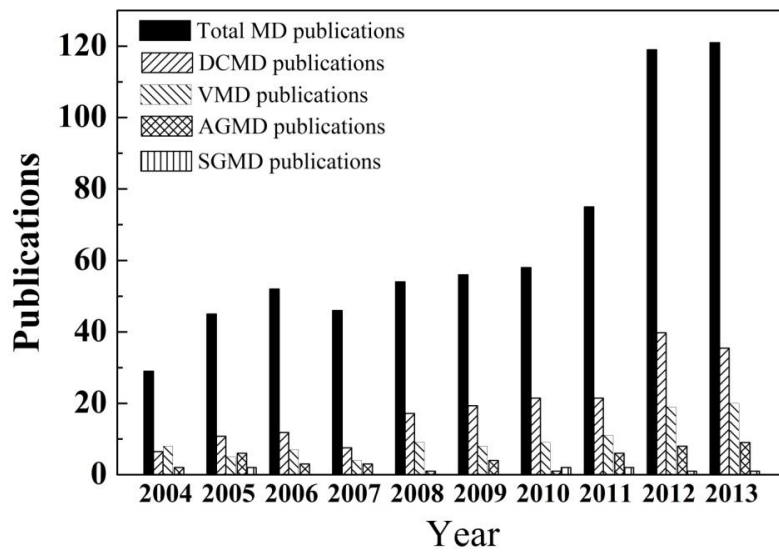


Figure 1-1. Growth of research activities of MD presented by the number of papers included in refereed database (Science Direct) per year

For the papers listed in **Figure 1-1**, most of them are about MD designs, mass transfer mechanism, heat transfer mechanism and the effects of MD operating conditions, and only 3.51% of published papers are focused on MD membrane fabrications. **Figure 1-2** shows the number of MD membrane fabrication papers in contrast with total MD papers in each year.

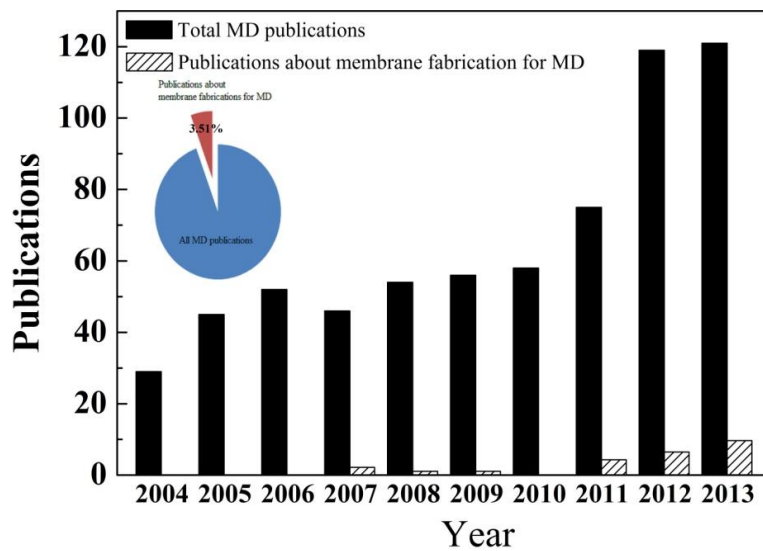


Figure 1-2. Number of papers about MD membrane fabrications included in refereed database (Science Direct) per year

It must be pointed out that although MD has attracted increasingly interests all over the world in recent years, MD still has little acceptance in industry applications due to some barriers, which include absence of specially designed MD membrane with high hydrophobicity, high porosity, competitive permeate flux, good long-term stability and robust mechanical strength.

1.3. Research objectives

This research aims to design and fabricate superhydrophobic composite membranes for DCMD application by electrospinning. Specifically, the main objectives of the study are:

- (1) To fabricate single-layer nanofibrous PVDF membranes for DCMD by electrospinning without any modification as a first trial:
 - Optimize polymer dope compositions, spinning parameters such as sprayer moving speed and chamber moisture to examine their effects on pore size distribution of the membranes;
 - Investigate the effect of inorganic additives on membrane pore size;
 - Perform heat-press post-treatment to improve fresh nanofiber membrane integrity, enhance water permeation flux, and help prevent membrane pores from wetting in DCMD operation;
 - Fabricate nanofiber MD membranes which have acceptable permeate flux and long-term MD performance, and could be used as good substrates for further works.
- (2) To prepare superhydrophobic membranes by surface modification on PVDF nanofiber membranes in order to increase membrane hydrophobicity and improve long-term performance in DCMD process:
 - Fabricate superhydrophobic PVDF nanofiber membranes by chemical modifications;
 - Reveal the effects of modification on membrane surface morphology and topology;
 - Compare the performances of modified superhydrophobic membranes with controlled membrane.

- (3) To construct superhydrophobic nanofiber membranes with robust superhydrophobicity and high porosity suitable for using in DCMD:
 - Design easily scaled up fabrication method to prepare superhydrophobic membranes for MD;
 - Demonstrate the newly developed superhydrophobic layer is robust to be used in long-term MD process;
 - Fundamentally understand the superhydrophobic effects on membrane wetting resistance during MD test.
- (4) To fabricate and compare highly porous nanofiber-supported dual-layer membranes with an ultrathin 3-dimensional (3D) superhydrophobic skin and mechanically robust non-woven-supported dual-layer membrane with a thicker 3D superhydrophobic structure for DCMD;
 - Enhance the mechanical properties of electrospun membranes by fabricating non-woven-supported dual-layer superhydrophobic membranes;
 - Improve roughness-induced superhydrophobicity by constructing membranes with a thicker 3D superhydrophobic structure;
 - Compare morphologies, pore sizes, mechanical properties as well as possible wetting procedures of nanofiber-supported and non-woven-supported superhydrophobic dual-layer membranes.

1.4. Thesis outlines

This thesis includes 7 chapters, which are highlighted as following:

Chapter 1: *Introduction* – Background information, challenges in the research area and the objectives of the study are provided.

Chapter 2: *Literature review* – A brief literature review is categorized into two parts. Firstly, the concepts and advantages about MD processes, MD applications and challenges, and current status of MD membrane fabrications are reviewed. Secondly, the electrospinning process is introduced. Mechanisms of electrospinning and parameter influences during the electrospinning process are

provided, followed by the review about few research for fabrication of electrospun MD membranes.

Chapter 3: *Fabrication of PVDF nanofiber membranes by electrospinning for DCMD* – PVDF nanofiber membranes were fabricated and optimized for DCMD application. Polymer dope compositions, spinning parameters such as sprayer moving speed and chamber moisture, inorganic additives, and heat-press post-treatment were optimized to examine their effects on pore size distribution of the membranes.

Chapter 4: *Engineering superhydrophobic surface on PVDF nanofiber membranes for DCMD* – Two types of superhydrophobic PVDF nanofiber membranes, integrally-modified and surface-modified PVDF membranes were successfully fabricated by electrospinning followed by surface modification, which includes dopamine surface activation, silver nanoparticle deposition and hydrophobic treatment. These novel composite nanofiber membranes have been characterized by a series of measurements and benchmarked against commercial PVDF flat sheet membrane for MD application.

Chapter 5: *Fabrication of bioinspired composite nanofiber membranes with robust superhydrophobicity for DCMD* – Superhydrophobic composite nanofiber membranes with robust superhydrophobicity and high porosity were developed for DCMD in this study, which consist of a superhydrophobic silica-PVDF composite selective skin formed on PVDF porous nanofiber scaffold via electrospinning. The effects of silica diameter on membrane contact angle, sliding angle and MD performance, and stability of the superhydrophobic layer were investigated thoroughly.

Chapter 6: *Electrospun superhydrophobic membranes with unique structures for membrane distillation* – The newly developed nanofiber-supported dual-layer membranes with an ultrathin 3D superhydrophobic layer and non-woven-supported dual-layer membranes with a thicker 3D superhydrophobic structure were fabricated by electrospinning. The morphology, pore size, porosity, mechanical

properties as well as possible wetting procedures of these superhydrophobic membranes are compared thoroughly.

Chapter 7: *Conclusions and recommendations* – The important findings of this study and recommendations for future work are provided in this chapter.

CHAPTER 2

Literature review

2.1. Membrane Distillation (MD)

2.1.1. Concept and advantages of MD

MD process is driven by the trans-membrane vapor pressure difference between the hot feed and cold permeate, in which only vapor molecules are transported through porous and hydrophobic membranes. The hot liquid feed in the MD module is in direct contact with one side of the membrane while condensation takes place on the cooler side of the membrane. The hydrophobic character of membrane and surface tension of the liquid will prevent the liquid from entering membrane pores. The liquid/vapor interfaces occur at the entrances of membrane pores. **Figure 2-1** shows the configuration of DCMD process.

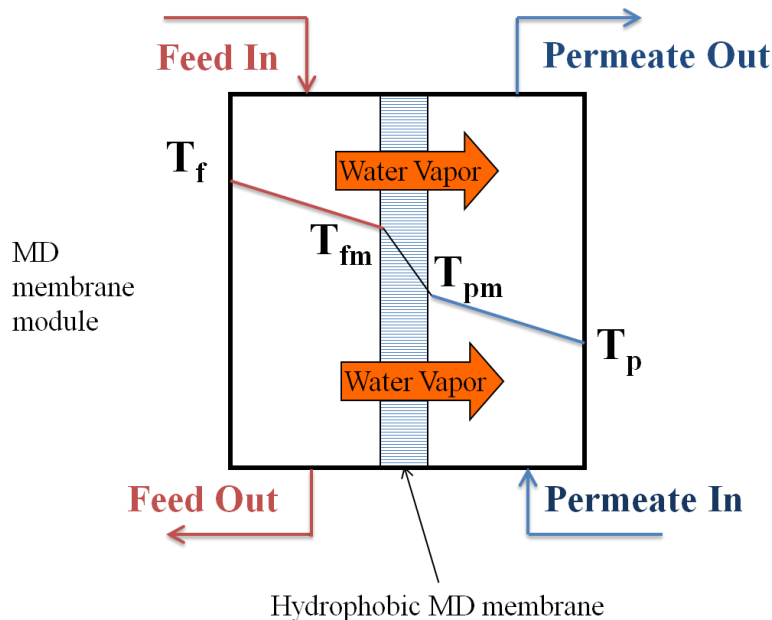


Figure 2-1. Schematic configuration of DCMD process. T_f , T_{fm} , T_{pm} and T_p are the temperature of feed side, on the membrane surface in feed side, on the membrane surface in the permeate side, and of permeate side, respectively. The water vapor would transport through the hydrophobic MD membrane.

Compared with traditional separation methods, the advantages of MD process include: (1) production of high purified distillate; (2) low operating temperature and pressure; (3) high rejection towards ions and non-volatile (100% theoretical rejection); (4) less stringent membrane property requirements; (5) low chemical interaction between membrane and feed solutions; (6) possibility to operate by low energy source such as waste heats, geothermal and solar; (7) easy integration with conventional desalination process to increase water recovery and improve system efficiency; (8) capacity to recover valuable crystal products from effluents in combination with a crystallizer, which is referred as membrane distillation crystallization (MDC) (Wu, Kong et al. 1991; Fujii, Kigoshi et al. 1992; Bouguecha and Dhahbi 2003; Koschikowski, Wieghaus et al. 2003; El Amali, Bouguecha et al. 2004; Tun, Fane et al. 2005; Mariah, Buckley et al. 2006; Banat, Jwaied et al. 2007; Chang, Wang et al. 2010; Guillén-Burrieza, Blanco et al. 2011).

2.1.2. MD applications and challenges

Due to the above-mentioned advantages, MD has great potential to apply for water desalination, water reuse, biomedical applications such as water removal from blood and the treatment of protein solutions, environmental waste cleanup, and food concentration processing (Barbe, Bartley et al. 1998; Laganà Barbieri et al. 2000; Cassano, Drioli et al. 2003; Lukanin, Gunko et al. 2003; Bagger-Jørgensen, Meyer et al. 2004; Jiao, Cassano et al. 2004; Alves and Coelhoso 2006; Błafi-Bakó and Koroknai 2006; Gunko, Verbych et al. 2006; Diban, Voinea et al. 2009; Valdés, Romero et al. 2009; Jensen, Christensen et al. 2011; Zhao, Zhu et al. 2011). In these applications, MD has been utilized to desalinate of seawater, to remove non-volatile compounds from water such as ions, colloids, and macromolecules, to separate trace volatile organic components from water like benzene, chloroform, trichloroethylene, and to extract organic compounds such as alcohols from aqueous solutions (Sarti, Gostoli et al. 1993; Couffin, Cabassud et al. 1998; Banat, Abu Al-Rub et al. 1999; Banat and Al-Shannag 2000; García-Payo, Izquierdo-Gil et al. 2000; Lee and Hong 2001; Wu, Tan et al. 2006).

However, although MD has been known for more than forty years, it has still limited use in industries. The obstacles impeding MD's commercial

implementation include: (1) lack of affordable specially designed MD membrane with high performance; (2) a relative lower permeate flux compared with other membrane process such as RO; (3) permeate flux delay due to temperature polarization; (3) membrane fouling in long-term process; (4) total or partial membrane pore wetting; (5) absence of available membrane modules with enhanced fluid dynamic to improve mass transfer and heat efficiency; (6) uncertain energy and economic costs for each MD configuration; (7) difficulty in achieving high permeate flux with high purity. Significant efforts are needed to overcome these impediments for MD large-scaled commercialization, especially for MD membrane design and fabrication.

It is generally known that flat-sheet or hollow fiber commercial micro-porous hydrophobic membranes which are used in MD process were primarily prepared for other filtration applications. Although these commercial hydrophobic membranes, made of polypropylene (PP) (Li, Xu et al. 2003; Marek 2007; Gryta, Grzechulska-Damszel et al. 2009; Tang, Jia et al. 2010), poly(vinylidene fluoride) (PVDF) (M 1996; Khayet, Feng et al. 2002; Bottino, Capannelli et al. 2005; Feng, Khulbe et al. 2008; Bonyadi and Chung 2009; Hou, Wang et al. 2009; Huo, Gu et al. 2009; Teoh and Chung 2009; Garc á-Payo, Essalhi et al. 2010; Yang, Wang et al. 2011) or polytetrafluoroethylene (PTFE) (Hwang, He et al. 2011; Lai, Liou et al. 2011; Teoh, Chung et al. 2011), meet the most required features of MD membranes, these membranes are still not satisfied either in long-term performance or permeate flux. Until now only few works have been done for designing MD membranes. To design and fabricate membranes for MD process, we need to know the requirements and specifications of MD membranes firstly.

2.1.3. *Requirements and current status of MD membranes*

➤ *Requirements of MD membranes*

The critical requirements and specifications of the MD membrane are outlined as following (Khayet 2011):

- 1) As mentioned above, in the MD process, the porous membrane plays a vital role of physical support on the liquid/gas interface. Because of hydrophobic

character of the membrane, the liquid cannot pass through membrane until the liquid entry pressure of water (LEP_w) is exceeded. Thus the first requirement of MD membrane is that it should be comprised of at least one hydrophobic layer. For multilayer MD membrane, at least the top layer facing feed solution is hydrophobic and porous.

- 2) Secondly, the MD membrane should have pore sizes in the range of several nanometers to few micrometers. To prevent the feed solution from entering the membrane pores, the pore size distribution should be as narrow as possible while the maximum pore size should be sufficiently small. However, small maximum and mean pore size may cause high membrane resistance and thus low permeate flux. Thus, a balance between the membrane wetting resistance and mass transfer efficiency should be made by choosing an appropriate pore size and pore size distribution.
- 3) The tortuosity factor, which is the measure of the deviation of the pore structure from straight cylindrical pores normal to the surface, should be as small as possible.
- 4) Additionally, the membrane porosity has a significant effect on the permeate flux. It is well-known that the membranes with higher porosity have more void spaces for vapor transfer and thus a higher permeation flux. In order to enhance permeate flux in the MD process, membranes with high porosity are preferable.
- 5) Thickness of the hydrophobic layer is another important factor which is inversely proportional to the rate of mass transport through the membrane. In the case of single-layer MD membrane, membrane thickness should have an optimized value which makes a higher mass transport rate and a lower heat transport rate. For multilayer membranes, the hydrophobic layer should be as thin as possible which decreases the mass transfer resistance while the overall membrane thickness should be as thick as possible to prevent heat loss.
- 6) It should be mentioned that most polymers have similar thermal conductivity coefficients within the same order of magnitude (between 0.04 W/m K to 0.06 W/m K). However, the air trapped inside the membranes is a better

isolate material than polymers (Thermal conductivity of air is only 0.025 W/m K). Thus, another way to diminish the membrane heat transport is to fabricate membrane with high porosity.

- 7) Furthermore, the MD membrane should be strong enough to prevent deflection and rupture, and should have excellent long-term performance.
- 8) Membrane materials should exhibit good thermal stability as MD process may be operated at temperature close to 90 ~ 100 °C, depending on the heat sources.
- 9) The membrane surface in contact with the feed solution in the MD process should possess high fouling resistance;
- 10) Finally, the MD membrane should provide stable permeation flux and long life.

➤ *Commercial MD membranes*

In the commercial market, microporous hydrophobic membranes made of PTFE, PP and PVDF in tubular, capillary or flat sheet forms are available. Because of unique characteristics of different polymers, they need different methods to prepare membranes. Although PTFE is the most ideal polymer for MD membrane manufacture due to its highest hydrophobic characteristic, best chemical resistance and thermal stability, PTFE membranes are most difficult to produce, which are usually fabricated by stretching, sintering, rolling or extrusion (Huang, Xiao et al. 2011; Adnan, Hoang et al. 2012). Moreover, PP membranes are manufactured through stretching or thermal induce phase separation (TIPS) process as PP cannot be dissolved in common solvent at room temperature. Compared with PTFE and PP, PVDF possesses relatively easier processability, which makes this polymer the most investigated material in laboratory for MD application (Tang, Jia et al. 2010; Khayet and Matsuura 2011). As PVDF can be dissolved in various solvents at room temperature, PVDF MD membrane could be easily fabricated by immersing the casting or extruding polymer solution in a coagulation bath via non-solvent induced phase separation (NIPS) method. However, these PVDF commercial membranes were mainly fabricated for MF purposes instead of MD, although some of them were investigated for MD application in literatures, as shown in **Table 2-1**.

Table 2-1. Commercial membranes commonly used in DCMD (membrane selective layer thickness, δ_s , μm ; total membrane thickness, δ_t , μm ; mean pore size, d_p , μm ; porosity, ε_m , %; membrane surface water contact angle, C_a , $^\circ$; DCMD permeate flux, J , $\text{kg}/\text{m}^2\text{h}$)

Name	Manufacturer	Material	δ_s (μm)	δ_t (μm)	d_p (μm)	ε_m (%)	C_a ($^\circ$)	J ($\text{kg}/\text{m}^2\text{h}$)	Observation	Ref.
Mp0.30	GE Osmonics	PVDF/non-woven	90	234	0.30	81	113	9	1 wt% NaCl solution as feed ; $T_f=60\text{ }^\circ\text{C}$; $T_p=20\text{ }^\circ\text{C}$	(Zhang, Dow et al. 2010)
PVDF (capillary)	PV390, Memtec	PVDF	115	115	0.26	-	97	22	0.1 wt% NaCl solution as feed ; $T_f=80\text{ }^\circ\text{C}$; $T_p=20\text{ }^\circ\text{C}$	(Gryta and Barancewicz 2010)
Durapore GVHP	Millipore	PVDF	120	120	0.16	72	-	8	0.6 wt% NaCl solution as feed ; $T_f=40\text{ }^\circ\text{C}$; $T_p=20\text{ }^\circ\text{C}$	(Mart ínez and Rodríguez-Maroto 2008)
GVHP	Millipore	PVDF	118	118	0.27	70	110	16	pure water solution as feed ; $T_f=60\text{ }^\circ\text{C}$; $T_p=20\text{ }^\circ\text{C}$	(Khayet, Imdakm et al. 2010)
GVHP	Millipore	PVDF	126	126	0.22	62	-	21	pure water as feed ; $T_f=60\text{ }^\circ\text{C}$; $T_p=20\text{ }^\circ\text{C}$	(Phattaranawik, Jiratananon et al. 2003)
HVHP	Millipore	PVDF	116	116	0.45	66	-	23	pure water as feed ; $T_f=60\text{ }^\circ\text{C}$; $T_p=20\text{ }^\circ\text{C}$	(Phattaranawik, Jiratananon et al. 2003)
PVDF	Millipore	PVDF	110	110	0.45	75	-	25	5 wt% NaCl solution as feed ; $T_f=61\text{ }^\circ\text{C}$; $T_p=21\text{ }^\circ\text{C}$	(Schofield, Fane et al. 1990)

➤ *Lab-fabricated MD membranes*

Compared to membranes used for other membrane processes, few research have been carried out for specially designing and preparing MD membranes. As mentioned previously, MD membrane must have its own special architecture to satisfy specific requirements. Thus, the research focusing on MD membrane design and fabrication are urgent and necessary. During last few years a number of laboratories have achieved progresses in fabricating MD membranes in order to enhance both the permeate flux and permeation water quality. **Table 2-2** summarizes these works for fabrications of PVDF MD membranes, characteristics of the resultant membranes and their MD performances.

Highly porous and macrovoid-free PVDF hollow fiber membranes were fabricated by applying a two phase flow (combining a solvent and a dope solution) in the air gap region when spinning via NIPS (Bonyadi and Chung 2009). It was found that membrane morphology and hydrophobicity have influences on the membrane wettability (Gryta and Barancewicz 2010). The investigation revealed that membranes with a sponge-like structure have better anti-wetting performance and membrane wettability could be retarded after PTFE particles were added into the polymer matrix, which enhanced the membrane hydrophobicity. Multichannel rectangular membranes were fabricated through NIPS with the aid of a specially designed spinneret (Teoh, Peng et al. 2011). These unique membranes were designed to combine the advantages from hollow fiber, flat sheet membranes and woven or nonwoven spacers. Dual-layer membranes with a more hydrophobic surface layer were fabricated for MD process in order to enhance permeation flux. Dual-layer hollow fiber with a fully finger-like macrovoid inner-layer and a sponge-like outer-layer has been fabricated for MD process (Wang, Teoh et al. 2011). It was found that the morphological characteristics of membranes had great effects on permeation flux and long-term performance in MD process. It also suggested that the hydrophilic-hydrophobic hollow fiber membrane maybe a promising approach for MD (Bonyadi and Chung 2007). When the

hydrophobic and hydrophilic clay particles were incorporated in the outer layer dope and inner layer dope respectively, the surface tension characteristic of the dual layer membrane was changed and the membrane mechanical strength was improved.

Moreover, LiCl and polyethylene glycol (PEG) 1500 were added into the dope as additives to fabricate high porosity and hydrophobic PVDF membrane for DCMD (Hou, Wang et al. 2009). Graphite particles and multiwall carbon nanotubes were embedded into membrane hydrophilic layer to enhance MD permeation flux via improving conducting network in membranes (Su, Teoh et al. 2010). Carbon nanotubes could be used as additives for MD membrane fabrication to provide preferable properties such as high porosity, high hydrophobicity and high specific surface area (Dum  , Germain et al. 2011). The resultant membranes possess higher contact angle and higher liquid entry pressure. Hydrophobic modified calcium carbonate nanoparticles were dispersed in a PVDF casting solution and the mixture of LiCl and PEG were added as non-solvent additives to fabricate PVDF composite hydrophobic hollow fiber membranes for DCMD (Hou, Wang et al. 2012). The addition of hydrophobic nano-particle would prepare sandwich-like morphology, optimize pore size distribution, enhance membrane porosity, increase membrane hydrophobicity, improve mechanical properties and provide composite membrane with better performance stability. The effects of hydrophobic self-synthesized fluorinated silica (FSi) particles on membrane morphology and membrane's MD performance were studied (Edwie, Teoh et al. 2012). It was argued that the stability of membrane long-term performance was not improved by the enhancement of hydrophobicity of membrane spun with FSi particles due to the existence of the hydrophilic hydroxyl group on the particle surface.

Table 2-2. Lab-fabricated PVDF membranes for DCMD (membrane selective layer thickness, δ_s , μm ; total membrane thickness, δ_t , μm ; mean pore size, d_p , μm ; maximum pore size, d_m , μm ; porosity, ε_m , μm ; membrane surface water contact angle, C_a , $^\circ$; liquid enter pressure, LEP, Kpa; DCMD permeate flux, J, $\text{kg}/\text{m}^2\text{h}$)

Institution	Material	δ_s (μm)	δ_t (μm)	D_p (μm)	D_m (μm)	ε_m (%)	C_a ($^\circ$)	LEP (Kpa)	J ($\text{kg}/\text{m}^2\text{h}$)	Observation	Ref.
Xi'an Jiaotong University	PVDF, hollow fiber	199	199	0.14		79	100		16	9.09 wt% NaCl solution	(Tang, Li et al. 2012)
		210	210	0.31		75			14	as feed; $T_f=65$ $^\circ\text{C}$;	
		215	215	0.38		69	87		10	$T_p=21$ $^\circ\text{C}$	
National University of Singapore	PVDF /PTFE, hollow fiber	6	140		0.26	86	95	104	22		(Teoh, Chung et al. 2011)
		13	145		0.26	83	114	466	20	3.5 wt% NaCl solution	
		20	150		0.27	82	111	387	18	as feed; $T_f=60$ $^\circ\text{C}$;	
		14	115		0.28	85	113	407	22	$T_p=17.5$ $^\circ\text{C}$	
National University of Singapore	PVDF /PAN, hollow fiber	14	145		0.27	82	111	396	20		(Su, Teoh et al. 2010)
		50	277	0.41		80			18	3.5 wt% NaCl solution	
		50	282	0.41		80			20	as feed; $T_f=60$ $^\circ\text{C}$; $T_p=15$	
		50	271	0.41		80			33	$^\circ\text{C}$	
Chinese Academy of Sciences	PVDF	130	130	0.35	0.50	69	85		5		(Hou, Wang et al. 2009)
		130	130	0.5	0.90	72	118		16	3.5 wt% NaCl solution	
		130	130	0.15	0.23	78	93		11	as feed; $T_f=60$ $^\circ\text{C}$; $T_p=20$	
		130	130	0.25	0.50	80	105		20	$^\circ\text{C}$	
National University of Singapore	PVDF/clay particles	50	380	0.41	0.60	80	137		21	3.5 wt% NaCl solution as feed; $T_f=63.3$ $^\circ\text{C}$; $T_p=16.6$ $^\circ\text{C}$	(Bonyadi and Chung 2007)
National University of Singapore	PVDF	100	100		0.07	63	88		8	3.5 wt% NaCl solution	(Bonyadi and Chung 2009)
		100	100		0.08	65	130		22	as feed; $T_f=60$ $^\circ\text{C}$; $T_p=17$	
		50	50		0.08	65	130		26	$^\circ\text{C}$	

To be continued on the next page

To be continued with the previous page

Institution	Material	δ_s (μm)	δ_t (μm)	D_p (μm)	D_m (μm)	ε_m (%)	C_a (°)	LEP (Kpa)	J ($\text{kg}/\text{m}^2\text{h}$)	Observation	Ref.
National University of Singapore	PVDF, hollow fiber	140	140	0.16	0.29	86	88		18		
		145	145	0.13	0.22	81	93		14	3.5 wt% NaCl solution as feed; $T_f=60$ °C;	(Teoh and Chung 2009)
	PVDF/PTFE, hollow fiber	145	145	0.11	0.21	74	103		12	$T_p=17.5$ °C	
		140	140	0.18	0.27	73	103		15		
		130	130	0.19	0.29	76	105		14		
		110	110	0.24	0.31	80	108		13		
		130	130	0.32	0.75	80	105	307	20		
Chinese Academy of Sciences	PVDF, CaCO_3 , hollow fiber	150	150	0.29	0.62	82	107	356	20		(Hou, Wang et al. 2012)
		150	150	0.25	0.56	85	110	403	21	3.5 wt% NaCl solution as feed; $T_f=60$ °C; $T_p=20$ °C	
		150	150	0.18	0.43	83	115	516	20		
		150	150	0.09	0.18	79	120	1180	15		
		150	150	0.03	0.11	73	123	1920	12		
National University of Singapore	PVDF	150	27	0.48		78	133		38		(Edwie, Teoh et al. 2012)
		120	29	0.47		75	138		39	3.5 wt% NaCl solution as feed; $T_f=60$ °C; $T_p=15$ °C	
	PVDF, Silica	107	30	0.35		69	139		37		
National University of Singapore	PVDF	198	78			89	106	70	30		(Yang, Wang et al. 2011)
		164	70			87	107	70	40	3.5 wt% NaCl solution as feed; $T_f=60$ °C; $T_p=15$ °C	
		141	39			84	110	70	50		
		143	104			74	113	100	18		
West Pomeranian University of Technology	PVDF, capillary	111	111	0.26			97		22		(Gryta and Barancewicz 2010)
		216	216				95		32		
	PVDF /PTFE, capillary	135	135	0.26			88		27	1000 ppm NaCl solution as feed; $T_f=80$ °C; $T_p=20$ °C	
		133	133	0.25			103		23		

2.2. Development of nanofiber membranes by electrospinning

2.2.1. Introduction of electrospinning

As mentioned above, compared with traditional membranes prepared by NIPS, electrospun nanofiber membranes have attractive characteristics, including large surface-to-volume ratio, high porosity and high orientations of structural elements, which make them have great potential for MD. The advantages and disadvantages of various membrane fabrication methods are listed in **Table 2-3**.

The principle of electrospinning was first illustrated by Formhals in the 1930s and the first patent related with electrospinning in US was submitted in 1902 (Morton 1902; Formhals 1934). The considerable attention of electrospinning process was regained since 1990s. Within last decade electrospinning of polymers has become a globally highly recognized technology for preparation of polymeric nanofibers with diameters down to a few nanometers. The number of papers and patents for fabrication and application of electrospun membranes has increased in recent years, as indicated in **Figure 2-2**.

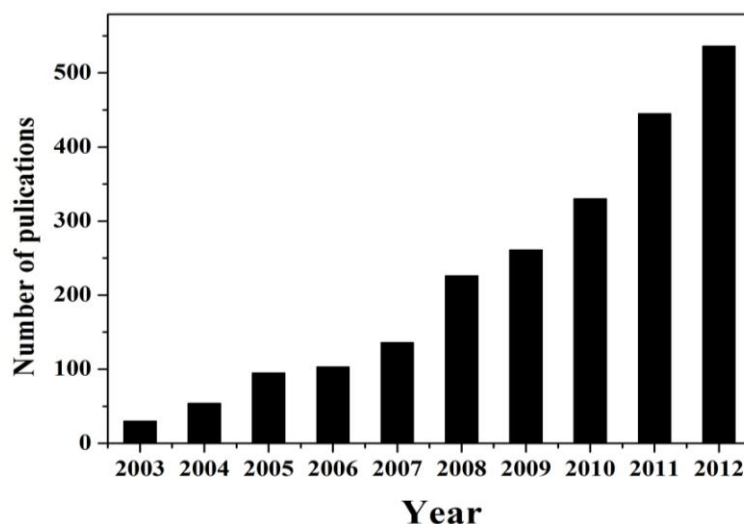


Figure 2-2. Annual number of publications on the subject of electrospinning, as provided by the search engine of Science Direct Scholar

Table 2-3. Advantages and disadvantages of different membrane fabrication methods

Membrane fabrication method	Advantages	Disadvantages
Electrospinning	<p>Easy to scale-up</p> <p>High level of versatility to allow control over fiber diameter, microstructure and arrangement</p> <p>Vast materials selection</p> <p>Cost effective</p> <p>Non-toxic solvent such as water can be used to prepare dope</p> <p>Easy to add additive into fibers</p> <p>Fabricate membranes with high porosity above 90% and high surface-to-volume ratio</p>	<p>2-D dimensional pore or microstructure arrangement</p> <p>Hard to achieve pores below 100 nanometers</p> <p>Slow yield speed</p>
Sintering	<p>Prepare symmetric membrane with pore size between 0.1 to 10 microns</p> <p>Suitable for chemically stable materials such as PTFE, PE, metals and ceramics</p> <p>No need solvent</p>	<p>Requires particles with narrow size distribution</p> <p>Hard to achieve pores below 100 nanometers</p> <p>Low porosity: 10-20%</p> <p>Need high temperature</p>
Stretching	<p>Prepare symmetric membranes with pore size between 0.1 to 3 microns</p> <p>Ladder like slits</p> <p>Porosity between 60% to 80%</p> <p>Can be used for PTFE, PE, PP and ceramics</p>	<p>Need high temperature</p>

To be continued on the next page

To be continued with the previous page

Membrane fabrication method	Advantages	Disadvantages
Track-etching	Prepare symmetric membrane with pore size between 0.02 to 10 microns Tight pore size distribution Cylindrical pores	Limited range of suitable polymers Low porosity 10% High price Thicknesses of membranes are limited by the particle energy Hard to achieve nano-pores
Template Leaching	Prepare symmetric membrane with pore size between 0.5 to 10 microns Extremely narrow pore size distribution High flux	High price Difficult to scale up Complex procedures
Phase inversion	Can be used for a wide variety of polymers Can fabricate flat and tubular membranes Simple to prepare and easy to scale up Fast yield speed Easy to optimize membrane thickness and pore size High porosity around 80% Form small surface pores and large bulk pores naturally	The polymer must be soluble in a solvent or solvent mixture

Among different methods of producing nanofibers such as melt fibrillation and gas jet techniques, the electrospinning has advantages with its comparative low cost and relatively high production rate (Iwamoto, Nakagaito et al. 2007; Lin, Yao et al. 2008). Nanofiber membrane formation in electrospinning is governed by self-assembly processes as induced by electric charges. A typical electrospinning setup is composed of three basic parts: a high voltage supply, a capillary (including polymer solution syringes, syringe pump and spinnerets) and a grounded metal collator as shown in **Figure 2-3**. During an electrospinning process, the precursor solution is extruded from a spinneret to form a small droplet at the feeding units/tips of die in the presence of an electric field. Then the charged solution jets are extruded from the droplet/cone. Briefly the fluid extension starts in uniform filaments, then follow with vigorous whipping and/or splitting motion because of fluid and electrically driven bending instabilities (Reneker and Yarin 2008). Finally, the continuous as-prepared fibers are deposited and collected on counter electrodes/substrates.

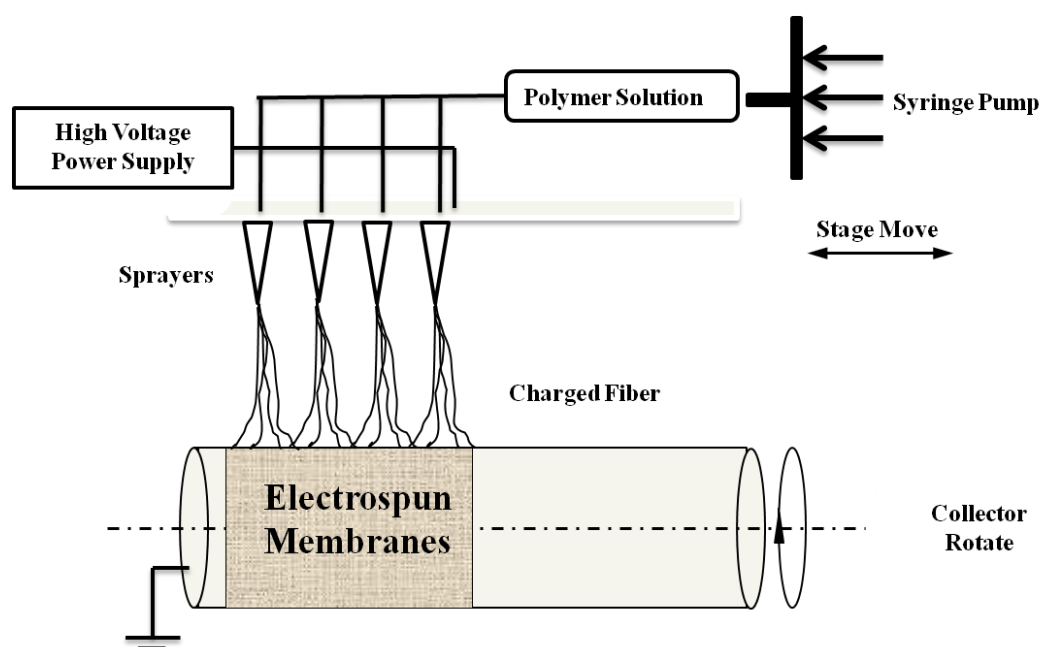


Figure 2-3. Schematic illustration of the basic setup for electrospinning

Since significant progress have been achieved in not only understanding the complex electrospinning processes and also in the strict control of fiber formation by operating parameters and materials, these achievements have in turn allowed for an extension of electrospinning technologies toward many applications including membrane fabrication, tissue engineering, drug delivery, energy storage, defense and security (Ramakrishna, Fujihara et al. 2006; Sill and von Recum 2008; Chen, Liu et al. 2013; Liao, Wang et al. 2013). Many companies such as eSpin Technologies and NanoTechnics are seeking to reap the unique advantages offered by electrospinning, while other companies as Donaldson and Freudenberg companies have commercialized the electrospun fibers in their filtration products within last two decades. In this section, the details in electrospinning process and parameters affecting the electrospinning including the intrinsic properties of the solution, operational condition as well as the temperature and humidity of surrounding will be further illustrated.

2.2.2. Understanding the complex process of electrospinning

During electrospinning process, polymeric nanofiber membranes are formed by creation and elongation of an electrified fluid jet. The forces, including electrostatic force, drag force, gravity, Coulombic repulsion force, surface tension and viscoelastic force, act on the charged fluid jet when it flies with an accelerated high speed under the electric field as shown in **Figure 2-4**. In order to control the morphology and structure of nanofibrous membranes, it is necessary to understand quantitatively how electrical forces interact with surface tension to change the shape of viscoelastic fluids into jets that finally solidify into nanofibers. Recently, the theoretical and experimental research have demonstrated that the electrospinning process generally composed of following three stages as shown in **Figure 2-5** (Reneker Darrell and Fong 2006): (1) onset of jetting and rectilinear jet development; (2) bending deformation with looping and spiralling trajectories; (3) solidification and deposition on counter electrodes/substrates.

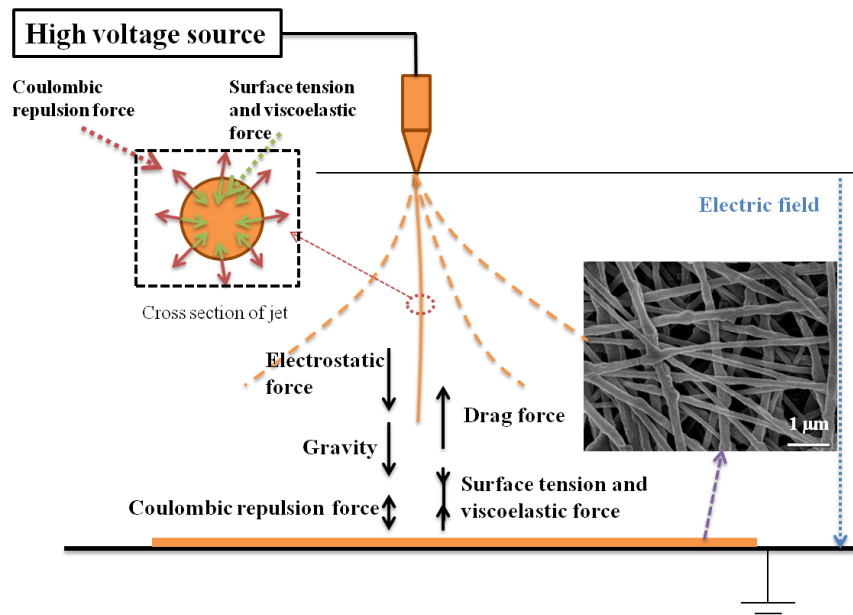


Figure 2-4. Schematic diagram illustrating the possible mechanism of nanofiber formation during electrospinning process

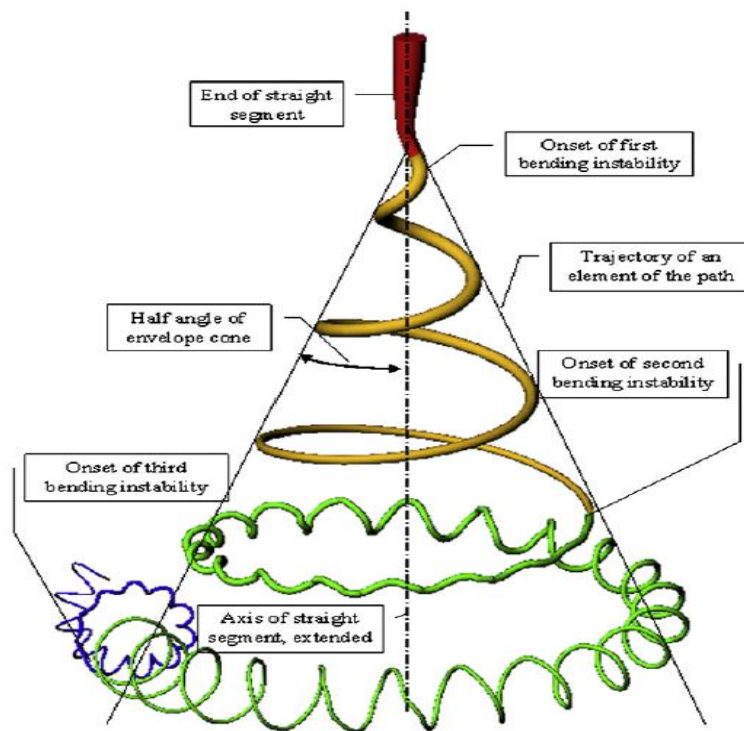


Figure 2-5. A diagram showing the prototypical instantaneous position of the pathway of an electrospinning jet [figure adopted from (Reneker Darrell and Fong 2006)]

➤ Onset of jetting and rectilinear jet development

During electrospinning process, an electrical potential difference, measured in volts, was applied between a droplet of polymer fluid which was suspended at an orifice by surface tension and viscoelastic stresses, and an electrically conducting grounded collector. As shown in **Figure 2-6**, the time zero was set as the first jet appeared while electrical field was applied before 28 ms (Fong and Reneker Darrell 2000). With an increase of applied voltage, the shape of solution tip will be transformed part of the way toward a conical shape. Then the rounded droplet became shaper and a jet emanated from the Taylor Cone (Taylor 1964). After milliseconds, the droplet had a round shape while a rapidly elongating and thinning jet with electrical charge flowed from the droplet. This cone shape was stable as long as appropriate amount of polymer solution was flowing in and replace the droplet. The critical voltage at which the droplet at the cone tip would overcome the surface tension and generate jets would be calculated by Taylor' calculation (Taylor 1969):

$$V_c^2 = 4 \frac{H^2}{h^2} \left(\ln \left(\frac{2h}{R} \right) - 1.5 \right) (1.3\pi R \gamma) (0.09) \quad (2-1)$$

where V_c is the critical voltage, H is the distance from the needle tip to the collecting screen, h is the length of the liquid column, R is the needle outer radius, and γ is the surface tension of the solution. Thus, through this equation it is obvious that the critical voltage which can generate the nanofibers from a given dope solution is decided by the dope surface tension, need radius and distance between needle tip and collecting screen. Higher critical voltage is needed when the dope possesses higher surface tension, the needle radius is larger, and the distance between needle and collector is increased.

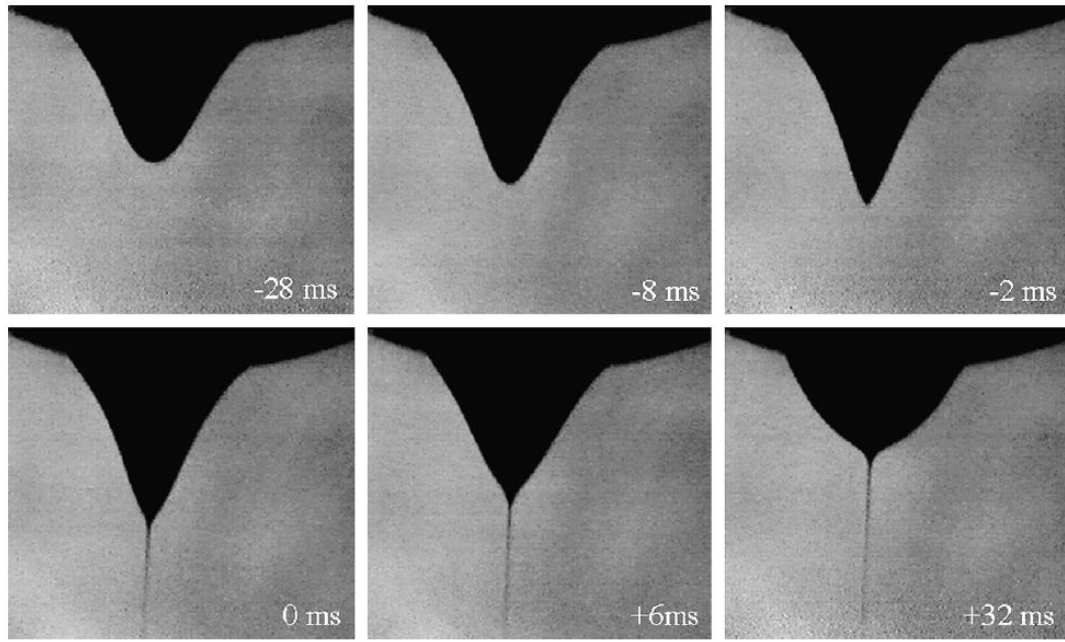


Figure 2-6. Evolution of the shape of a fluid drop in electrospinning process [figure adopted from (Fong and Reneker Darrell 2000)]

After the nanofiber is initiated and before the onset of first bending instability, the jet of polymer solution would follow the nearly straight electric field lines for a certain distance away from the tip as show in **Figure 2-5** (Reneker, Kataphinan et al. 2002). The critical length of the straight jet was predicted by applying Chauchy's inequality (He, Wu et al. 2005):

$$L = \frac{4kQ^3}{\pi\rho^2I^2} (R_0^{-2} - r_0^{-2}) \quad (2-2)$$

where L is the critical length of the straight jet, $R_0 = (2\sigma Q/\pi\rho kE)^{1/3}$, Q is the flow rate, σ is the surface charge, k is the dimensionless conductivity, E is the applied electric field, I is the current passing through the jet, ρ is the liquid density and r_0 is the initial radius of the jet. Therefore, the critical length is proportional to dope flow rate, conductivity and applied electric field but inversely proportional to liquid density and current passing through the jet. These equations provide us with a deep understanding about the first step of electrospinning.

➤ Bending deformation with looping and spiraling trajectories

As shown in **Figure 2-5**, after the path of jet as a straight segment, it is elongated driven by electrical forces caused by charges carried with jet, and followed by a series of successively bending coils having turns of increasing radius (Reneker, Yarin et al. 2000; Yarin, Koombhongse et al. 2001; Reneker, Kataphinan et al. 2002). It was demonstrated that the key role in causing bending and stretching of jet at high frequencies and reducing the jet diameter from a micrometer to a nanometer was played by a non axisymmetric or electrically driven bending instability (Shin, Hohman et al. 2001; Shin, Hohman et al. 2001). Three types of instabilities have been found and modeled to analysis the phenomenon. The classical Rayleigh instability dominated by surface tension and suppressed at high electric field is given as following:

$$(\epsilon - \epsilon')E_0^2 + \frac{4\pi^2\sigma^2}{\epsilon} = \frac{2\pi\gamma}{l} \quad (2-3)$$

where E_0 is the initial applied electric field, σ is the surface charge density, γ is the surface tension, l is the radius of the jet, ϵ and ϵ' are the dielectric constant inside and outside of the jet separately. According to the Rayleigh instability equation, the radius of the jet is decreased when the applied electric field and surface charge density is increased.

The second axisymmetric instability often occurs at higher electric field than Rayleigh instability while the third one is bending or whipping instability which is not axisymmetric instability. The latter two instabilities are caused by electrically driven force due to fluctuations in the dipolar component of the charge distribution and essentially independent of surface tension of polymer solution. And the bending instability of electrospun nanofibers were demonstrated by images of electrospinning Polycaprolactone (PCL) as shown in **Figure 2-7** (Reneker, Kataphinan et al. 2002).

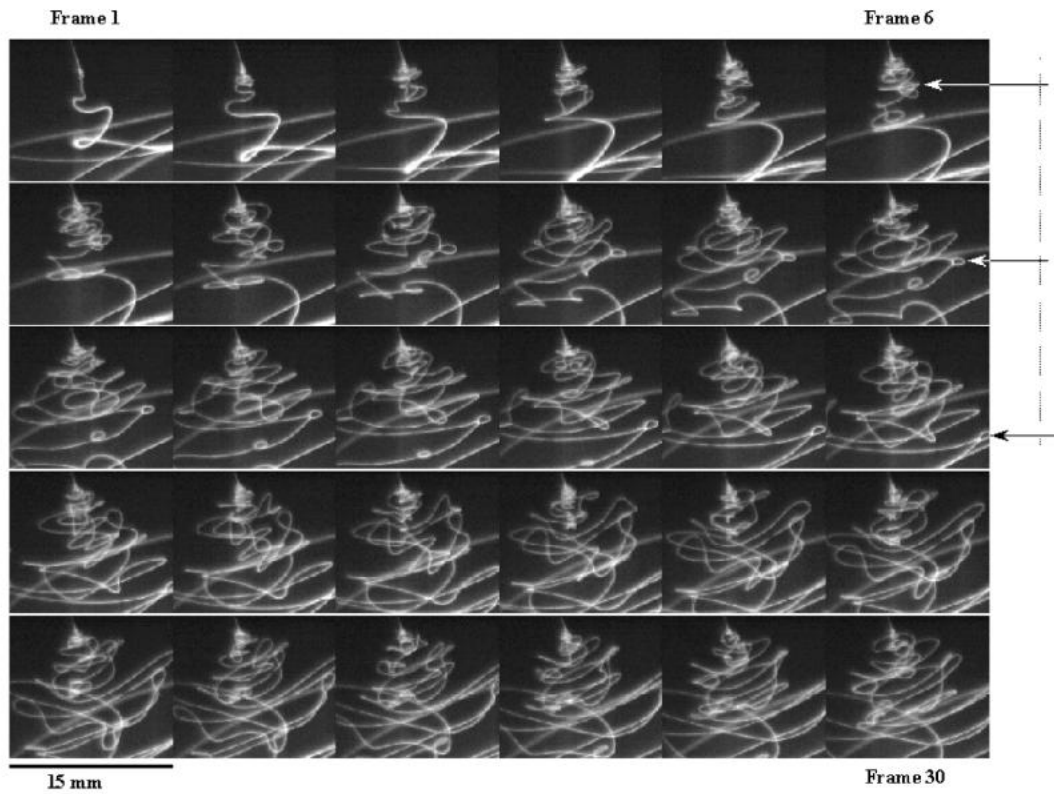


Figure 2-7. Frame images that show the evolution of the bending instability on a jet of 15 wt% PCL in acetone [figure adopted from (Reneker, Kataphinan et al. 2002)]

Additionally, other characteristic instabilities such as branching and formation of physical beads have been illustrated. Branches occurred more frequently in higher concentrated solution and at a higher electric field, while the capillary instability tended to cause a cylindrical fluid jet to break up into droplet at smaller electrical charge per unit, which lead to formation of beaded nanofibers (Huebner and Chu 1971; Fong, Chun et al. 1999).

➤ Solidification and deposition on counter electrodes/substrates

During the process of nanofiber bending and elongation, the solvent in fibers evaporate simultaneously, which consequently produce dry polymer fibers on counter electrodes/substrates. The equations accounting for solvent evaporation and

polymer solidification were developed to calculate the jet paths during the course of nonlinear bending instability which led to formation of nanofibers (Yarin, Koombhongse et al. 2001). In the calculation, the cross-sectional radius of a dry fiber after elongation and solvent evaporation is related with initial radius of the jet. The diameter of final dry nanofiber was decreased as the initial jet radius decreased. Additionally, because of the longitudinal compressive force from jet impingement on a solid flat surface, the buckling instability may occur resulting in bending fibrous structures with sinuous folding and overlapping (Han, Reneker et al. 2007).

Furthermore, the design of electrospinning apparatus is essential for the morphology and structure of fabricated nanofibers (Park, Park et al. 2007). The schematics of electrospinning systems with various nozzle types and target electrodes, and the morphologies of resultant nanofibers are shown in **Figure 2-8**:

- (A) Nanofiber membranes with uniform thickness could be manufactured by a multi-jet electrospinning (Liao, Wang et al. 2013). Multiple spinnerets enhance productivity, as well as increase the potential to fabricate bi-component and multi-component nanofibers;
- (B) Multiple jet could also be deposited onto a porous tubular surface (Dosunmu, Chase et al. 2006);
- (C) The electrospinning setup with a coaxial spinneret resulted in new nanofibers possessing inner core-outer shell structure. This technology could also be used to generate hollow nanofibers and nanochannels when air is blew inside instead of polymer B (Li and Xia 2004). If the outer tube jacketed the electrospun nanofiber with gas saturate with the corresponding polymer solution, it could provide a smooth fiber surface (Larsen, Spretz et al. 2004);
- (D) The electrospinning setup with bicomponent-jet spinnerets had advantages in spinning two different polymers with a side-by-side arrangement to combine the properties of polymers (Lin, Wang et al. 2005);

- (E) A scanning tip with a droplet of polymer dope on top after dipping in dope can control the deposition of nanofibers to manufacture nanofiber-based electronics and sensors (Kameoka, Orth et al. 2003);
- (F) A one dimensional nanofiber could be achieved by using an optical chopper motor (Subramanian, Vu et al. 2005);
- (G) Residual solvent could be removed in a coagulation bath, which forces fiber to crystallize (Smit, Büttner et al. 2005);
- (H) The charged jet could be concentrated on the sharp edge of collector because the electrical field was increased by the sharp edge points (Theron, Zussman et al. 2001);
- (I) When the rotating speed of cylindrical collector was fixed at appropriate speed, the fiber possessed best alignment (Bhattarai, Edmondson et al. 2005);
- (J) Double-edge steel bladed in line had been developed to obtain highly aligned fibers (Teo and Ramakrishna 2005);
- (K) The electrospinning system with a copper ring was used to concentrate jets (Deitzel, Kleinmeyer et al. 2001);
- (L) The effects of rectangular frame collector on prepared fibers were also studied (Huang, Zhang et al. 2003);
- (M) The tubular shape nanofiber membranes could be fabricated using a rotating and traversing mandrel-type collector (Kidoaki, Kwon et al. 2005);
- (N) Three-dimensional nanofibrous tubes could be achieved by controlling architectures (Zhang and Chang 2008);
- (O) Different fiber arrangements at various location on the gap were fabricated by using designed grounded collector (Teo and Ramakrishna 2006);
- (P) Additionally, the electrospinning provides a versatile method for generating spider-web-like nano-nets with ultrafine fiber diameter less than 20 nm under higher voltages (Wang, Ding et al. 2011).

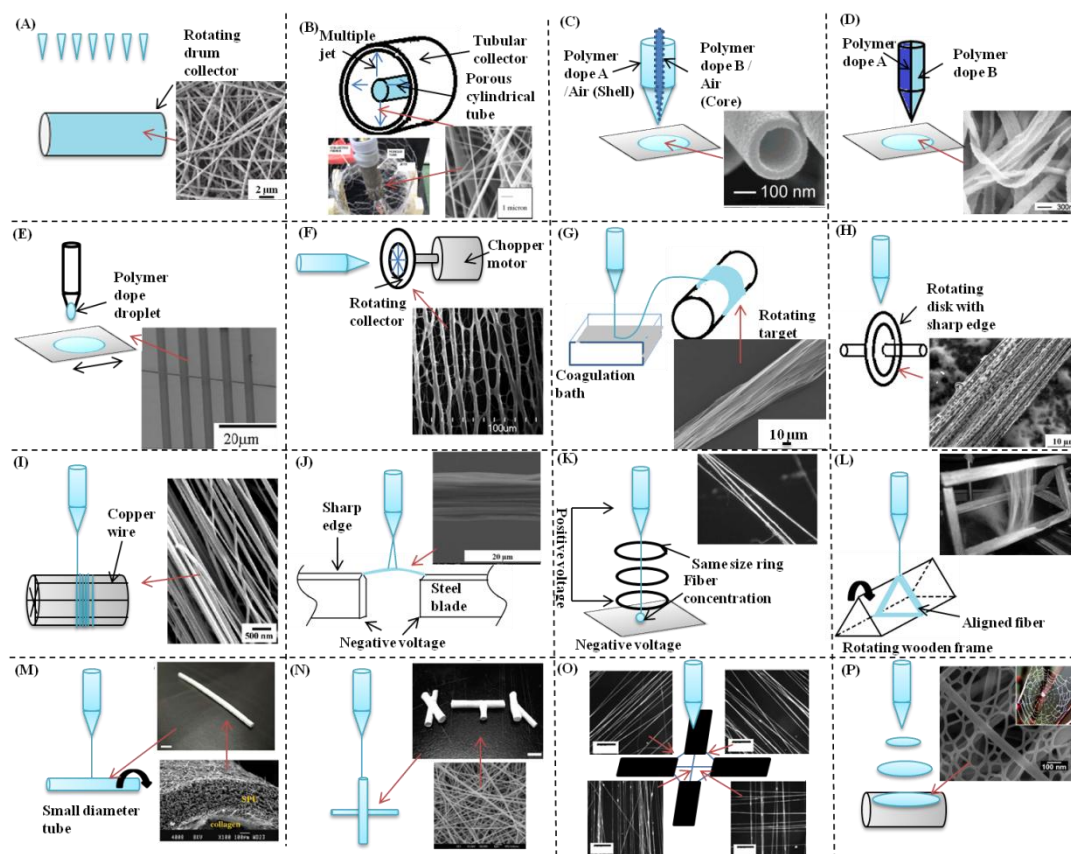


Figure 2-8. Schematics of electrospinning systems with various spinnerets and various target electrodes, and resultant nanofiber morphologies [surface morphology images inserted in this figure are adopted from (Deitzel, Kleinmeyer et al. 2001; Theron, Zussman et al. 2001; Huang, Zhang et al. 2003; Kameoka, Orth et al. 2003; Larsen, Spretz et al. 2004; Li and Xia 2004; Bhattarai, Edmondson et al. 2005; Kidoaki, Kwon et al. 2005; Lin, Wang et al. 2005; Smit, Büttner et al. 2005; Subramanian, Vu et al. 2005; Teo and Ramakrishna 2005; Dosunmu, Chase et al. 2006; Teo and Ramakrishna 2006; Zhang and Chang 2008; Wang, Ding et al. 2011; Liao, Wang et al. 2013)]

Technologically, to extend the possible usage of nanofibers easily, the electrospinning assemblies used to produce nanofibers have been improved by modifying the collector.

2.2.3. *Parameters affecting electrospinning process*

Although electrospinning technology is not novel and easy to use, many parameters can influence the formation of polymer dope into nanofibers significantly. These parameters could be classified into three parts: (1) Intrinsic properties of polymer dopes; (2) Operational conditions; (3) Surrounding conditions. The effects and influence degrees are summarized in **Table 2-4**, and details of these effects are discussed as following.

➤ **Effects of intrinsic properties of polymer dopes**

Progress has definitely been made in recognizing the effects of various parameters to affect the electrospinning of nanofibers (Sun, Long et al. ; Li and Xia 2004; Li, McCann et al. 2006; Agarwal, Greiner et al. 2013; Wang, Ding et al. 2013). Considered was the control of intrinsic properties of solution including polymer dope concentration, dope viscosity, solution conductivity, solution density, surface tension, solvent, vapor pressure and vapor diffusivity.

It was well-known that the electrospun membrane structure and morphology as well as the fiber diameter are influenced by the concentration/viscosity of polymer solutions (Deitzel, Kleinmeyer et al. 2001; Huang, Zhang et al. 2003; Lee, Kim et al. 2003; Ryu, Kim et al. 2003). Because of variations of solution viscosity and surface tension, the concentration decides limiting boundaries of production of electrospun fibers. Polymer solutions with low concentration form bead-on-string fibers while the polymer solutions with higher viscosity tend to change the shape of beads from spherical to spindle-like and then produce uniform fiber shapes (Reneker and Chun 1996; Bhardwaj and Kundu 2010). And with further enhancement of viscosity, the diameter of fibers is increased.

Table 2-4. Effects of different parameters on electrospun nanofibers

Parameters		Effects on nanofiber morphology	Reason	Influence Degree
Intrinsic properties of solutions	Polymer concentration increases	Fiber diameter increases	The jet elongation becomes more difficult and slowly	☆☆
	Dope viscosity increases	Fiber diameter increases	The jet elongation becomes more difficult and slowly	☆☆☆
	Solution conductivity increases	Suppress the formation of beads, fiber diameter decreases	The charges carried by jet increase. Thus the repel force in jet is increased and jets elongate fast.	☆☆☆
	Solution density increases	Fiber diameter increases	The jet elongation becomes more difficult and slowly	☆☆
	Surface tension decreases	Fiber diameters decrease	Small surface tension make jets elongate easy	☆
	Solvent	Good solvents tend to give rise to beads; partial solubility systems tend to form stable nanofibers; poor solvents could not support effective spinning.	Dielectric constant of solvents shows a direct correlation with average electrospun fiber diameter.	☆☆
	Vapor pressure increases	Fiber diameters increase. Fibers with high surface porosity are produced	Jets have less time to elongate before solidified. Phase separation can be induced by high vapour pressure of solvent.	☆☆
	Vapor diffusivity decreases	Fiber diameters decrease	Jets have more time to elongate before solidified.	☆

To be continued on the next page

To be continued with the previous page

Parameters		Effects on nanofiber morphology	Reason	Influence Degree
Operational conditions	Applied voltage increases	An initial decrease in fiber diameters after increasing applied voltage. If applied voltage is further increase, the fiber diameters could be increased also.	Possible reason is that at first the jets carry more charges to elongate fast. But after increasing voltage more, higher voltage will eject more jets also.	☆☆
	Distance between needle and collector increases	Fiber diameters decrease but beads tend to form	The jet elongation time is increased. It also make the fiber unstable	☆☆☆
	Orifice radius/initial jet decreases	Fiber diameters decrease	The initial diameter of jet decreases.	☆☆☆
	Flow rate increases	Fiber and beads diameters increase; the effects are interreacted with effects from volumetric charge density effects	A higher flow rate ejects more dope in a jet and makes the initial jet diameter larger.	☆
Surrounding conditions	Ambient temperature decreases	Fiber diameters decrease	The jet elongation time increase.	☆
	Ambient humidity increases	Fiber diameters decrease, fiber-sticking and beads increase. The density and size of pores on fibers are increased	The jet elongation time increase.	☆

In addition, increasing electric conductivity of dope solution changes rheological behavior and considerably influences spinnability of the dope solution (Subbiah, Bhat et al. 2005; Rutledge and Fridrikh 2007). Solution conductivity is mainly determined by the type of polymer, solvent and the availability of ionisable salts (Bhardwaj and Kundu 2010). During electrospinning process, the highly conductive solutions are extremely unstable and tend to manufacture fibers with significant decreasing diameter, dramatic bending and a broad diameter distribution (Sill and von Recum 2008; Liao, Wang et al. 2013). Furthermore, the instability of Taylor cone could be enhanced by increasing dope conductivity, which in turn produces more micro-sized droplets and dense-nets (Wang, Ding et al. 2011). It was investigated that the ions with smaller atomic radius could impose a stronger elongation force on the jet due to the higher charge density and higher mobility (Zong, Kim et al. 2002; Barakat, Kanjwal et al. 2009; Yang, Wang et al. 2011; Liao, Wang et al. 2013). Besides, the addition of formic acid to dope solution could also increase the dope conductivity due to the high dielectric constant of formic acid, which thus favor the formation of thinner fibers and dense nano-nets (Wang, Ding et al. 2010; Wang, Ding et al. 2011).

Furthermore, it was revealed that surface tension was likely to play a role to regulate the morphology of nanofibers by adjusting it via addition of surfactants (Lin, Wang et al. 2004; Talwar, Krishnan et al. 2010; Hu, Wang et al. 2011; Yang, Wang et al. 2011). Due to surface tension effect of reducing surface area, nano-nets are more regular and uniform, which was attributed to the stable jets encountering fewer perturbations. However, if the concentration of surfactants is too high, the nanofiber morphology may show defects as the surfactants may self-assemble to form colloidal aggregates.

As the nanofibers were formed by solvent evaporation on the way of flight in the high electric field, the selection of solvent is one of the primary factors to decide fiber morphologies. The fibrous membranes formed from various kinds of

solvent have been investigated (Wang, Ding et al. 2011; Yang, Wang et al. 2011). It was suggested that the dope solution prepared by good solvent with high solubility was relatively hard to make good electrospinning compared with lower solubility solvent (Luo, Nangrejo et al. 2010). Detailed impacts on a qualitative level of the quality of solvent on the electrospinning has been studied based on model systems comprising 28 different solvents as well as mixture of them with non-polar biocompatible polymer and it was found that good solvent tend to electro spraying whereas partial solubility systems prefer to produce stable electrospinning of nanofibers (Luo, Nangrejo et al. 2010). The spinnability-solubility maps are constructed for easy selection of solvents for electrospinning (Luo, Nangrejo et al. 2010).

So it is apparent that changes of intrinsic properties of solution may modulate the molecular structure, alter theological and surface tension of fibers, and are critical factors in the successful preparation of nanofiber membranes by electrospinning.

➤ Effects of operational condition

The operational conditions of electrospinning also play significant roles in determining the morphologies and structures of electrospun membranes. The strength of applied electric field is an important element which decides the charge amount to the droplet located on the top of spinneret as well as the electrostatic force (Hu, Wang et al. 2011). It was investigated that the enhancement of applied voltage could favor formation of thinner fibers and completely split nano-nets (Wang, Ding et al. 2011). The average diameter of nanofibers was decreased along with the applied voltage (Ding, Li et al. 2006). However, a higher applied voltage could also eject more fluid in a jet which manufactures fibers with larger diameter (Demir, Yilgor et al. 2002).

Additionally, the distance between the tip and collector can also affect the prepared nanofibers as the nanofibers need a minimum distance to give sufficient time to evaporate solvent. Recently it was illustrated that if the distance is either too close or too far, the beads tend to form (Zhang, Reagan et al. 2009). And a decrease of the orifice size was found to decrease the fiber diameter (Katti, Robinson et al. 2004). It was also revealed that the diameter of nanofibers was increased with the enhancement of flow rater (Agarwal, Greiner et al. 2013).

➤ Effects of surrounding conditions

Besides the above parameters, ambient temperature and humidity also have influences on the achieved nanofibers. It was demonstrated that at a lower temperature, the average diameter of nanofiber was decreased as the evaporation rate of solvent was decelerated and thus the nanofiber possessed longer time to elongate and solidify while at higher temperature the polymer chains had less freedom to move and force the jet to solidify faster and consequently produce thicker nanofibers (Wang, Ding et al. 2011; Wang, Wang et al. 2012). Furthermore, according to recent reports, variation of relative humidity (RH) can control fabrication of nanofiber membranes. It was observed that compared with samples obtained at lower humidity, the fibers fabricated in higher humidity would possess a light fiber-sticking structure (Ding, Li et al. 2006; Hu, Wang et al. 2011; Wang, Ding et al. 2011; Wang, Ding et al. 2011).

As shown in **Table 2-4**, it was investigated that solution conductivity, distance from nozzle to collector, dope viscosity and initial jet radius have the most significant effects on resulting fiber diameters. Five other parameters including polymer concentration, solution density, solvent, vapor pressure and applied voltage play moderate roles while else parameters have minor effects (Thompson, Chase et al. 2007). So it is apparent that experimental and theoretical investigations have been carried out to unravel the effects of spinning parameters in controlling

nanofiber morphologies and structures. Nevertheless, the possible cross-influences between different parameters such as various polymer solutions under similar operational conditions should need further studies, which would possibly push the understanding level of electrospinning process from a qualitative to a predominantly quantitative level. Furthermore, the effects of these parameters on bulk membrane pore size, porosity, surface hydrophobicity and topologies are still uncertain, which are significant for water treatment applications and need our further investigations.

2.2.4. Current status of nanofiber membrane fabrication for MD process

Nanofiber membranes are attractive for MD applications due to their high water flux, low trans-membrane pressure, high water contact angle, high porosity, interconnected open pores and unique surface structures. PVDF nanofiber membranes were firstly fabricated by C. Feng for AGMD to produce drinking water from saline water (Feng, Khulbe et al. 2008). The membrane flux was comparable to those obtained by commercial microfiltration. Furthermore, electrospun PVDF-clay nanocomposite nanofiber membranes were fabricated and tested in DCMD application as well (Prince, Singh et al. 2012). The incorporation of clay nanocomposite could enhance the hydrophobicity of the membranes and increase the melting point of PVDF-clay electrospun nanofiber membrane. Polyvinylidene fluoride-co-hexafluoropropylene (PVDF-HFP) nanofiber membrane were prepared via electrospinning for membrane distillation (Lalia, Guillen-Burrieza et al. 2013). The thickness effects on membrane performance have been investigated by electrospinning PVDF nanofiber membranes for MD (Essalhi and Khayet 2013).

So far, only these few researches have been done to fabricate hydrophobic nanofiber membranes by electrospinning for MD process. The long-term performances and permeation flux of these membranes still need to be enhanced before commercialization. Thus, in this research we proposed to design and fabricate superhydrophobic membranes by electrospinning for DCMD process.

CHAPTER 3

Fabrication of PVDF nanofiber membranes by electrospinning for DCMD

3.1. Introduction

As described in Chapter 2, one of the major barriers impeding MD industry applications is the availability of specially designed MD membranes which can fulfill the requirements for MD process. This part of my work aims to fabricate electrospun PVDF nanofiber membranes as a first trial, and optimize the pore sizes by varying polymer dope compositions and electrospinning process parameters such as spinning needle moving speed and chamber moisture, and investigate the effect of heat-press post-treatment on membrane performance by testing the PVDF nanofiber membranes before and after heat-press treatments in a DCMD setup under the same operating conditions. It is expected that this study can help have a better understanding of optimal electrospinning and post-treatment conditions to fabricate new nanofiber membranes suitable for membrane distillation with enhanced performance.

3.2. Experiments

3.2.1. *Membrane materials and chemicals*

The membrane materials, commercial polymer polyvinylidene fluoride (PVDF) Kynar HSV 900 with a higher molecular weight and Kynar 761 with a lower molecular weight were purchased from Arkema Inc., Singapore, and were dried at 50 °C under vacuum for at least 1 day before use. N, N-Dimethylacetamide (DMAC), N, N-Dimethylformamide (DMF) and acetone from Fisher, Singapore

were used as solvents. Lithium chloride (LiCl) as an additive was purchased from Merck, Singapore. Isopropyl alcohol (IPA) with analytical grade was obtained from VWR Co. Ltd, Singapore. All the reagents were used as received. A commercial PVDF membrane, Durapore® Membrane filter, was purchased from Millipore, Ireland to compare with the nanofiber PVDF membranes.

3.2.2. Dope preparation, dope viscosity and conductivity measurements

Different PVDF polymer dope solutions for electrospinning were prepared by dissolving PVDF 761 or PVDF HSV 900 in DMAC and a mixture of DMF and acetone with a weight ratio of 6 to 4. A desired amount of LiCl (0.004 wt %) was added into some dope solutions to improve dope electrospun ability, optimize the nanofiber membrane porosity and control membrane pore sizes. All dope solutions were stirred mechanically for at least 1 day at 60 °C. The homogenous dope solutions were then cooled down and degassed at room temperature for overnight before electrospinning.

Rheological characteristics of all the dope solutions were measured by a rheometer (Pysica MCR 101, Anton Paar, supplied from Singapore). The measurements were carried out under a steady-state shear rate ranging from 0.01 s^{-1} to 1000 s^{-1} at 25 °C using a 25 mm measuring plate (CP25-1-SN16699). Each dope was tested at least five times and the viscosity of the dope solution was taken an average value at the shear rate of 10 s^{-1} . In order to investigate the effects of inorganic additives on dope conductivity and resultant nanofiber membrane morphology, the conductivity of desired dopes were tested by Mettler Toledo SevenMulti Meter ($0.01\text{ }\mu\text{S/cm}$ to 1000 mS/cm , $\pm 0.5\%$) which was provided by Mettler, Singapore.

3.2.3. *Electrospinning of PVDF nanofiber membranes and post-treatment*

Figure 2-3 shows schematic diagram of an electrospinning setup. Basically, a polymer dope solution in a thin PTFE tube was pushed slowly into high voltage charged sprayers by a syringe pump. The sprayers were connected to a high voltage supplier which can generate positive voltages of up to 30 kV. A positive voltage of 25 or 28 kV was applied across a distance of 12 cm or 15 cm between the tip of the sprayers and the grounded collector. The spinning sprayers can be moved slowly and evenly by a motor during electrospinning. The moisture in the chamber can be altered by pumping dry air.

During electrospinning process, nanofibers were produced and collected on non-woven textiles posted on the rotating collector when the applied electric field overcomes the surface tension of the polymer dope solution. Solvents in the nascent nanofibers were evaporated and nanofibers started to bend concurrently. In order to eliminate the effect caused by the residual solvent in the membrane, the PVDF nanofiber membranes were subsequently placed in a fume cupboard under vacuum condition at 60 °C for overnight to ensure that all solvents have been evaporated completely from the fresh membranes. Then a heat-press post-treatment was applied. The dry PVDF nanofiber membranes were pressed between two flat glass panes and placed in an oven at 170 °C just below polymer melting point for an hour to compress all the nanofiber layers together.

3.2.4. *Characterizations of PVDF nanofiber membranes*

The surface and cross-sectional morphologies of PVDF nanofiber membranes were sputtered with gold and then observed using a scanning electron microscope (SEM) (EVO 50, Carl Zeiss AG, Singapore).

The membrane porosity is defined as the volume of the pores divided by the total volume of the membrane. It can be determined by gravimetric method. After

immersing the PVDF nanofiber membranes into IPA which penetrates into the pores of the membrane, the membrane weight with IPA was measured after IPA on membrane surface was removed. The membrane porosity, ε_m , can be calculated by following equation:

$$\varepsilon_m = \frac{(\omega_1 - \omega_2) / D_i}{(\omega_1 - \omega_2) / D_i + \omega_2 / D_p} \quad (3-1)$$

where ω_1 is the weight of the wet membrane, g; ω_2 is the weight of the dry membrane, g; D_i is the isopropyl alcohol density, g/m³; D_p is the polymer density, g/m³.

The pore size of membranes was determined by a capillary flow porometer (model CFP 1500A, from Porous Material. Inc. (PMI) in Singapore). Its working principle is based on the bubble-point and gas permeation tests. The contact angles of the electrospun membranes were measured using the sessile drop method by a goniometer (Contact Angle System OCA, from Data Physics Instruments GmbH in Singapore). One 5 μ L water droplet was dropped onto a levelled membrane surface and the images of the water drop on the membrane surface were captured by an optical system to calculate the contact angle. Each sample was tested at least 5 times.

A homemade setup for LEP measurement is shown in **Figure 3-1**. A digital pressure gauge was installed on top of a stainless steel tank which was used as the reservoir for a 3.5 wt% NaCl solution. A tested nanofiber membrane with an effective membrane area as 10 cm² was installed in one flat-sheet membrane cell. The feed side of the flat-sheet membrane cell was filled with the NaCl solution. Meanwhile, 800 mL distillation water with conductivity below 5 μ S/cm was circulated in the permeation side of the cell. During the LEP test, hydraulic pressure provided by compressed N₂ was applied on the nanofiber membrane surface at the feed side. The hydraulic pressure was increased with a step of 2 psi and each

pressure was maintained for 10 min. The conductivity of water in the permeation side was monitored by COND3110 handheld conductivity meter (0-1000 ms/cm, $\pm 0.1 \mu\text{s/cm}$, Gobal Water in Singapore). The pressure read at digital pressure gauge was recorded as LEP when permeation conductivity was increased gradually in 10 min.

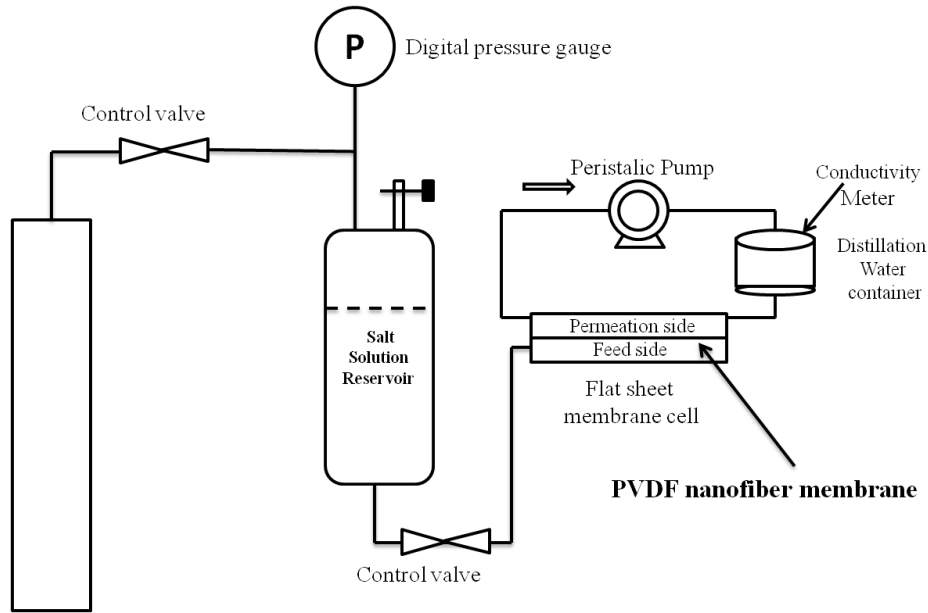


Figure 3-1. Schematic diagram of homemade LEP test setup

3.2.5. MD performance tests

The flat-sheet PVDF electrospun membranes were tested in a DCMD setup with an effective membrane area of 38 cm^2 . The MD experimental setup is shown in **Figure 3-2**. Both the feed and permeate solutions were cycled through the flat-sheet membrane cell. On the hot feed side, the feed solution was synthetic seawater with conductivity around 60 ms cm^{-1} (3.5 wt% sodium chloride), which was heated in the range of 323-353 K by one 1500W water heater and circulated by a peristaltic pump ($0.4\text{-}2 \text{ L min}^{-1}$). On the cold permeate side, the permeate water (DI water with conductivity below $5 \mu\text{s/cm}$) was cooled down to 293 K by one 400 W water cooler and circled by another peristaltic pump ($0.1\text{-}0.5 \text{ L min}^{-1}$). The inlet and outlet

temperatures on both feed and permeate sides were measured by temperature meters while the conductivities in the feed and permeate tanks were monitored by conductivity meters. The permeate flux was collected in an overflow tank locating on one digital balance. Over the duration of the MD experiment all the tubes were insulated to prevent heat loss and all the data were logged into a computer automatically.

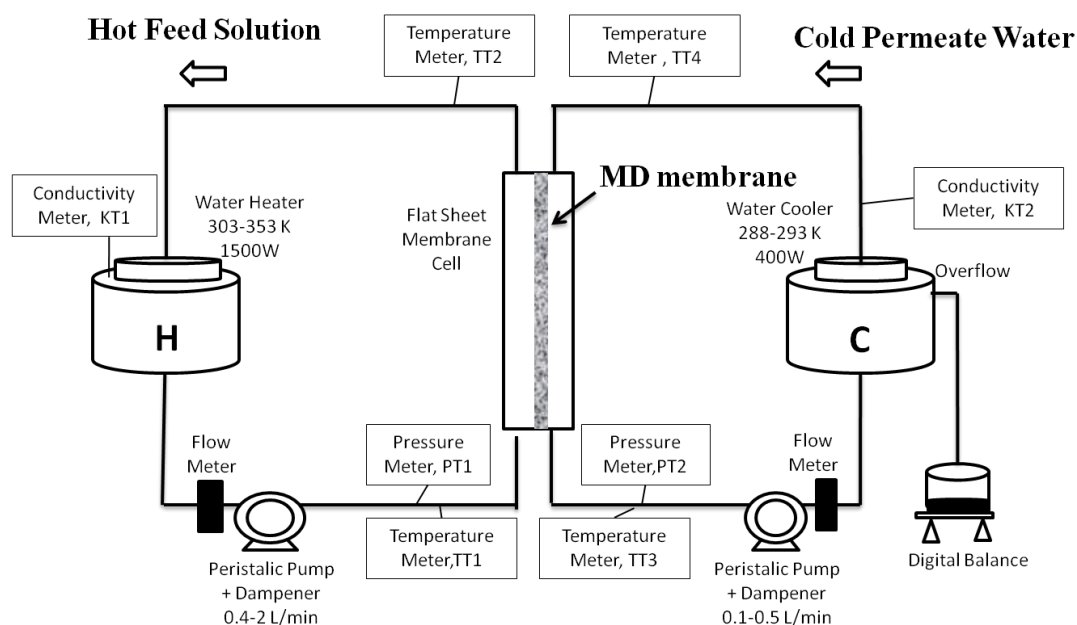


Figure 3-2. Schematic diagram of direct contact membrane distillation

3.3. Results and discussion

3.3.1. Determination of appropriate polymer concentrations and solvents

Table 3-1 tabulates the viscosity of all the polymer dope solutions used in the study. Dope 1, made by 12 wt% PVDF HSV900 in DMAC, presents the highest viscosity of 8.00 Pa s. This viscosity is found to be too high to spin as it is difficult to push the dope into the sprayers by the syringe pump. In addition, the forces of the viscosity and the surface tension of the dope determine the upper and lower

boundaries of the polymer concentration used to ensure the success in spinning. Polymer dope solutions with a relatively low viscosity can be obtained by using low molecular weight PVDF 761 or reducing PVDF HSV900 concentration. For example, the viscosity of dope 2, in which 15 wt% PVDF 761 was dissolved in DMAC, is 0.8 Pa·s. The dope 3 made by 11 wt.% PVDF 761 dissolved in the mixed solvent of DMF/acetone has a low viscosity of 0.20 Pa s, while it only needs 5 wt% PVDF HSV900 dissolved in the same solvent to achieve a similar viscosity as 0.18 Pa s (dope 8).

Table 3-1. Viscosity of different dope solutions

Dope code	Polymer type	Solvent	Concentration (wt%)	Additive	Dope viscosity (Pa s)
1	PVDF HSV900	DMAC	12	NA	8.00
2	PVDF 761	DMAC	15	NA	0.80
3	PVDF 761	DMF/Acetone	11	NA	0.20
4	PVDF HSV900	DMF/Acetone	8	NA	1.00
5	PVDF HSV900	DMF/Acetone	7	NA	0.50
6	PVDF HSV900	DMF/Acetone	6	NA	0.30
7	PVDF HSV900	DMF/Acetone	6	LiCl, 0.004 wt%	0.33
8	PVDF HSV900	DMF/Acetone	5	NA	0.18
9	PVDF HSV900	DMF/Acetone	5	LiCl, 0.004 wt%	0.26

It can also be seen from **Table 3-1** that some polymer dopes were prepared using a mixed solvent of DMF/acetone. This is because the membranes were transparent (indicating the membranes were wet) using the dope solution dissolved in DMAC (dopes 1-2). The intention of using a solvent mixture is to accelerate solvent evaporation, as the vapour pressure of DMF (0.38 kPa at 20 °C) and acetone (25 kPa at 20 °C) are higher than DMAC (0.18 kPa at 20 °C). It turns out that white and almost dry membranes were obtained when the dope solution was prepared using DMF/acetone as the solvent (dopes 3-9). Therefore, to ensure smooth spinning and obtain good membranes, low concentrated PVDF HSV900 dopes with a mixed solvent of DMF and acetone were used in further studies (dope 4–9). The membranes fabricated by different dopes are named as M(membrane)-dope code-HS(High sprayer speed)/LS(Low sprayer speed)-LM(Low moisture)/NA.

3.3.2. *Effect of polymer dope solution*

Figure 3-3 shows the surface morphology of M-4-HS and M-5-HS membranes. It can be seen that the composition/viscosity of the polymer dope affects the dimension of the nanofibers, and thinner nanofibers can be obtained by low viscosity dopes as shown in **Figures 3-3C** and **3-3D**. The diameters of nanofibers of membrane M-4-HS spun by a 8 wt% PVDF HSV900 solution (dope 4) are in the range of 1.0-1.5 μm while the diameters of nanofibers membrane M-5-HS spun by a 7 wt% PVDF HSV900 solution (dope 5) are in the range between 0.2 to 0.5 μm , and some big beads and even small pieces of the polymer can be observed in M-5-HS nanofibers due to its low concentration (viscosity) and insufficient time to evaporate all the solvent. It is argued that the big beads and small pieces of polymer are formed when the wet polymer fibers are laid on the grounded collector without strain force and self-repulsion force by the electric field, which made the fibers to relax, melt partially and solidify (Zong, Kim et al. 2002). The undulating morphology caused by the beads and polymer pieces resulted in membrane porosity reduction.

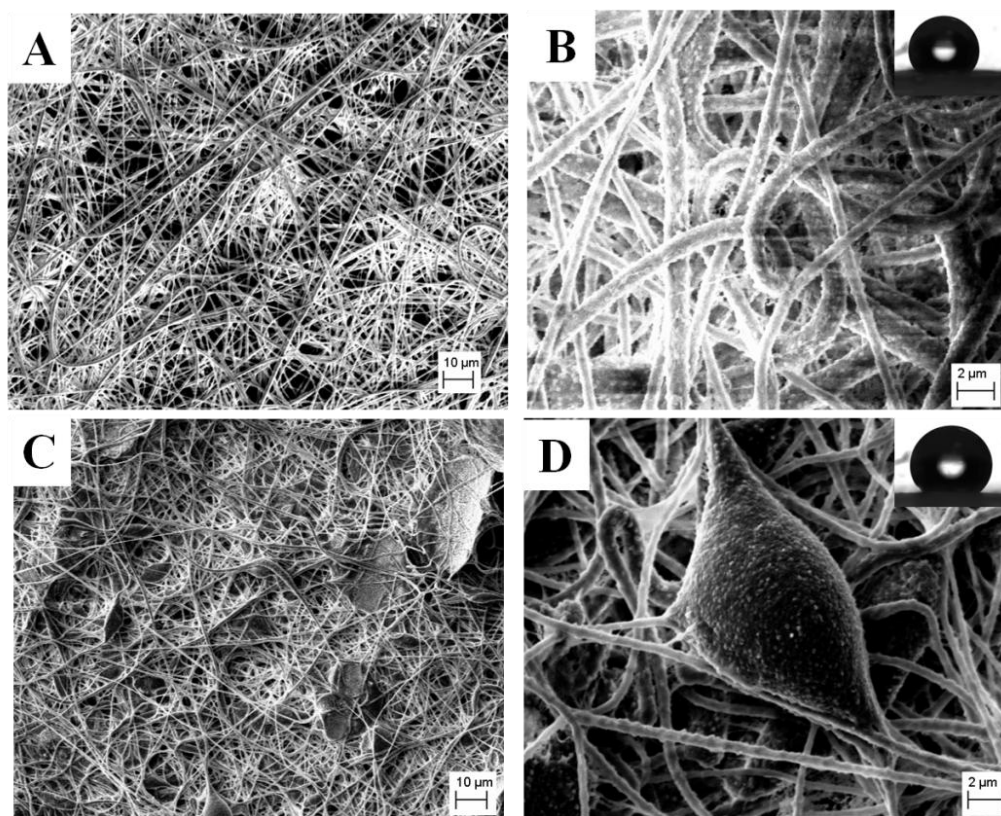


Figure 3-3. Surface morphology and water contact angle of M-4-HS (A: 500 ×; B: 3K ×) and M-5-HS (C: 500 ×; D: 3K ×) membranes

The surface properties of membranes M-4-HS and M-5-HS are listed in **Table 3-2**. It is found that the nanofibers with varied diameters produced by different dope solutions impose a significant influence on the membrane properties. As shown in **Table 3-2**, the membrane M-4-HS has a maximum pore size of 1.72 μm and a mean pore size of 0.91 μm . Compared with M-4-HS, the membrane M-5-HS prepared by a lower concentration dope #5 possesses maximum and mean pore sizes of 1.12 μm and 0.75 μm , respectively. When the polymer concentration was further reduced to 6 wt%, the membrane with a maximum pore size of 1.10 μm and a mean pore size of 0.50 μm can be achieved (membrane M-6-HS). Clearly, a low viscosity dope can make membranes with smaller pore sizes. It is easy to

understand that the pores formed by thinner nanofiber overlapping should be smaller than by the nanofibers with larger diameters.

Table 3-2. Surface properties of PVDF membranes made under different conditions

Dope code	Sample code	Processing conditions					Membrane surface property		
		Voltage (kV)	Needle speed (mm s ⁻¹)	Distance (cm)	Humidity (%)	Temperature (°C)	Mean pore size (μm)	Max pore size (μm)	Contact angle (°)
4	M-4-HS	21	1.00	15	70%	20	0.91	1.72	136
5	M-5-HS	21	1.00	15	70%	20	0.75	1.12	137
6	M-6-HS	21	1.00	15	70%	20	0.50	1.10	139
6	M-6-LS	21	0.10	15	70%	20	0.32	0.88	137
7	M-7-LS	27	0.10	12	70%	20	0.41	0.75	141
9	M-9-LS	27	0.10	12	70%	20	0.30	0.54	142
9	M-9-LS-LM	27	0.10	12	50%	20	0.18	0.36	138

3.3.3. Effect of sprayer moving speed

Electrospinning parameters were varied to explore their impacts on the membrane structure of resultant membranes. As shown in **Table 3-2**, while maintaining the same other processing conditions including the same polymer dope extrusion speed, if the sprayers were moved more slowly, the electrospun membranes may have a smaller mean and maximum pore size (membranes M-6-LS vs. M-6-HS). When dope #6 was spun at a 1 mm s⁻¹ needle speed, the maximum pore size of membrane M-6-HS is 1.10 μm and mean pore size is 0.50 μm. When the needle speed was decreased to 0.1 mm s⁻¹, the maximum and mean pore size of

membrane M-6-LS are reduced to 0.87 μm and 0.33 μm , respectively. This change may be due to the fact that when the needles move slowly on the top of grounded rotating collector, the solvent in the nascent nanofibers did not have sufficient times to evaporate before more nanofibers overlapped on pervious wet nanofibers, which caused membrane more compact and thus membrane pore sizes became smaller. Subsequently, the needle speed as 0.1 mm s^{-1} was chosen in further investigation to obtain nanofiber filters with small pore sizes.

3.3.4. Effect of inorganic additives

As mentioned in section 3.3.2, an undulating morphology caused by the large beads and polymer pieces was present in the membrane (M-5-HS) fabricated by a low viscosity dope. But low viscosity is preferred to produce desired membranes with small pore sizes. Therefore, in order to balance these contradictory effects, inorganic additives were added into the dope solutions (dope 7 and dope 9).

The effect of ionic salt additives on the membrane structure was examined in **Figure 3-4**. The membrane M-6-LS spun by dope #6 without any additive has many beads on the nanofibers, which present various diameters in a wide distribution (**Figure 3-4A**). In contrast, the membrane M-7-LS made of dope #7 with 0.004 wt% LiCl as an additive has distinctly better nanofibers with relatively thinner and more uniform diameters as shown in **Figure 3-4B**. However, dope #8 with an extremely low concentration of 5 wt% PVDF HSV900 without any additive cannot be utilized to produce good nanofibers due to its too low viscosity. The addition of 0.004 wt% LiCl into the dope (dope 9) made the resulting nanofibers thin and uniform as shown in **Figure 3-4D**.

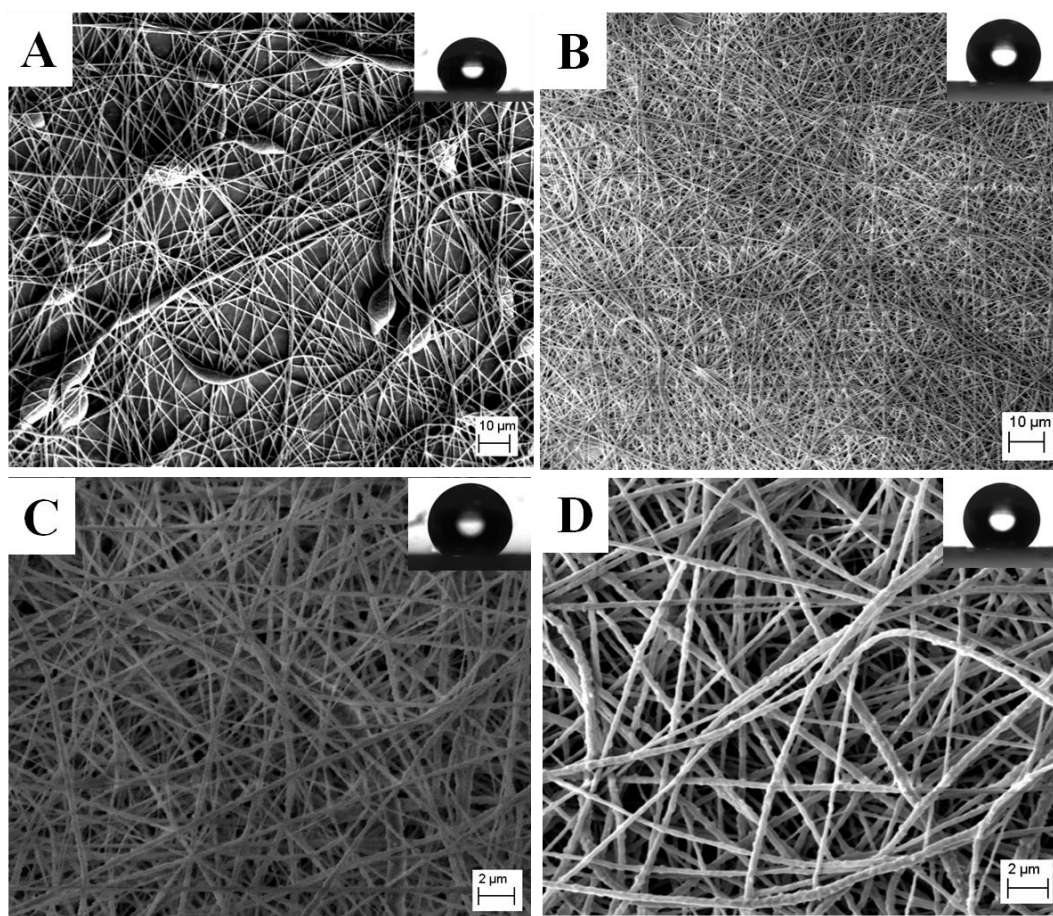


Figure 3-4. Surface morphology and water contact angle of M-6-LS (A: 500 ×), M-7-LS (B: 500 ×; C: 3K ×) and M-9-LS (D: 3K ×) membranes

The impact of LiCl additives on the membrane structure may be due to two reasons. Firstly, it was reported that LiCl interacts more strongly with NMP solvent than PVDF polymer to form stable LiCl-NMP complexes and thus decrease the strength of the solvent (Lee, Won et al. 2002). The increased viscosity of the polymer dope solution after adding LiCl additives in the current study (shown in **Table 3-3**, the dope 7 and dope 9 do have a bit higher viscosity than dope 6 and dope 8, respectively), suggests good affinity of LiCl with DMF/Acetone than with PVDF. However, this small enhancement in dope viscosity may not be sufficient to produce stable and uniform nanofibers since dope 5 with an even higher viscosity of

0.50 Pa s cannot produce uniform fibers (membrane M-5-HS shown in **Figures 3-3C** and **3-3D**).

Table 3-3. Additive effects on dope viscosity and conductivity

Dope code	Dope viscosity(Pa s)	Dope conductivity(μ s)
6	0.30	2.07
7	0.33	45.75
8	0.18	2.00
9	0.26	46.27

Thus, the attention should be drawn to the variation of the dope conductivity caused by the addition of the inorganic salt. As shown in **Table 3-3**, the original dopes without the additive (dope 6 and dope 8) have low conductivity as 2.07 μ s/cm and 2.00 μ s/cm. After a small amount of LiCl (0.004 wt%) was blended in the dope solutions, the conductivity of both dopes were increased significantly into 45.75 μ s/cm and 46.27 μ s/cm, respectively. The presence of LiCl may bridge electrostatic interaction between DMF/acetone mixture solution and PVDF polymer, consequently, enhancing the conductivity of the polymer solution. A higher conductive polymer solution can generate a higher charge density on the surface of the charged jet. Since the self-repulsion of the charges on the jet determines the over tension in fibers and higher charges result in a larger self-repulsion force, therefore, the diameters of nanofibers become thinner and the nanofibers are ejected faster. Moreover, the ions with a smaller atomic radius such as chloride ions have a higher charge density and mobility, thus generating a larger elongation force (Zong, Kim et al. 2002). This may be reason why LiCl played a role in the formation of electrospun membranes.

3.3.5. *Effect of relative humidity (RH)*

The moisture in electrospinning chamber was optimized to further reduce membrane pore sizes. It is found that moisture in the chamber has a significant influence on the membrane structure. As shown in **Table 3-2**, the membrane M-9-LS spun by dope 9 under relative humidity of 70 %, which is the lab humidity without any control, has a mean pore size of 0.30 μm and a maximum pore size of 0.54 μm . With the reduction of the humidity in the chamber by pumping dry air, the pore sizes of resultant membranes are decreased accordingly. PVDF nanofiber membranes M-9-LS-LM spun at relative humidity of 50 % possess a mean pore size of 0.18 μm and a maximum pore size of 0.36 μm .

This phenomenon can occur for some reasons. Firstly, the presence of more water molecules in the electrospinning chamber at high moisture would decrease the excess charges on the nanofibers because of molecular polarization (Mattoso, Offeman et al. 2008; Tang, Qiu et al. 2009). The lower charges on the nanofibers have a lower self-repulsion force to stretch fibers, resulting in thicker nanofibers and consequently, the membranes formed exhibited larger pores. Another possible mechanism for the phenomenon is due to the phase separation (Mattoso, Offeman et al. 2008; Tang, Qiu et al. 2009). At high humidity, water from air may cause fiber surface to precipitate before depositing on the collector surface. On the contrary, at low moisture, relatively wet nanofibers have a longer time for elongation before collection. Thus the membranes with small pores could be obtained at lower humidity.

It is worth to mention that all the PVDF eletrospun membranes have impressive water contact angles (136 ° to 142 °) as compared with flat sheet PVDF membranes fabricated by other methods such as phase inversion. These micro- and nano-structure surfaces arranged by electrospun nanofibers not only provide sufficient roughness for high hydrophobicity but also have a high adhesive force

with water, which is so-called “petal effects” (Feng, Zhang et al. 2008). A water droplet on the surface of these electrospun membranes can keep a sphere shape and would not roll off from the surface even if these membranes are turned upside down. Membranes with thinner nanofibers have a higher contact angle as the surface roughness is higher. Moreover, as shown in **Table 3-2**, the contact angle of the membranes spun by the dope with LiCl additive have a relatively higher water contact angle (138° - 142°) than without additives (137° - 139°) due to their thinner nanofibers and rougher surfaces.

3.3.6. *Effect of heat-press post-treatment*

To improve membrane integrity and mechanical strength, a heat-press post-treatment was applied. The membrane morphology before and after the post-treatment were observed by SEM, shown in **Figure 3-5**, which include the surface, cross-sectional and water contact angle images of PVDF naofiber membrane M-9-LS-LM. The original membrane had a thickness of $71\ \mu\text{m}$ with a water contact angle of 141° . If the membrane was treated by heat-pressing at 160°C , the membrane remained fluffy morphology as the fresh membrane. After heat-pressing at 170°C , the thickness of the membrane was reduced to $42\ \mu\text{m}$ with a lower contact angle of 138° due to the nanofiber compaction as shown in **Figures 3-5 B1**, **3-5 B2**, and **3-5 B3**. If the membranes were treated in an even higher temperature of 180°C , the fibers tended to melt more severely. This consequently sacrificed the advantages of high hydrophobicity and high porosity of nanofiber membranes. As shown in **Figure 3-5 C1**, the connection points at the surface of the nanofiber sheet were melt together. The thickness and water contact angle of membrane were further reduced to $20\ \mu\text{m}$ and 120° , respectively. Thus, 170°C is considered as the optimal post-treatment temperature in the current study. It has been reported that with an appropriate heat-press post-treatment, the nanofiber sheets can be used as self-supported membranes without non-woven support due to its sufficient mechanical strengthen (Gopal, Kaur et al. 2006).

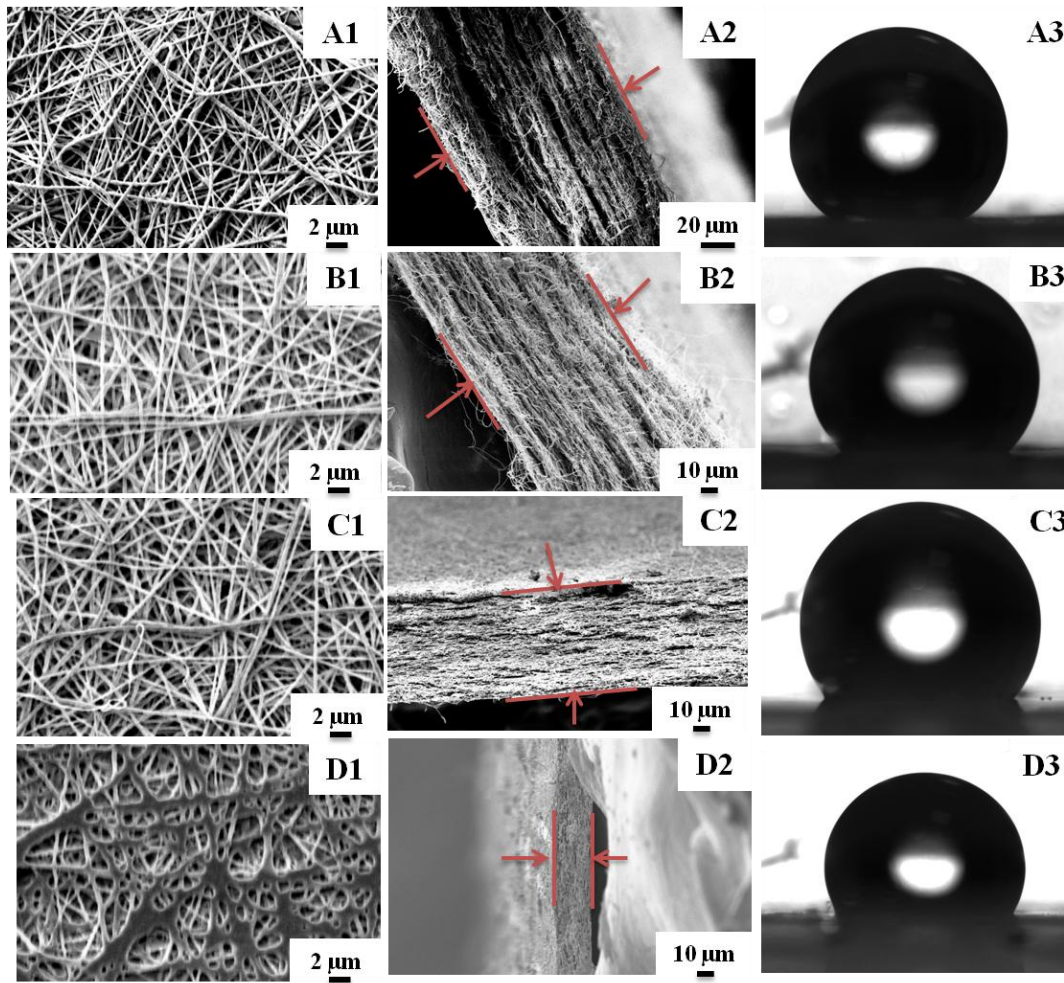


Figure 3-5. SEM pictures of electrospun PVDF membrane M-9-LS-LM before heat press (A1: 3K \times ; A2: 500 \times cross section; A3: water contact angle), after 160 $^{\circ}\text{C}$ heat press (B1: 3K \times ; B2: 500 \times cross section; B3: water contact angle), after 170 $^{\circ}\text{C}$ heat press post-treatment (C1: 3K \times ; C2: 500 \times cross section; C3: water contact angle) and 180 $^{\circ}\text{C}$ heat press post-treatment (D1: 3K \times ; D2: 500 \times cross section; D3: water contact angle)

The effects of heat-press post-treatment on the pore size, porosity and LEP of PVDF nanofiber membranes are shown in **Table 3-4**. It reveals that the heat-press post-treatment decreased membrane pore size, water contact angle and porosity due to the compaction, but increased LEP of nanofiber membranes. It has

been reported that tensile strength and tensile modulus of electrospun membranes increase after heat-press, while the crystalline of PVDF did not change too much before and after hot-press (Na, Zhao et al. 2008). Additionally, with an appropriate heat-press post-treatment, the nanofiber sheets can be used as self-supported membranes without non-woven support due to its sufficient mechanical strength (Gopal, Kaur et al. 2006)

Table 3-4. Effect of heat-press post-treatment on membrane properties

Dope code	Sample code	Mean pore size(μm)	Max pore size(μm)	Contact angle ($^{\circ}$)	Porosity (%)	LEP (bar)
9	M-9-LS-LM	0.18	0.36	138	71.4	0.24
9	M-9-LS-LM-Heat	0.21	0.33	136	53.7	0.35

3.3.7. Preliminary evaluation of membrane performance in DCMD

The electrospun PVDF membranes without/with hear-press post treatment were tested in the DCMD setup to examine their potential for membrane distillation application. As shown in **Figure 3-6**, the permeation flux of the fresh PVDF nanofiber membrane without heat-press post-treatment (membrane M-9-LS-LM) and same batch nanofiber membrane with heat-press post-treatment at 170 $^{\circ}\text{C}$ (membrane M-9-LS-LM-heat) have been measured over 15 hours. It can be seen that the permeation flux of membrane M-9-LS-LM-heat is around $21 \text{ kg m}^{-2} \text{ h}^{-1}$ when the hot feed and cold permeation temperatures were set as 323 K and 293 K, respectively. This permeation flux is competitive as under the same MD test conditions, the permeation flux of commercial membranes is around $15 \text{ kg m}^{-2} \text{ hr}^{-1}$ (Yang, Wang et al. 2011). However, under the same MD test conditions, the flux of membrane M-9-LS-LM was decreased to $11 \text{ kg m}^{-2} \text{ h}^{-1}$ after one hour test which

is much lower than the treated membrane even though the membrane M-9-LS-LM possesses a higher porosity than its counterpart.

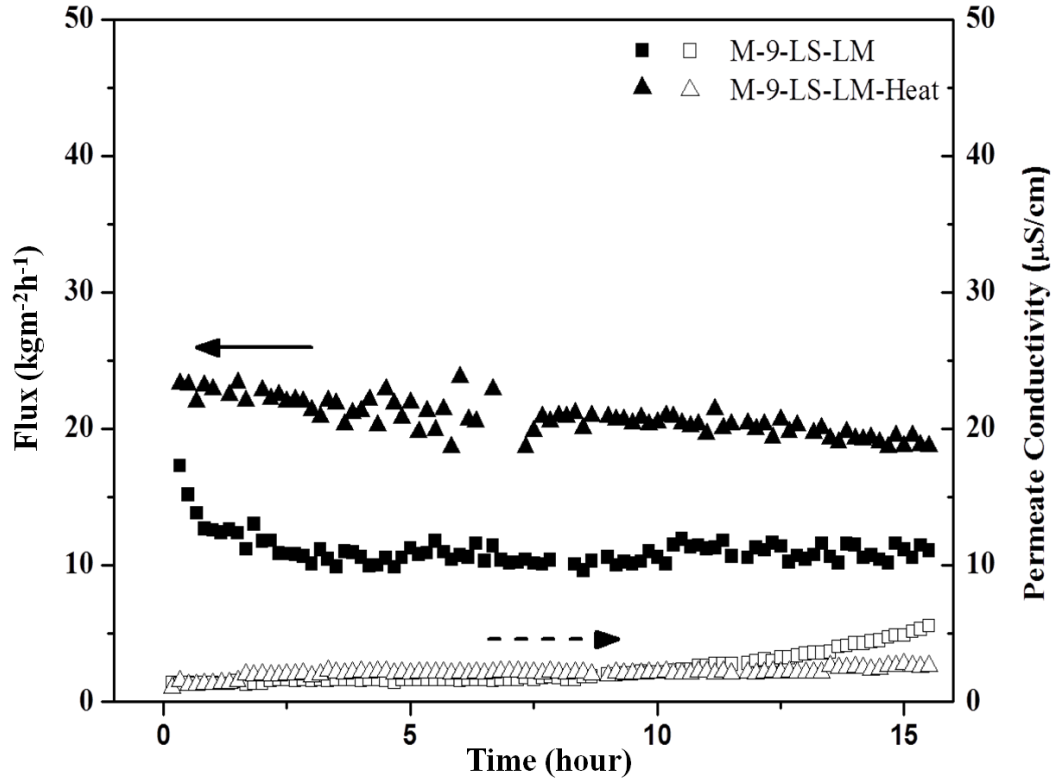


Figure 3-6. Effects of heat-press post-treatment on permeation flux and long term performance of PVDF membranes for DCMD application (3.5 wt% NaCl solution as feed, $T_f = 323$ K, $T_p = 293$ K, flow rate at feed side= 0.6 L/min, flow rate at permeate side= 0.6 L/min)

To fully understand the results shown in **Figure 3-6**, an analysis on the structure of electrospun nanofiber membranes is necessary. As illustrated in **Figure 3-7**, the fresh (non-heat treated) nanofiber membrane may be considered as a matrix consisting of multiple nano-sheet layers where each layer may have a gap/pores due to the nature of electrospinning (**Figure 3-7A**). The optical and SEM images of the fresh nanofiber membrane are shown in **Figures 3-7 A(2)** and **3-7 A(3)**. When a hot salt solution in the feed side is scouring on the membrane surface, because of loose

overlapping, small salt water drops may enter into the nanofiber-sheet layers fast and accumulate within the gap/pores, as shown schematically in **Figure 3-7B**. A certain amount of stagnant water droplets were collected between the nanofiber layers of the fresh membranes after tested in DCMD setup, which confirmed the hypothesis (**Figure 3-7 B(2)**). The cross-sectional morphology of the membrane after MD operation is shown in **Figure 3-7 B(3)**, which illustrates that a gap was formed between nanofiber layers due to the stagnant water. The stagnant water may decrease the temperature difference between the feed and permeate sides significantly, which is the driving force, thus lead to severe permeate flux reduction. Compared with fresh nanofiber membrane, the heat-press treated membrane did not contained salt water droplets after 15 hours DCMD test as shown in **Figure 3-7 C**. According to **Figure 3-7 C(3)**, no gaps are shown between nanofiber layers. It demonstrated that the heat-press post-treatment improved membrane integrity and prevented salt solution from intruding into nanofiber layers.

Figure 3-6 also shows the permeate conductivity of the two membranes over a period of around 15-h operation. It can be seen that both membranes delivered sustainable fluxes for the test period, but, for the untreated PVDF nanofiber membrane, there was a slow and gradual conductivity build-up of the distillate after about 10 h test, while the treated nanofiber filter exhibited a stable performance and better water quality over 15 h of testing. Due to relatively open structure of untreated nanofiber textile, the small molecules of water incline to penetrate inside the membrane resulting in membrane wetting and thus severe flux falloff. Therefore, the advantages of the post-treated membranes over fresh membranes are not only enhancing permeation flux, but also greatly reducing membrane pore wetting. Obviously, even the heat-press treatment decreased the porosity of electrospun membranes, the benefits obtained from adaptive heat-press treatment are far beyond detrimental effects for MD application.

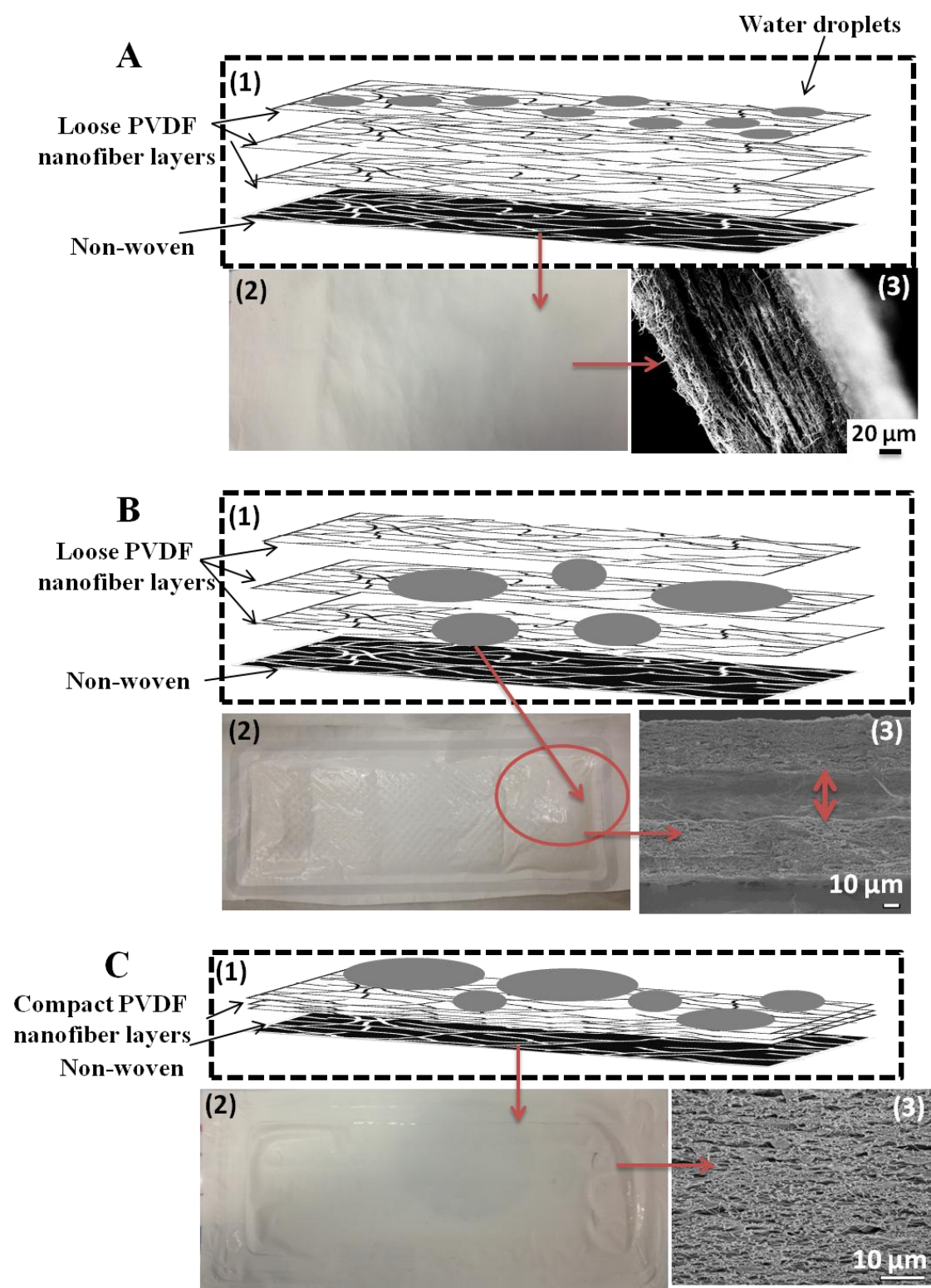


Figure 3-7. Illustration of water entrapment in a nanofiber membrane

3.3.8. Comparison with other flat-sheet PVDF MD membranes

The DCMD performance of the PVDF nanofiber membrane M-9-LS-LM-Heat was compared with commercial PVDF membranes (Phattaranawik, Jiraratananon et al. 2003; Martínez and Rodríguez-Maroto 2008; Zhang, Dow et al. 2010) and PVDF-clay nanocomposite nanofiber membrane (Prince, Singh et al. 2012), as shown in **Table 3-5**. For a better comparison, the commercial membrane Durapore® supplied by Millipore from Singapore was tested at same DCMD setup as the membrane M-9-LS-LM-Heat. It can be seen that a noticeable flux enhancement has been achieved in the current work. This is believed to be attributed to the open surface pore structure and a thinner thickness of the PVDF nanofiber membrane. It demonstrates the PVDF nanofiber membrane has potential to be used as MD membranes for membrane distillation application.

Table 3-5. DCMD performances of flat-sheet PVDF membranes

Membrane	Mean pore size	Contact angle	Porosity	Feed solution property			Permeate solution property	Permeation flux	
	(μm)	(°)	(%)	Solution	v _f (m s ⁻¹)	T _{f,in} (°C)	T _{p,in} (°C)	v _p (m s ⁻¹)	(kg m ⁻² h ⁻¹)
Durapore ^a	0.28	135	48	3.5 wt% NaCl solution	0.05	60	20	0.14	10.6
GE Osmonics (Zhang, Dow et al. 2010)	0.30	113	81	1wt% NaCl solution	0.36	60	20	0.36	9.1 ^b
GVHP (Mart ínez and Rodr íguez-Maroto 2008)	0.16	-	70-75	1 M NaCl solution	0.35	40	20	0.35	8.1 ^b
GVHP (Mart ínez and Rodr íguez-Maroto 2008)	0.22	-	62	Pure water	laminar flow	60	20	laminar flow	8.4 ^b
HVHP(Phattaranawik, Jiraratananon et al. 2003)	0.45	-	66	Pure water	laminar flow	60	20	laminar flow	10.3 ^b
PVDF-Clay nanofiber membranes(Prince, Singh et al. 2012)	0.58	154	82	3.5 wt% NaCl solution	-	80	17	-	5.7 ^b
M-9-LS-LM-Heat (current work)	0.21	136	54	3.5 wt% NaCl solution	0.07	50	20	0.14	20.6

a. The data was tested in our lab using the commercial Millipore Durapore membranes.

b. The flux was read from figures shown in papers and converted the permeation flux in the same unit

3.4. Conclusions

Nanofiber PVDF membranes have been fabricated using the electrospinning method. In order to improve and stabilize the membrane performance in the DCMD process, the structures and properties of resultant membranes were optimized by controlling a series of factors including polymer dope compositions and spinning parameters. And the heat-press post-treatment effect on the MD performance of membranes has also been examined.

Experiments reveal that dope solution properties and electrospinning process parameters are key factors to determine the membrane structures. By means of controlling polymer concentration and adding suitable additives in the dope solution, the nanofibers with a small diameter could be fabricated and membranes formed by the nanofibers possess small pore sizes. In addition, the membranes with small pore sizes can be prepared by slowing down the sprayer moving speed and reducing the moisture in the spinning chamber. Surface contact angle measurements confirm that all the electrospun PVDF membranes exhibit a rougher surface with high hydrophobicity.

Moreover, the heat-press post-treatment is considered as a necessary step to improve fresh nanofiber membrane integrity, enhance water permeation flux and help prevent membrane pores from wetting in DCMD operation. The post-treated PVDF nanofiber membranes were able to present a steady water permeation flux of about $21 \text{ kg m}^{-2}\text{h}^{-1}$ throughout the entire test of 15 h, which is 100% higher than the untreated fresh membrane. It suggests that PVDF electrospun nanofiber membranes have good potential for MD application.

CHAPTER 4

Engineering superhydrophobic surface on PVDF nanofiber membranes for DCMD

4.1. Introduction

As demonstrated in Chapter 3, electrospinning is a simple and effective way to fabricate continuously polymeric nanofiber membranes composed of microscale and nanoscale fibers for MD process, which have high porosity and high surface-to-volume ratio (Bhattarai, Bhattarai et al. 2004; Gopal, Kaur et al. 2006; Rao, Geng et al. 2012). However, the uniform nanofiber structures fabricated by pure polymer dopes without hydrophobic additives do not possess enough wetting resistance. In particular, the micro- and nano-structured surface provides a high adhesive force with water as mentioned in section 3.3.5. The water droplet cannot roll off even if the membrane is turned upside down. Thus to further enhance the hydrophobicity of nanofiber membranes, superhydrophobic membranes are proposed to make in this chapter.

Superhydrophobic surfaces exhibit both a high water contact angle above 150° and a low water roll-off angle below 10° (Bhushan and Jung 2011). Water droplets are able to roll off on such a surface with some slip, providing the surface self-cleaning property known as “Lotus Effect” as the contaminants on the surface can be taken with them (Barthlott and Neinhuis 1997; Neinhuis and Barthlott 1997). Since 1990s, materials and biological scientists began to investigate natural superhydrophobic surfaces such as Lotus (Wagner, Fürstner et al. 2003; Burton and Bhushan 2006). The Lotus leaves have a hierarchical structure with microscale roughness composed of papillose epidermal cells and nanoscale asperities

consisting of three-dimensional epicuticular waxes which are long chain hydrophobic hydrocarbons. This hierarchical structure facilitates the formation of air pockets on the solid surface, making applied water droplets have the lowest contact surface with the solid. As a result, the adhesive force between the solid surface and water can be reduced significantly (Nosonovsky and Bhushan 2007; Bharat and Yong Chae 2008; Bhushan 2008).

Fundamentally, the methodologies used to achieve superhydrophobic surfaces are to increase surface roughness and then modify the surface with low energy and non-polar molecules. It is worth mentioning that surface roughness is usually more critical than the low surface energy, as both moderately hydrophobic and very hydrophobic materials can possess similar superhydrophobic property when roughened. To date, the layer-by-layer (LBL) assembly has been introduced into the electrospun fibers to construct a superhydrophobic surface (Tasuku, Bin et al. 2007). In this approach, the nanofiber membranes need to be immersed in TiO_2 colloid solution for 15 min, rinsed in three pure water baths and then placed into an anionic solution for another 15 min. The adsorptions and rinsing steps need to be repeated more than 10 times to achieve enough roughness. Later the membranes were dried to immerse into fluoroalkylsilane (FAS) solution for 6 h to modify the surface to be superhydrophobic. The entire procedure is complicated and time-consuming. It was also reported that combining electrospinning with initiated chemical vapour deposition (CVD) is an effective approach to prepare superhydrophobic fabrics (Ma, Mao et al. 2005). Moreover, Yoon et al. have demonstrated that CF_4 plasma is an alternative method to fabricate superhydrophobic micro/nanofibrous cellulose triacetate (CTA) membrane (Zhaohui, Changquan et al. 2009). However, these modification processes require the usage of special equipments, such as chemical vapour deposition reactor and CF_4 plasma equipment.

In this work, a facile method for preparation of superhydrophobic nanofiber membranes by surface modification was explored. It involves three steps of modification: (1) the nanofiber surfaces were firstly coated by poly-dopamine (PDA) to improve the adhesive force between the fibers and silver nanoparticles which were deposited on the fiber surface at the second step; (2) the PDA activated nanofibers were coated by silver nanoparticles during chemical reduction to optimize the morphology and roughness of the membrane; (3) in order to alter the surface chemistry, 1-Dodecanethiol (C12) was applied to react with silver nanoparticles in mild conditions. The whole modification procedure could be finished in 3 h. The PDA modification method is versatile because of its applicability to many types of materials with complex shapes, simple ingredients, mild reaction conditions and strong binding force (Lee, Dellatore et al. 2007). Moreover, the PDA coating layer performs well as a binding agent even with metals (Liao, Cao et al. 2009; Wang, Jiang et al. 2011). These advances make this modification method available for all types of nanofiber membranes including PVDF nanofiber membranes used in current study. Subsequently the modified membranes were evaluated in DCMD process to compare with commercial membranes for potable water production.

4.2. Experiments

4.2.1. Membrane materials and chemicals

Dopamine hydrochloride, tris (hydroxymethyl) aminomethane (tris), 1-dodecanethiol (C12), D-(+)-glucose and silver nitrate plant cell were purchased from Sigma-Aldrich, Singapore. Ethanol and ammonia solutions used in the modification process were received from Merck, Singapore. All the reagents were used as received. Water was purified with a Milli-Q system (Millipore Co. Singapore). Other materials have been described in section 3.2.1.

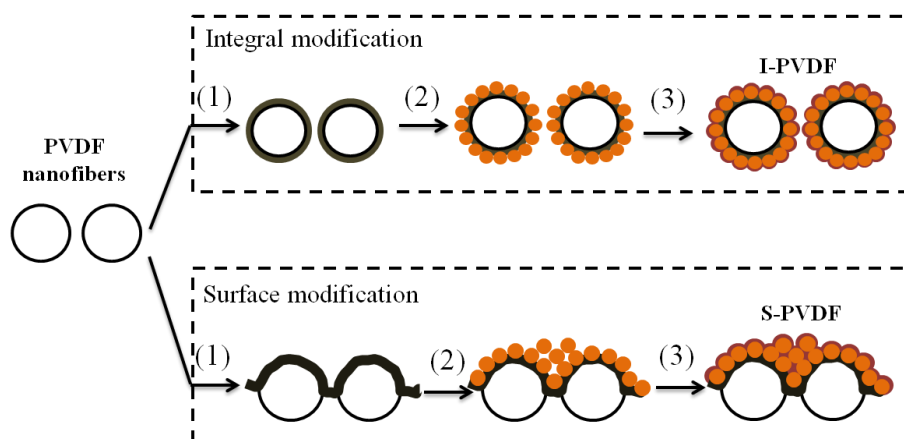
4.2.2. *Electrospinning of PVDF nanofiber membranes and post-treatment*

A 5 wt% PVDF polymer dope solution for electrospinning was prepared by dissolving a pre-weighted PVDF HSV 900 in a mixture of DMF and acetone with a weight ratio of 6 to 4. A desired amount of LiCl (0.004 wt%) was added into the dope solution to improve dope electrospun ability, optimize the nanofiber membrane's porosity and control membrane pore sizes (Zong, Kim et al. 2002; Liao, Wang et al. 2013). The dope solution was stirred mechanically for at least 1 day at 60 °C. The homogenous dope solution was then cooled down and degassed at room temperature for overnight before electrospinning. Then, the polymer solution was electrospun into nanofiber webs using an electrospinning setup equipped with a high voltage supply. A positive voltage of 28 kV was applied across a distance of 12 cm between the tip of the sprayers and the grounded drum. The spinning sprayers can be moved slowly and evenly by a motor during electrospinning. Nanofibers were spun over a course of 3 h to prepare continuous fibrous membrane. In order to eliminate the affect from residual solvents in the membrane, the PVDF nanofiber membranes were subsequently placed in a fume cupboard under vacuum condition at 60 °C for overnight to ensure all solvents evaporated from the fresh membranes. The dry PVDF nanofiber membranes were then pressed between two flat glass panes and placed in an oven at 170 °C just below polymer melting point for an hour to compress all the nanofiber layers together.

4.2.3. *Membrane modification*

Two types of modification which are integral and surface modifications were carried out as shown in **Figure 4-1**. The difference between the integral and surface modifications lies in the pre-activation by the DPA. Nanofiber membranes were firstly wetted by a mixed solution of IPA and water to ensure that the chemical solution can flow inside the membranes and react on all fibers, which were used to make integrally modified PVDF membranes (designated as I-PVDF). Compared

with the I-PVDF membrane, surface-modified PVDF membranes (designated as S-PVDF) were prepared by directly treating the dry PVDF nanofiber membrane which did not allow the reagents to intrude into the membrane pores and ensured that the modification only occurred on the membrane surface.



(1) PDA modification; (2) Silver nanoparticle coating; (3) 1-dodecanethiol hydrophobic modification

Figure 4-1. Schematic diagram of preparing superhydrophobic PVDF nanofiber membranes by silver nanoparticle and 1-dodecanethiol hydrophobic modification

In the subsequent modification process, the as-prepared PVDF membranes were dipped into the aqueous dopamine solution with a fixed concentration (2 mg of dopamine per millilitre of 10 mM tris, at pH of 8.5) for 1 h to form a thin adhesive PDA film on the fiber surface. Then the pre-activated PVDF membranes (PDA-PVDF) were taken out and washed with a large amount of deionized water at room temperature. In next step, the PDA-PVDF membranes were placed in an electroless silver-plating bath for predetermined time to prepare silver-deposited PVDF membrane (Ag-PVDF). The composition of the solution in the plating bath was as followings: 1 wt% AgNO_3 , 1 wt% D-(+)-glucose and 0.02 wt% ethanol. The Ag-PVDF membranes were raised in deionized water to remove unattached silver nanoparticles. To apply a hydrophobic material on nanofiber membrane surfaces, the Ag-PVDF membranes were subsequently immersed in an ethanol solution of 10

mM 1-dodecanethiol. Prior to a series of characterizations and DCMD test, the 1-dodecanethiol-coated membrane (C12-PVDF) was rinsed with a copious amount of absolute ethanol and then dry in vacuum at 100 °C for 1 h.

4.2.4. Characterizations of PVDF electrospun membranes

In order to analyze the chemical composition on membrane surface precisely, X-ray photoelectron spectroscopy (XPS) tests were conducted using a Theta Probe XPS provide by Thermo Fisher Scientific (Singapore), equipped with a monochromatic Al K α X-ray source (1486.68 eV) and a hemispherical analyzer. The survey spectrums were collected from 0 to 1300 eV with pass energy of 200 eV and 1 eV of energy step size while high resolution scans were done with pass energy of 40 eV. The core-level signals were obtained at a photoelectron take-off angle of 50 ° with respect to the sample surface. Binding energies were calibrated with respect to C 1s hydrocarbon bond at 284.6 eV.

The surface morphologies and elemental compositions of the samples were observed by a field emission scanning electron microscope (FE-SEM, JSM-7600F, JEOL Asia Pte Ltd, Japan) equipped with an Energy-dispersive X-ray spectroscopy (EDX) detector. Prior to characterisation, the samples were mounted on the sample studs by carbon double-sided adhesive tapes and sputtered with a thin platinum layer. The FE-SEM tests were carried out at an accelerating voltage of 5 kV and the FE-SEM-EDX measurements were carried out at 20 kV.

The topography of the C12-PVDF membranes surfaces were characterized by means of a XE-100 atomic force microscope (AFM), manufactured by Park Systems, Korea. In each case, an area of 2.5 μm \times 2.5 μm was scanned using the tapping mode, and an arithmetic mean of the surface roughness (R_a) was calculated from the roughness profile determined by AFM. All measurements were performed in air at 26 °C.

The contact angles, mean pore size and pore size distribution, porosity and LEP of as-prepared membranes were determined by the same method as mentioned in section 3.2.4. The mechanical strength of the membranes was measured using a Zwick/Roell BT1-FR0.5TN.D14 testing machine at a constant elongation velocity of 50 mm min⁻¹ under room temperature (26 °C), which was purchased from Singapore. The resultant PVDF membranes were tested in a DCMD setup with an effective membrane area of 38 cm² as mentioned in section 3.2.5.

4.3. Results and discussion

4.3.1. Chemical modification reactions on the PVDF nanofiber membranes

As the first step, pristine PVDF membranes were treated by dopamine. During the dopamine oxidative self-polymerization, the transparent dopamine solution turned to be pink and then deep dark, indicating that the polymerization may form melanin (Lee, Dellatore et al. 2007). A possible reaction pathway for dopamine modification is shown in **Figure 4-2A**.

The surface chemical compositions of poly(dopamine)-activated PVDF membrane (PDA-PVDF) and pristine PVDF nanofiber membrane were compared via the XPS measurements, as shown in **Figure 4-3**. It can be seen that the wide-scan spectrum of pristine PVDF nanofibers contains the C 1s and F 1s peaks (**Figure 4-3A**). The C 1s core-level spectrum can be curve-fitted with two peak components, one at binding energy (BE) of 284.6 eV for the carbon bonded to hydrogen (CH_x) and the other at BE of 290 eV for the carbon singly bonded to fluorine (C-F₂) (**Figure 4-3B**) (Moussaif, Pagnoulle et al. 2000). The distinct differences in the wide-scan spectra between pristine PVDF (**Figure 4-3A**) and the PDA-PVDF (**Figure 4-3C**) are the presences of the N1s and O1s peaks, which are the elements from poly(dopamine). The presence of poly(dopamine) on the PDA-PVDF nanofibers surface is further ascertained by the changes in the XPS C 1s

core-level line shape. The C 1s core-level spectrum of the PDA-PVDF shows other two peaks in addition to $\underline{\text{C}}\text{H}_x$ and $\underline{\text{C}}\text{-F}_2$, which are at 285.6 eV for the $\underline{\text{C}}\text{H-N}$ and $\underline{\text{C}}\text{H-C(O)}$ species and at 286.4 eV for the $\underline{\text{C}}\text{-O}$ species (Liao, Cao et al. 2009). These additional peaks are all measured due to the emitted photoelectrons from poly(dopamine) layers. Furthermore, the result that the $\underline{\text{C}}\text{-F}_2$ peak component associated with the PVDF substrate persists in C 1s spectrum of the PDA-PVDF suggests that thickness of the deposited PDA layer is below the probing depth of the XPS technique (less than 10 nm for this equipment).

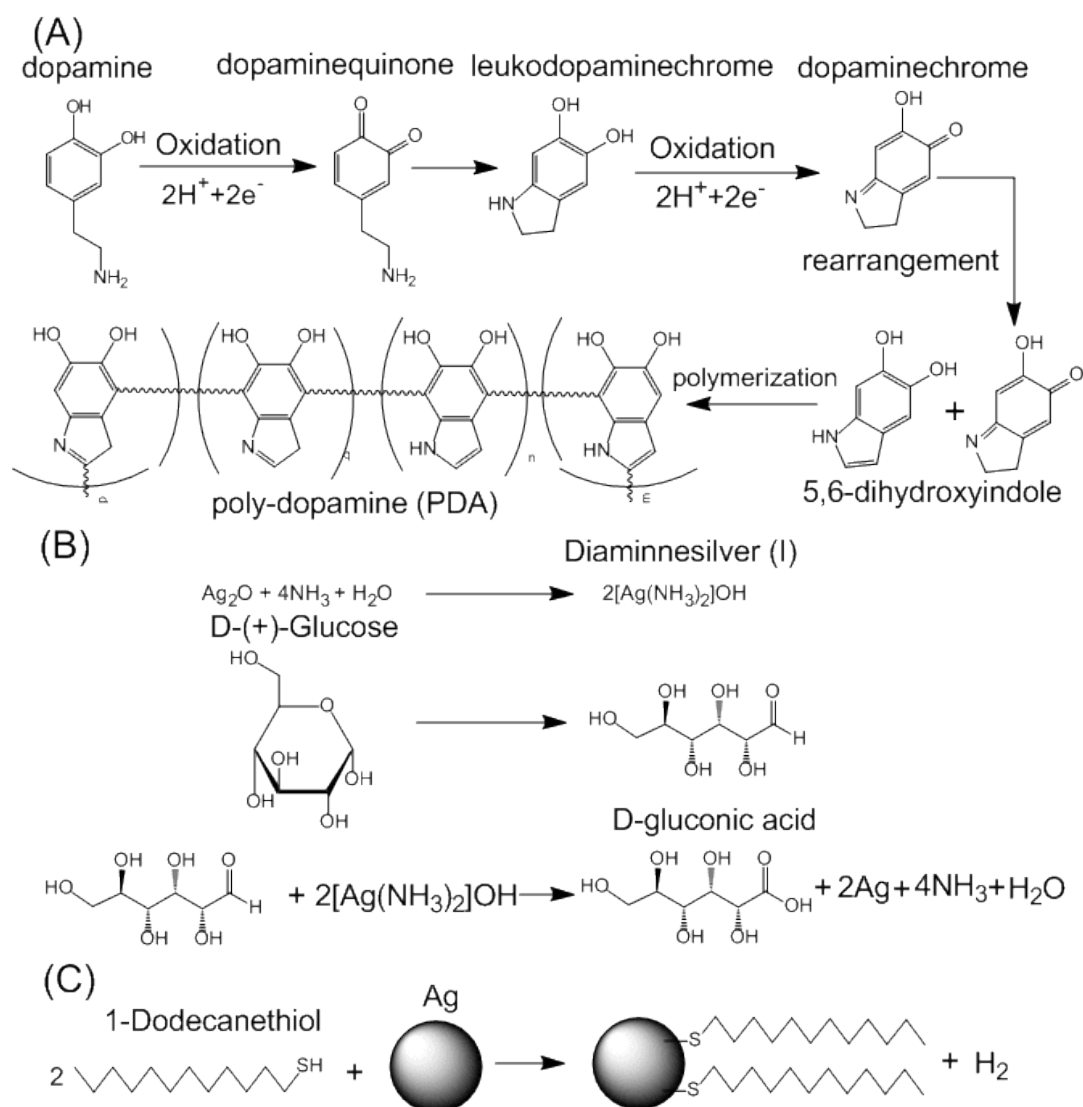


Figure 4-2. Possible reaction pathways of superhydrophobic membrane preparation

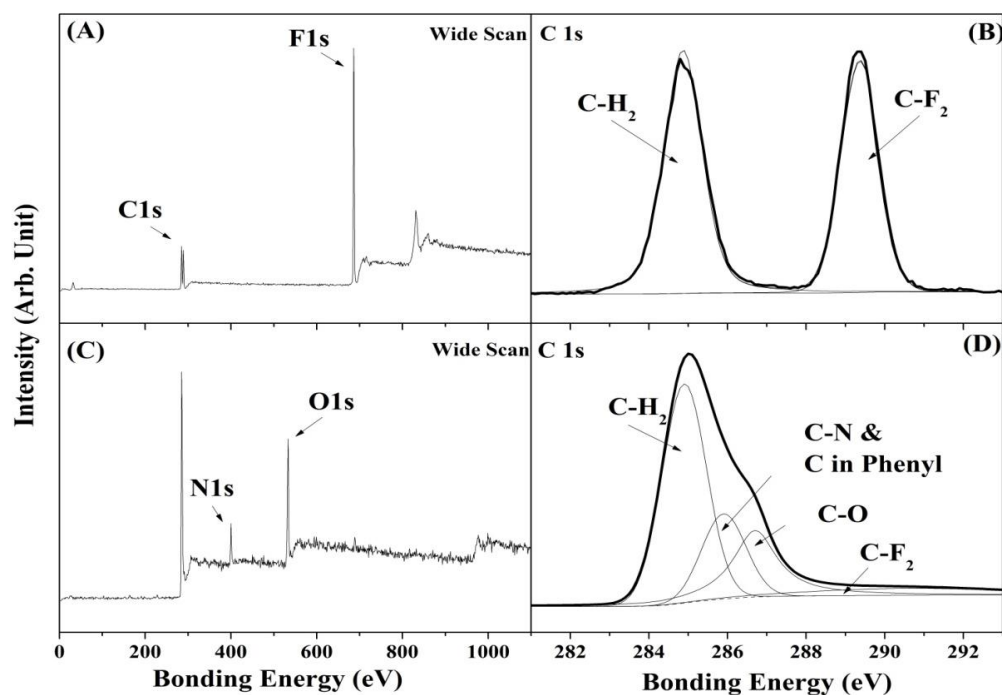


Figure 4-3. The XPS wide-scan and C 1s core-level spectra of (A and B) PVDF membrane and (C and D) dopamine-modified PVDF membrane (PDA-PVDF).

The metal-binding ability of catechol and N-containing groups present in the PDA layer and reduced agents (glucose in this study) was exploited to deposit adherent silver nanoparticle coatings on to the PDA-PVDF membranes (Nosonovsky and Bhushan 2007; Wang, Jiang et al. 2011). An ammoniacal silver nitrate solution was prepared as an electroless bath solution. The possible mechanism of the silver reduction is shown in **Figure 4-2B**. As silver ions in the ammoniacal silver solution have high redox potential, which can be easily reduced to Ag and causes bulk reduction, a small amount of ethanol was added to enhance the stability of the bath. The strong signal of Ag at BE of about 370 eV at **Figure 4-4A** demonstrates that silver layers were successfully deposited on membrane surfaces. The Ag 3d core-level spectrum shown in **Figure 4-4B** can be curved into two peaks which are Ag 3d_{5/2} peak at BE of 368.0 eV and Ag 3d_{3/2} peak at BE of

374.0 eV (Wang, Jiang et al. 2011). Both peaks further demonstrate that the coated silvers are in the zero valent state.

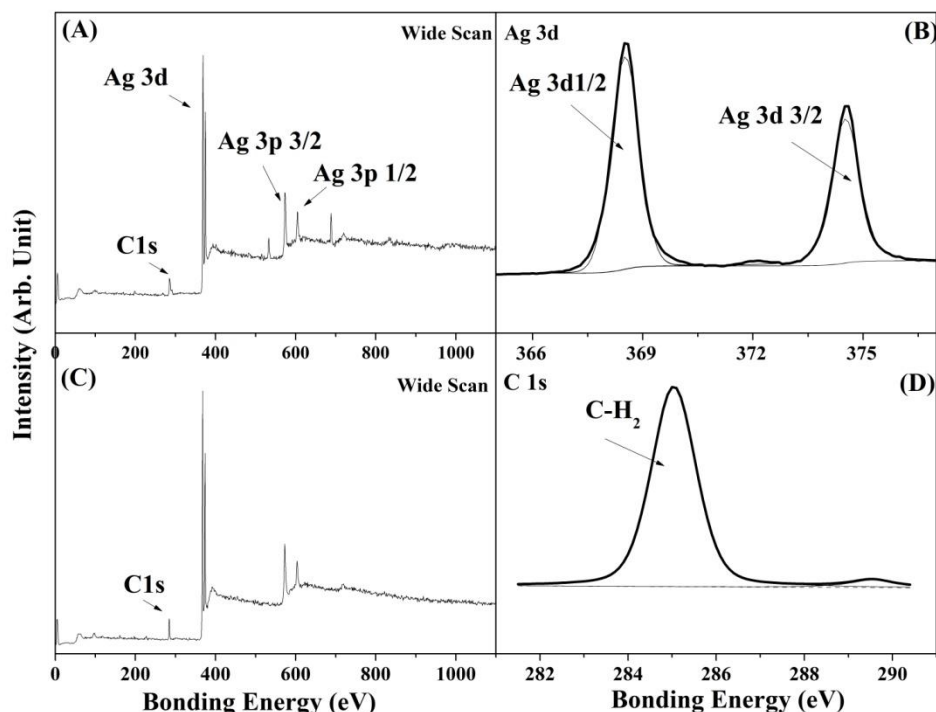


Figure 4-4. The XPS wide scan and Ag 3d core-level spectra of silver deposited PVDF membrane (Ag-PVDF) (A and B), and XPS wide scan and C 1s core-level spectra of modified PVDF membrane (C12-PVDF) (C and D).

A self-assembled monolayer of thiol was subsequently reacted on the silver nanoparticle surface to change the surface to be hydrophobic as shown in **Figure 4-2C**. The wide-scan spectrum of 1-dodecanethiol-coated PVDF (C12-PVDF) and the C 1s core-level spectrum are shown in **Figures 4-4C** and **4-4D**. The wide-scan spectrum only have strong peaks for C 1s, Ag 3d and 3p, which demonstrate that after the final modification step, there are mainly carbon and silver on membrane surfaces. Furthermore, the C 1s core-level spectrum can be curve-fitted into only one peak at BE of 284.6 eV for $\underline{\text{C}}\text{H}_x$, which is the chemical composition in the coated thiol layer (1-dodecanethiol). These XPS information fully confirms that the

modification reactions shown in **Figure 4-2** have been carried out on the membrane surface.

4.3.2. Membrane surface morphologies

The surface morphologies of pristine PVDF nanofiber membrane (**Figures 4-5 A1 and 4-5 A2**), modified I-PVDF nanofiber membrane (**Figures 4-5 B1 and 4-5 B2**) and S-PVDF nanofiber membrane (**Figures 4-5 C1 and 4-5 C2**) were observed by FE-SEM. It can be seen from **Figures 4-5 A1 and 4-5 A2** that the pristine PVDF nanofiber membranes have a nanofiber fabric surface consisting of PVDF nanofibers with a diameter of $\sim 150 \pm 57$ nm. The water contact angle images (inserted images in **Figure 4-5 A1**) show that pristine PVDF nanofiber membrane has a high contact angle of $138^\circ \pm 1^\circ$ and exhibits a high adhesive force with water droplet. Even when the membrane is turned upside down, the water droplet on the surface still kept spherical in shape and cannot roll off from the membrane surface, which is so-called petal effect (Feng, Zhang et al. 2008).

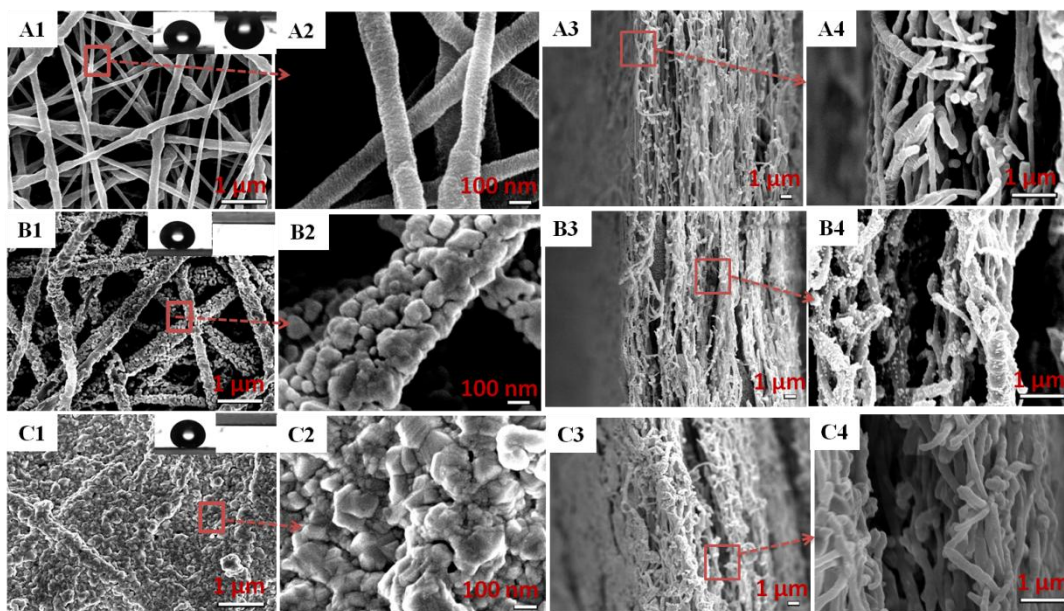


Figure 4-5. FE-SEM images of pristine PVDF (A1, A2), I-PVDF (B1, B2) and S-PVDF (C1, C2) nanofiber membranes. Cross section images of pristine PVDF (A3, A4), I-PVDF (B3, B4) and S-PVDF (B3, B4) nanofiber membranes

On the other hand, silver nanoparticles could be observed clearly on the I-PVDF fiber surface as shown in **Figures 4-5 B1** and **4-5 B2**. According to the FE-SEM image, the I-PVDF membrane surface was still formed by nanofibers with a larger diameter of 293 ± 86 nm. The existence of Ag and S elements on the surface of the I-PVDF nanofiber membranes proved by XPS analysis and introduced by modifications demonstrates that silver nanoparticles and a hydrophobic layer were successfully formed on the nanofibers surfaces as a layer with a thickness about 70 nm. The I-PVDF nanofiber membrane is superhydrophobic, which has a high water contact of $153^\circ \pm 4^\circ$ and a low water sliding angle less than 10° . The water droplet cannot stay on the membrane surface when it is turned upside down as shown in contact angle images (small inserts in **Figure 4-5 B1**). The membrane has “Lotus effect” instead of “Petal effect” due to the surface roughness optimization. Compared with the I-PVDF membrane, the S-PVDF membrane surface was covered with a layer of silver nanoparticles and hydrophobic monolayers as shown in **Figures 4-5 C1** and **4-5 C2**. It is hard to observe distinguished nanofibers from the surface image. However, due to the surface roughness provided by silver nanoparticles, this membrane still has superhydrophobic property as the I-PVDF, which exhibits a high water contact of $158^\circ \pm 3^\circ$ and a low water sliding angle less than 10° .

Furthermore, the cross sections of PVDF nanofiber membrane (**A3, A4**), I-PVDF (**B3, B4**) and S-PVDF (**C3, C4**) were also examined by FE-SEM as shown in **Figure 4-5**. From these images it can be seen that small silver nanoparticles are deposited on the inner nanofiber surface of the I-PVDF membrane. In contrast, nanofibers inside the S-PVDF membrane have similar morphology as pristine PVDF nanofibers, which are not covered by nanoparticles. It demonstrated that the modification reaction occurred on all nanofibers for the I-PVDF membrane while it only modified the surface layer for the S-PVDF membrane.

4.3.3. Effects of surface modification conditions on membrane superhydrophobicity

The deposition of silver nanoparticles layers on the PDA-activated PVDF membrane surface is a critical step to optimize surface roughness and enhance membrane hydrophobicity. Different deposition times in the electroless coating bath from 5 to 20 min were selected to investigate the deposition time effect on membrane surface properties. The contact angles of as-prepared I-PVDF and S-PVDF membranes are shown in **Figure 4-6**. The contact angle of the pristine PVDF nanofiber membrane is $138^\circ \pm 1^\circ$ and the water droplet adheres to the membrane surface even when the membrane is tilted to handstand.

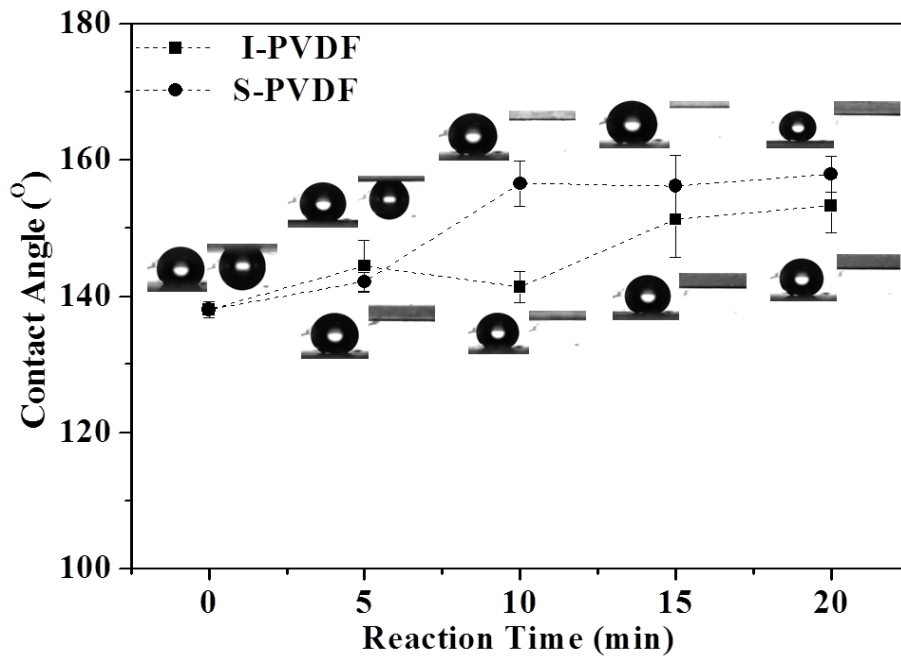


Figure 4-6. Effect of silver nanoparticle treatment time on the contact angle

Generally, when water contact with a flat surface as shown in **Figure 4-7A**, the contact angle can be obtained by the well-known Young equation as following:

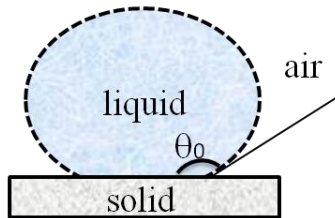
$$\cos \theta_0 = \frac{\gamma_{SA} - \gamma_{SL}}{\gamma_{LA}} \quad (4-1)$$

The characteristic angle θ_0 is called the static contact angle. γ_{SA} and γ_{SL} are the surface energies of solid against air and liquid, respectively, and γ_{LA} is the surface energy of liquid against air (Bhushan and Jung 2011). If a water droplet is placed on a rough surface with a homogeneous interface (as shown in **Figure 4-7B**), the area of interface increases with respect to that for a smooth surface. The Wenzel equation (Wenzel 1936) could be used to predict the contact angle:

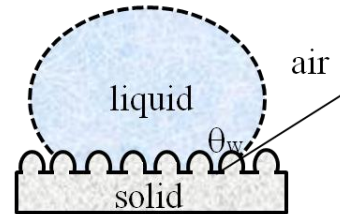
$$\cos \theta_w = R_f \cos \theta_0 \quad (4-2)$$

where θ_w is the contact angle of a water droplet upon a rough solid surface calculated by Wenzel equation. R_f is the non-dimensional surface factor, equal to the ratio of the surface area to its flat projected area. This Wenzel model also illustrates that a hydrophobic surface ($\theta_0 > 90^\circ$) becomes more hydrophobic with an increase of surface roughness (R_f).

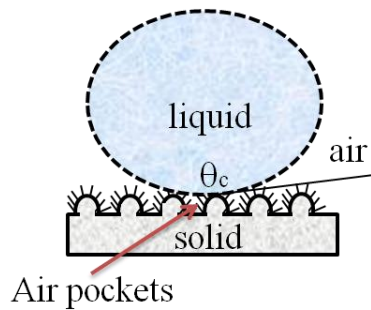
A. Flat surface



B. Microstructured surface



C. Hierarchical surface



D. Nanostructured surface

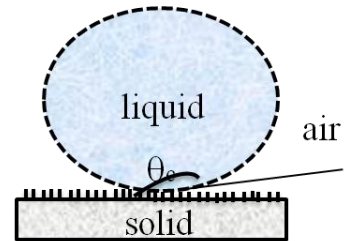


Figure 4-7. Schematic illustrations of water drops on different membrane surfaces

Thus, compared with PVDF flat membrane which usually has a contact angle of around 90° (Yang, Wang et al. 2011), the nanofiber PVDF membrane have a higher contact angle as 138° . At the same time, the microstructures of nanofiber PVDF membrane also provide a high adhesive force with water. The nanofiber PVDF membrane can capture maximal water droplets up to 25 mg. As water droplets can intrude into the large-scale grooves on the nanofiber membrane surfaces, as shown schematically in **Figure 4-7B**. It can be easily understood that the water sealed in the grooves between nanofibers would be clung to the membrane surface, showing a high contact angle hysteresis, even when the surface is tilted to any angle or even turned upside down. The contact angle hysteresis is determined by the difference between advancing and receding contact angles.

As shown in **Figure 4-6**, except for the original PVDF nanofiber membrane, the I-PVDF membrane modified for 5 min also shows high adhesive force with water. It may be because when the membrane was modified for a short period of time, the nanoparticle layers are too thin to reduce the gaps between the nanofibers, which are still big enough to allow water droplets to penetrate inside.

Furthermore, as shown in **Figure 4-6**, the I-PVDF membranes modified over 5 minutes show higher contact angles and weaker adhesive forces with water. After modified for more than 10 minutes, the membranes show superhydrophobic properties which have a high water contact angle above 150° and a low water sliding angle below 10° . Similar to a lotus surface, in addition to the microscale roughness provided by PVDF nanofibers, the surface of these microstructures is also rough with nanoscale asperities (silver nanoparticles) covered by hydrophobic long chain hydrocarbons. This hierarchical structure as shown schematically in **Figure 4-7C** provides air pocket formation, leading to the lowest contact area with an applied water droplet and resulting in reduction of contact angle hysteresis and adhesive force. For the case of this composite interface, consisting of a solid-liquid

fraction and liquid-air fraction, the Cassie-Baxter equation (Cassie and Baxter 1944) was employed to predict the contact angle as following:

$$\cos \theta_c = f_{SL}(R_f \cos \theta_0 + 1) - 1 \quad (4-3)$$

where θ_c is the contact angle calculated by Cassie-Baxter equation and f_{SL} is the fraction of the water droplet in direct contact with the surface. According to the equation, it can be easily predicted that the surface having a lower contact area between water and solid (a low f_{SL} value) have a higher contact angle.

For the S-PVDF membranes, after dipped in the electroless silver bath for only 5 minutes, the S-PVDF membranes already have a superhydrophobic surface. As observed from **Figures 4-5 C1** and **4-5 C2**, the S-PVDF membranes were covered by a layer of nanoparticles. The contact area between the water droplet and the surface is reduced by this nanostructured surface as shown schematically in **Figure 4-7D**. It is likely that the water droplet is constantly advancing and receding at unstable contact line points and moves easily. The contact angle for this surface can also be predicted by Cassie Baxter equation. After 20 minutes modification, the weights of I-PVDF and S-PVDF were increased by 42% and 8% respectively. More weight gain of I-PVDF is due to the modification carried out on bulk membrane.

4.3.4. Confirmation of nanostructures of modified membrane surfaces

In order to further observe the surface of membranes and prove the above explanations, the topologies of pristine PVDF and modified PVDF membranes were observed by AFM at tapping mode as shown in **Figure 4-8**. For each sample, a 3D map and a flat map along with a 2D profile in a given location (red line in figures) of the flat 3D are shown. A scan size of $2.5 \mu\text{m} \times 2.5 \mu\text{m}$ was measured to obtain a sufficient amount of bumps to characterize the surfaces and to maintain enough resolution to achieve an accurate test. The structures found with the AFM measurement correlate well with the FE-SEM images shown in **Figure 4-5**.

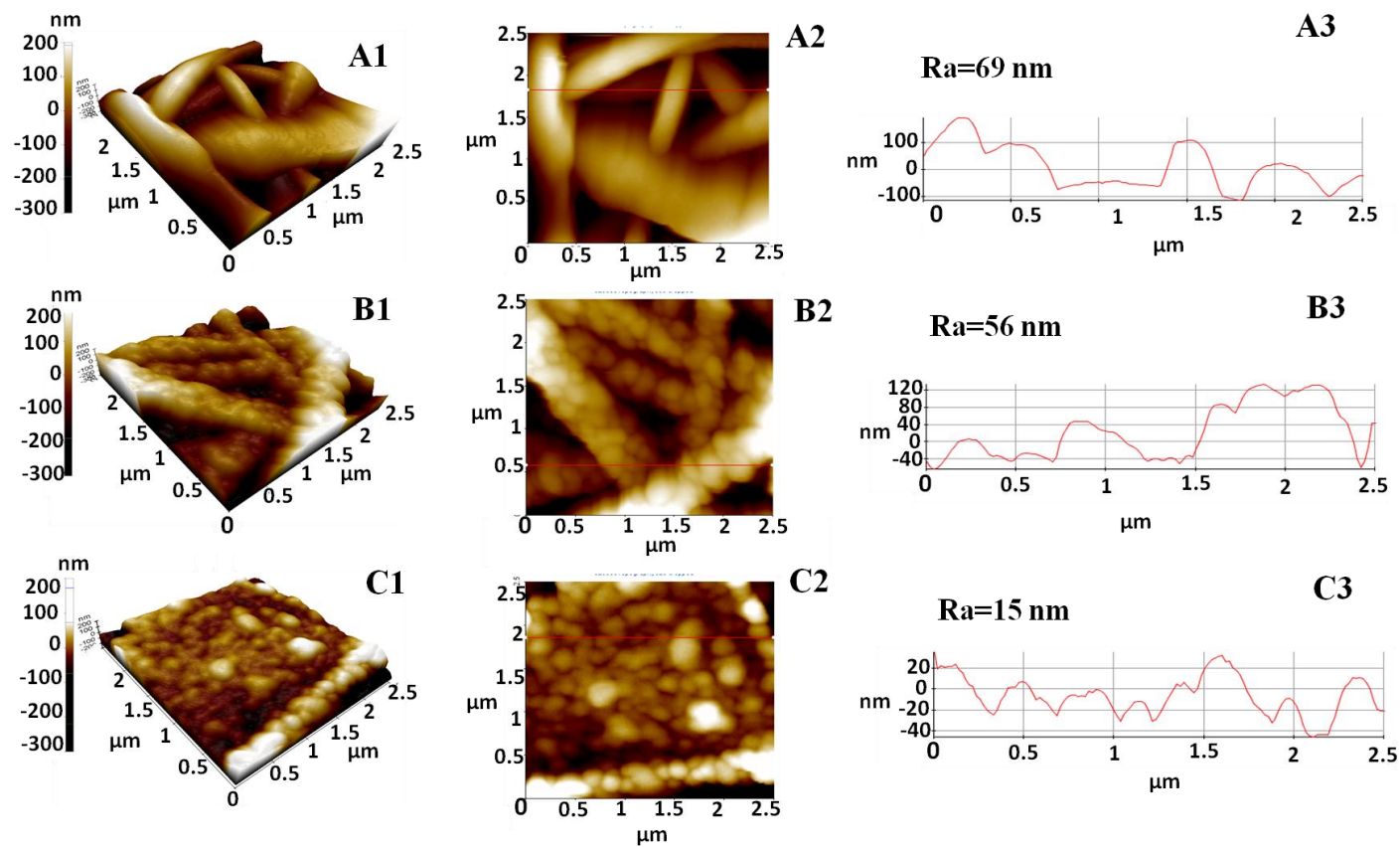


Figure 4-8. Surface height maps and flat maps along with 2D profiles in a given location of PVDF nanofiber membranes: (A1, A2, A3) original PVDF nanofiber membrane; (B1, B2, B3) I-PVDF; (C1, C2, C3) S-PVDF

As shown in **Figures 4-8 A1, 4-8 A2 and 4-8 A3**, the bumps caused by nanofibers in original PVDF membrane have higher heights and larger distances exist between each bump, which may make water droplet intrude into the grooves easily. The distances between the bumps on the I-PVDF surface are smaller, making the probability of air pockets formation increase and thus enhancing membrane hydrophobicity. It can be seen that more number of bumps exists in the S-PVDF surface. Even though the height of bumps on the S-PVDF surface are lower than those on other surfaces, the number of small gaps between the bumps are increased, which may provide more air pockets and make the surface superhydrophobic. Furthermore, compared with original PVDF nanofiber membrane, although the I-PVDF membrane has similar surface roughness as the pristine membrane (similar R_a values), silver nanoparticles coated on each nanofiber (as shown in **Figures 4-8 B1 and 4-8 B2**) enhance the membrane roughness in nanoscale, resulting in a hierarchical structure. In the case of the S-PVDF membrane, the roughness of membrane was reduced significantly due to the coverage of an entire silver nanoparticles layer on the membrane surface. Although the S-PVDF membrane has a smoother surface with a lower R_a value, its nanostructures consisting of silver nanoparticles on the membrane surface are able to decrease the contact area between solid and liquid surfaces and thus enhance its hydrophobicity.

4.3.5. DCMD performance

Although electrospun PVDF membranes possess high porosity and hydrophobicity which are desirable for MD application, membrane wetting is still a challenging issue for this type of membranes (Liao, Wang et al. 2013). However, it was found that the PVDF hollow fiber membranes with a similar pore size distribution and even lower hydrophobicity presented stable performance in the DCMD process for over 30 days (Hou, Wang et al. 2012). Probably, the phenomenon of easy wetting of nanofiber membranes is mainly due to their surface property, which exhibits strong adhesive force with water droplets. Thus it is

hypothesized that if water droplets are able to roll off from the membrane surface easily instead of adhering to it, the membrane should present enhanced anti-wetting performance. In this section, the modified membranes are applied in DCMD process to verify this assumption.

The common characteristics of the unmodified/modified membranes as well as a commercial flat sheet membrane are shown in **Table 4-1**. It can be seen that the mean pore size and maximal pore size of the S-PVDF nanofiber membrane are reduced significantly while the I-PVDF membrane keeps similar pore size as original PVDF membranes. It may be because that the relatively dense layer on the S-PVDF surface reduce the membrane pore size a lot, but the silver nanoparticles wrapped around nanofibers do not have a significant impact on the membrane pores. The thicknesses of unmodified/modified membranes are in the same range. After modification, the contact angles of the I-PVDF and the S-PVDF membranes increase to over 150° and the LEPs increase from 0.41 bar to 1.46, 0.86 bar, respectively, which illustrate that the modification indeed enhances the membrane hydrophobicity and improves the anti-wetting property of the membranes. Even the S-PVDF membrane possess smaller pore sizes, the I-PVDF has a higher LEP. This may be due to the fact that each nanofiber layer in the I-PVDF membrane was modified into superhydrophobic, which improved the membrane wetting resistance more effectively. The porosity of membrane is reduced from 79 % to 68 % after surface modification due to the coverage by a much denser layer of silver nanoparticles, but the porosity of the I-PVDF was kept as 77 %.

Table 4-1. Characteristic properties of original PVDF, modified I-PVDF and S-PVDF nanofiber membranes and commercial PVDF membrane

Sample code	PVDF	I-PVDF	S-PVDF	Commercial PVDF
Contact angle (°)	138 ± 1	153 ± 4	158 ± 3	135 ± 1
Mean pore size (μm)	0.31 ± 0.02	0.34 ± 0.01	0.18 ± 0.01	0.28 ± 0.01
Max pore size (μm)	0.59 ± 0.01	0.55 ± 0.01	0.41 ± 0.03	0.46 ± 0.01
Thickness (μm)	48 ± 5	47 ± 4	52 ± 1	111 ± 1
Porosity (%)	79 ± 2	77 ± 1	68 ± 8	62 ± 1
LEP(bar)	0.41 ± 0.07	1.46 ± 0.12	0.86 ± 0.22	1.19 ± 0.48
Tensile modulus E _t (Mpa)	6.9 ± 3.0	17.0 ± 1.3	10.8 ± 7.5	10.2 ± 2.6
Tensile at break σ _B (Mpa)	11.3 ± 2.8	10.6 ± 3.2	8.9 ± 1.5	4.7 ± 1.8
Strain at break δ (%)	47 ± 17	41 ± 11	34 ± 11	19 ± 11

The tensile properties of the electrospun PVDF nanofiber mats before and after modification were also measured. The tensile modulus of the I-PVDF and S-PVDF membranes were significantly increased after modification, which may be due to the rigid modified layers on the nanofibers. This implied that the membrane rigidity was increased after modification while the elastic property or flexibility was lost a bit. It is worth mentioning that compared with the commercial PVDF membrane, the I-PVDF and S-PVDF membranes have higher tensile modulus and tensile at break, suggesting that these modified nanofiber membranes have better mechanical strength than commercial membranes. Besides, the pore size distributions of the PVDF, modified PVDF nanofiber membranes and the

commercial PVDF membrane are shown in **Figure 4-9**. According to **Figure 4-9**, the I-PVDF membrane has similar pore size distribution as unmodified PVDF membrane, while the S-PVDF membrane has a smaller maximum pore size.

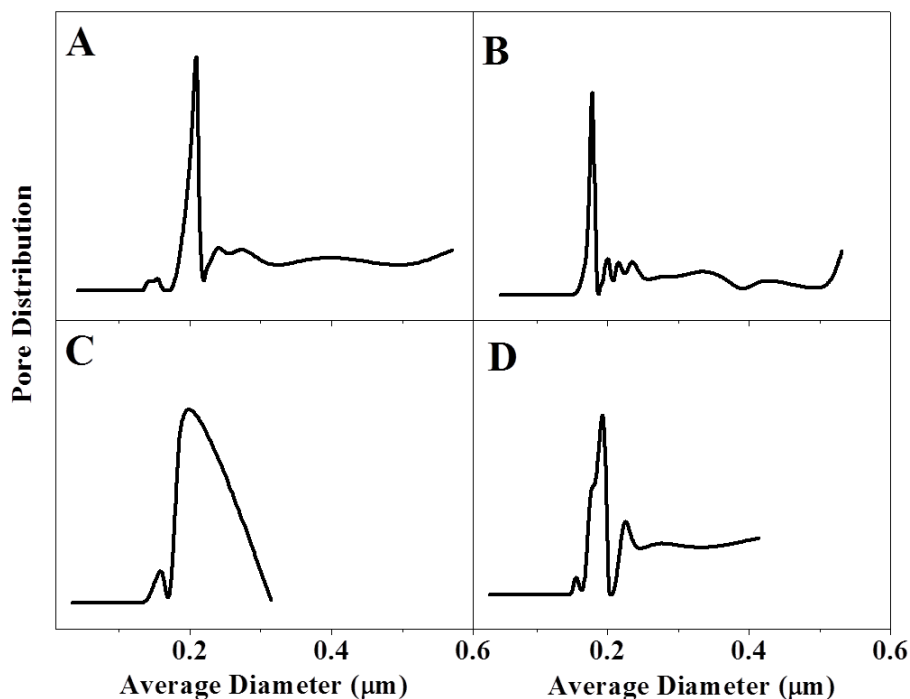


Figure 4-9. Pore size distribution of PVDF nanofiber membranes (A): original membrane; (B): I-PVDF; (C): S-PVDF membrane and (D): commercial PVDF flat sheet membrane

The continuous DCMD tests of the original PVDF nanofiber membrane, modified nanofiber membranes of the S-PVDF and I-PVDF as well as the commercial PVDF membrane are shown in **Figure 4-10**. It is observed from **Figure 4-10** that, although the PVDF nanofiber membrane presented a high flux of 35.7 kg/m²h, the membrane started to be wetted in less than 1 hour of operation. After integral modification, the I-PVDF nanofiber membrane showed a similar flux about 31.6 kg/m²h. And the conductivity at the permeation side remained a stable low value over the testing period of 8 h, indicating that the membrane did not suffer wetting. For the S-PVDF nanofiber membrane, though the membrane showed stable

performance, the flux of this modified membrane was much lower than original membrane, which is about $5.4 \text{ kg/m}^2\text{h}$. This result may be caused by the high mass transfer resistance generated by the dense modification layer on the membrane surface. Thus, compared with surface modification, the integral modification is preferred for DCMD application. Considering that the integral modification did not decrease membrane pores significantly, the main reason responsible for membrane anti-wetting improvement is believed to be the different surface morphology. The I-PVDF nanofiber membrane has a rough surface with hierarchical structures which causes water to roll off easily, while original nanofiber membrane has a rough surface with larger grooves which have a strong adhesive force with water droplets on the surface. The lotus-like self-cleaning property of the I-PVDF membrane prevents the membrane from wetting while the petal-like strong adhesive property of original PVDF membrane makes the membrane being wetted quickly. Furthermore, the I-PVDF has a higher flux than the commercial PVDF membrane as shown in **Figure 4-10**, suggesting that the superhydrophobic nanofiber membranes are a potential alternative for commercial MD membranes if its performance can be maintained for a sufficiently long time. A long-term performance test will be carried out in the next step.

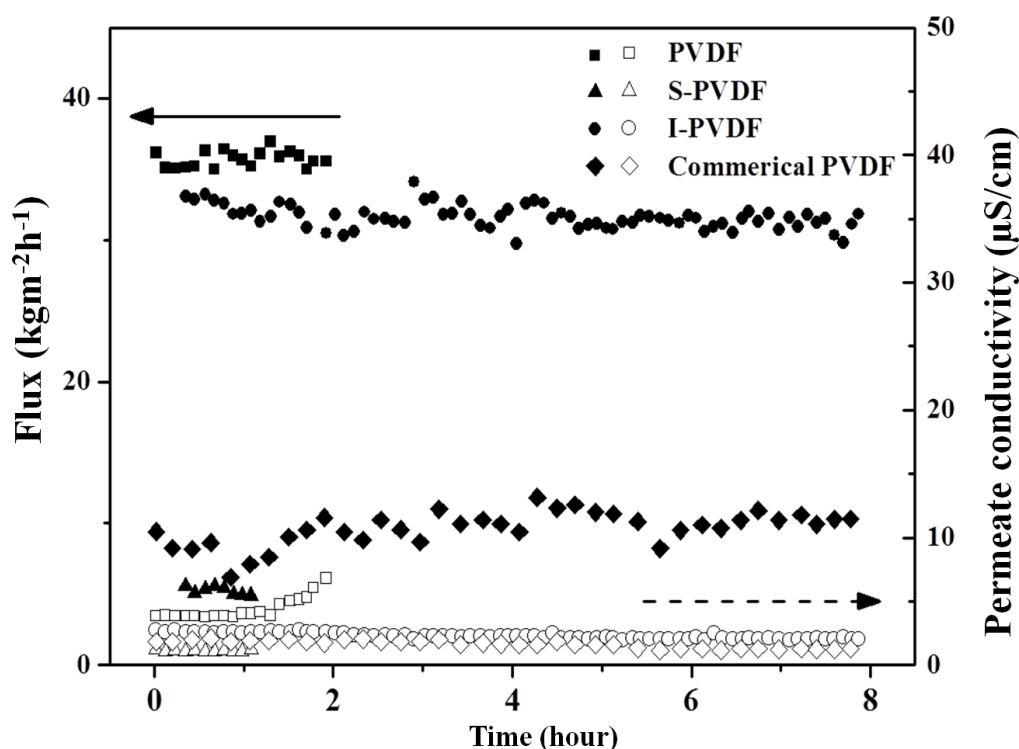


Figure 4-10. Continuous DCMD tests of the original PVDF, modified S-PVDF and I-PVDF and commercial PVDF membranes (3.5 wt% NaCl as feed, $T_f=333$ K, $T_p=293$ K, Flow rate at feed side=0.4 L/min, Flow rate at permeate side=0.6 L/min)

The DCMD performance of the I-PVDF nanofiber membrane was also compared with commercial PVDF membranes (Phattaranawik, Jiratananon et al. 2003; Martínez and Rodríguez-Maroto 2008; Zhang, Dow et al. 2010) and the PVDF-clay nanocomposite nanofiber membrane (Prince, Singh et al. 2012). As shown in **Table 4-2**, a considerable water flux enhancement has been achieved in this work. This is believed to be attributed to the open surface pore structure and thinner thickness of the PVDF nanofiber membrane with the aid of electrospinning. The superhydrophobic nature of the surface brought by the integral modification on all nanofibers renders the membrane anti-wetting property while remaining high water flux.

Table 4-2. DCMD performances of flat-sheet MD membranes for desalination

Membrane	Mean pore size	Contact angle	Porosity	Feed solution property				Permeate solution property	Permeation flux
	(μm)	($^{\circ}$)	(%)	Solution	v_f (m s^{-1})	$T_{f,in}$ ($^{\circ}\text{C}$)	$T_{p,in}$ ($^{\circ}\text{C}$)	v_p (m s^{-1})	($\text{kg m}^{-2} \text{h}^{-1}$)
Durapore ^a	0.28	135	48	3.5 wt% NaCl solution	0.05	60	20	0.14	10.6
GE Osmonics (Zhang, Dow et al. 2010)	0.30	113	81	1wt% NaCl solution	0.36	60	20	0.36	9.1 ^b
GVHP (Mart ínez and Rodr íguez-Maroto 2008)	0.16	-	70-75	1 M NaCl solution	0.35	40	20	0.35	8.1 ^b
GVHP (Mart ínez and Rodr íguez-Maroto 2008)	0.22	-	62	Pure water	laminar flow	60	20	laminar flow	8.4 ^b
HVHP(Phattaranawik, Jiraratananon et al. 2003)	0.45	-	66	Pure water	laminar flow	60	20	laminar flow	10.3 ^b
PVDF-Clay nanofiber membranes(Prince, Singh et al. 2012)	0.58	154	82	3.5 wt% NaCl solution	-	80	17	-	5.7 ^b
I-PVDF (current work)	0.34	153	66	3.5 wt% NaCl solution	0.05	60	20	0.14	31.8

a. The data was tested in our lab using the commercial Millipore Durapore membranes.

b. The flux was read from figures shown in papers and converted the permeation flux in the same unit

4.4. Conclusions

Superhydrophobic PVDF nanofiber membranes for DCMD application have been successfully fabricated by electrospinning followed by a surface modification to optimize surface morphology and roughness. This study reveals following points:

- The modification method including dopamine surface activation, silver nanoparticle deposition and hydrophobic treatment is an effective way to make the PVDF nanofiber membrane being superhydrophobic. This method is versatile not only because of simple reagents and mild reaction conditions used, but also due to its applicability to all nanofiber membranes made by any polymer.
- The surface morphology and topology of pristine and modified PVDF nanofiber membrane were studied to elaborate the reason causing superhydrophobic property of the modified membrane. It was found that water droplets on the hierarchical or nanostructured membrane surface are unstable and easy to roll off.
- Compared with unmodified membrane, the modified I-PVDF nanofiber membrane exhibits stable performance in DCMD process. As the pore size distribution of the two membranes are similar, the surface property is believed to play an important role in determining nanofiber membrane performance in MD. The high adhesive force with water make the pristine nanofiber membrane being wetted easily while the superhydrophobicity of modified I-PVDF nanofiber membrane would enhance membrane anti-wetting property.
- The I-PVDF can achieve a high and stable MD water flux of $31.6 \text{ kg/m}^2\text{h}$ using a 3.5 wt% NaCl as feed solution while the feed and permeate side temperature were fixed at 333 K and 293 K, respectively.

CHAPTER 5

Fabrication of bioinspired composite nanofiber membranes with robust superhydrophobicity for DCMD

5.1. Introduction

As demonstrated in Chapter 4, superhydrophobicity of fabricated membrane could enhance membrane stability in MD process. However, the robustness of superhydrophobic layer in long-term usage as well as the convenience to achieve superhydrophobicity are the issues we should further investigate.

Nature provides many inspirations for novel synthetic materials. FE-SEM images of the most well-known example of superhydrophobic natural plant, lotus leaf (inserted pictures in **Figure 5-1**), reveal that hydrophobic wax-like materials are decorated on the protrusions and valleys as the secondary structure. Superhydrophobic glass membranes with integrated arrays of nanopiked microchannels were prepared by glass fiber drawing, dissolving template materials from microchannels and chemical etching, which retarded fouling during operation due to reduce water-membrane contact area (Ma, Hong et al. 2009). However, the resultant membranes required a complicated preparation process and exhibited a low mass flux of 3.3 kg/m^2 per hour at 65°C when feed was 5 wt% salt solutions. A hierarchical structure with multilevel roughness on microporous PVDF membrane was constructed by means of TiO_2 deposition and following hydrophobic modification, which increased the LEP and water contact angle of commercial PVDF membrane (Razmjou, Arifin et al. 2012). The achieved membrane showed permeation flux around $10 \text{ L/m}^2\text{h}$ when salt concentration of feed solution was 3.5

wt%, and feed and permeation temperatures were set as 323K and 298K respectively, which needs further improvement.

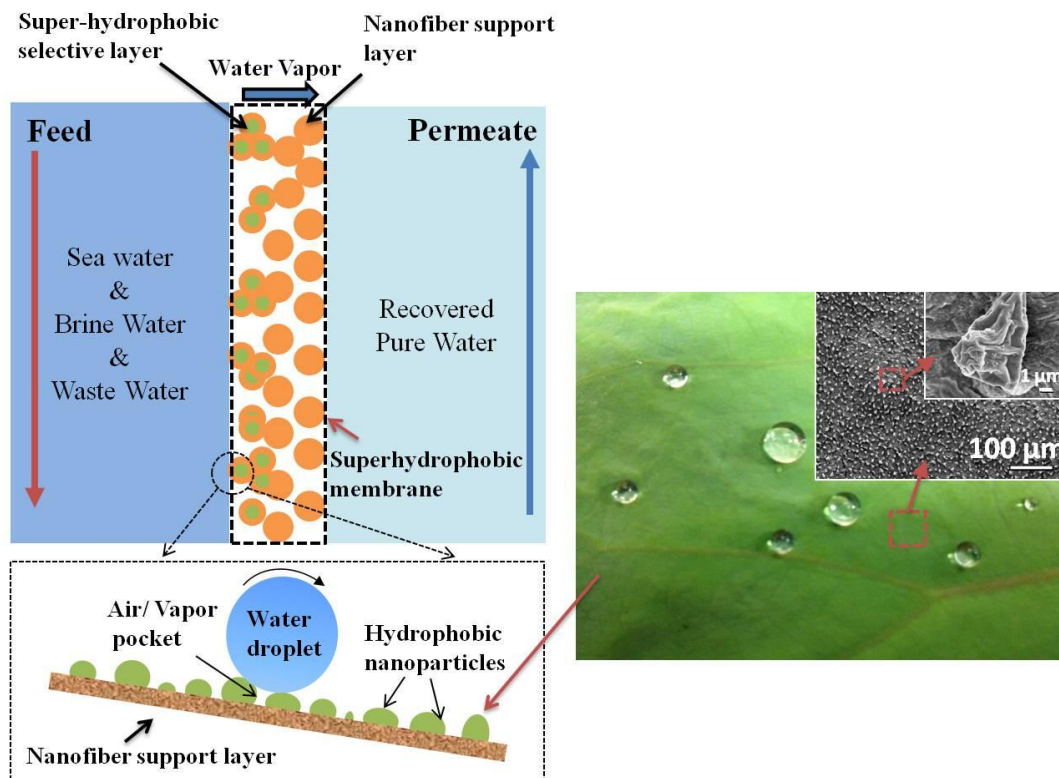


Figure 5-1. Schematic of an ideal MD membrane with a lotus leaf-like superhydrophobic selective layer and a scaffold-like nanofiber support layer

Inspired by the lotus leaf structure, in our current work, a novel nanocomposite MD membrane has been designed as shown in **Figure 5-1**. A scaffold-like PVDF nanofiber membrane made by electrospinning, with high porosity and low tortuosity, and an adjustable thickness, is used as a mechanical support. A silica-PVDF composite selective layer, which has an extremely high water contact angle ($>150^\circ$) and water repelling properties, is formed on the top of the support via the same electrospinning technique. It is expected that the silica-PVDF composite layer has a similar hierarchical structure to the lotus leaf, and is able to form air pockets or water vapour pockets on the membrane surface during

the MD process, leading to the lowest contact area between water and the membrane. The unstable contact line points can force the water droplets to roll off the membrane surface spontaneously. Furthermore, the effects of the diameter of silica on water contact angle, water sliding angle of resultant membranes were studied. The durability of the superhydrophobic selective layer was tested in ultrasonic treatment. Finally, the DCMD tests were performed to demonstrate the stable high performance of the newly developed membranes in long-term MD operations. Due to the unique architecture, the membranes would possess better performance than other superhydrophobic membranes mentioned above.

5.2. Materials and methods

5.2.1. Materials

Silica with an average aggregate particle size between 0.2 to 0.3 μm and in spherical shapes with a particle size of 5 – 15 nm were purchased from Sigma-Aldrich, Singapore. For the silica surface modification, α , ω -triethoxysilane terminated perfluoropolyether ((EtO)₃Si-PFPE-Si(OEt)₃) with an average molecular weight between 1750 to 1950 was obtained from Solvay Solexis under the trade name Fluorolink® S10 and was coded as FS10. Tetraethoxysilane (TEOS) (Merck, Singapore) was used as an additive to enhance the modification efficiency. N-hexane also provided by Merck in Singapore was used as a dispersive solvent for modification. All reagents were used as received. Other materials have been described in section 3.2.1.

5.2.2. Silica modification and dope preparation

Briefly, a desired amount of silica nanoparticles was stirred rapidly over night in N-hexane solution in which FS10 and TEOS with a mass ratio of 3:2 was added. The total concentration of FS10 and TEOS was 5 wt%. The modified SiO₂ nanoparticles were then separated by centrifugation and annealed in a vacuum oven

at 100 °C for 1 hour. The resultant white powder was stored over night in a vacuum oven at 50 °C prior to further experiments and characterization.

PVDF precursor solutions for the superhydrophobic layer were prepared by initially dissolving 5 wt.% PVDF HSV 900 in DMF. Then modified SiO₂ with different diameters were dispersed in prepared 5 wt% PVDF solution by stirring rapidly at room temperature. The mass ratio of modified SiO₂ particles/PVDF was fixed at 2:1 to guarantee the superhydrophobic effects (Wang, Li et al. 2011).

5.2.3. Electrospinning of PVDF nanofiber membranes and composite superhydrophobic membranes

The PVDF nanofiber membranes and superhydrophobic composite silica-PVDF membranes were prepared via an electrospinning setup as reported in our previous work (Liao, Wang et al. 2013). As shown in **Table 5-1**, the PVDF nanofiber support was fabricated by a 8 wt% PVDF dope. After spinning the porous substrate, the superhydrophobic surface layers were electrospun using two modified silica-blended PVDF dopes. One dope was the mixture of PVDF and small silica particles with diameters of 5-10 nm while another was prepared by dispersing larger hydrophobic SiO₂ particles with aggregate diameters of 0.2-0.3 μm in a 5 wt% PVDF dope. As the purpose was to investigate the effects of the superhydrophobic layer precisely on the membrane properties, all the composite membranes had the same substrate layer.

Table 5-1. Electrospinning conditions of PVDF nanofiber and composite membranes

Membrane ID	PVDF (support layer)	S-PVDF (selective layer)	L-PVDF
Dope composition (wt. %)	PVDF HSV900/DMF: 8/92 (0.004% wt LiCl)	PVDF HSV900/SiO ₂ (small diameter) /DMF: 5/10/95	PVDF HSV900/SiO ₂ (large diameter) /DMF: 5/10/95
Dope flow rate (mL min ⁻¹)	0.03	0.02	
Travel Speed (mm sec ⁻¹)	0.1		
Travel Distance (cm)	8		
Distance (cm)	15	12	
Voltage (kV)	28		

5.2.4. Characterizations of PVDF nanofiber and composite membranes

A homemade setup for liquid entry pressure of water (LEPw) measurement is shown in **Figure 5-2**. A digital pressure gauge was installed on top of a stainless steel tank which was used as the reservoir for distilled water. A tested nanofiber membrane with an effective membrane area as 10 cm² was installed in one dead-end flat-sheet membrane cell. During the LEPw test, hydraulic pressure provided by compressed N₂ was applied on the nanofiber membrane surface on the top of membrane. The hydraulic pressure was increased with a step of 2 psi and each pressure was maintained for 10 min. The pressure read at digital pressure gauge was recorded as LEPw when the first drop of permeate was observed.

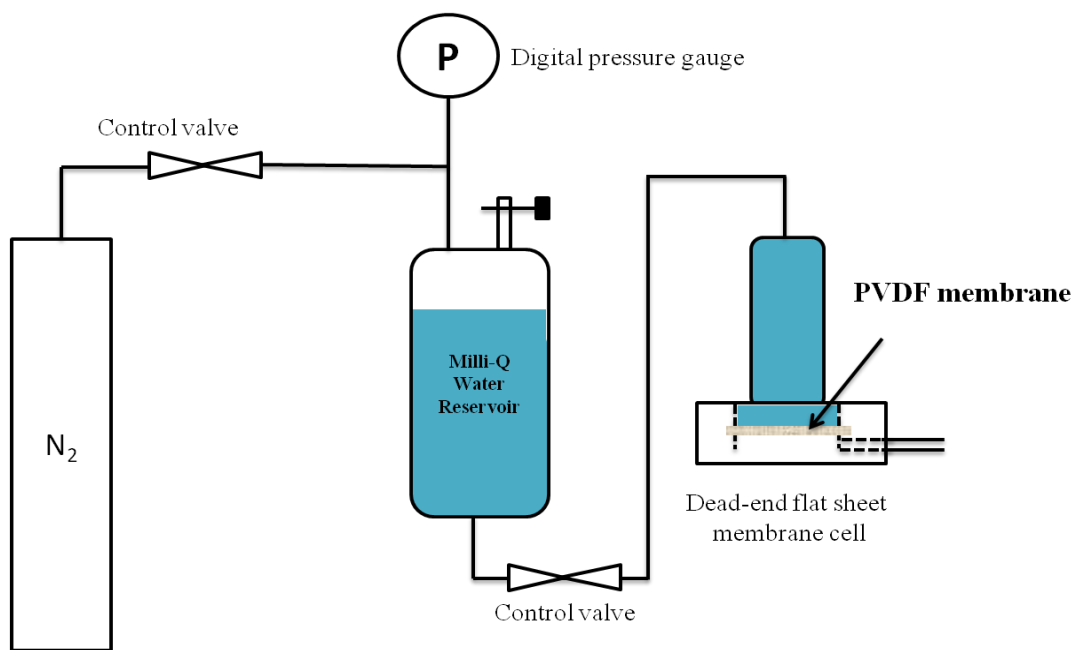


Figure 5-2. Schematic diagram of homemade LEPw test setup

To prepare a superhydrophobic and water-repellent surface, it is necessary to have high water contact angle and, more importantly, the contact angle hysteresis should be as small as possible, which leads to a small water sliding angle (SA). As shown in **Figure 5-3**, the water SA of the membrane was determined by placing a 10 μL water droplet on the horizontal membrane surface, which was then inclined to tilt gradually until the water droplet started to roll off from the surface. The SA was calculated by the equation:

$$\tan \theta_{SA} = \frac{a}{b} \quad (5-1)$$

where a is the raised height of composite membrane and b is the corresponding horizontal length of the membrane when the droplet started moving downward. θ_{SA} is the water sliding angle of each sample. Each sample was tested at least 5 times.

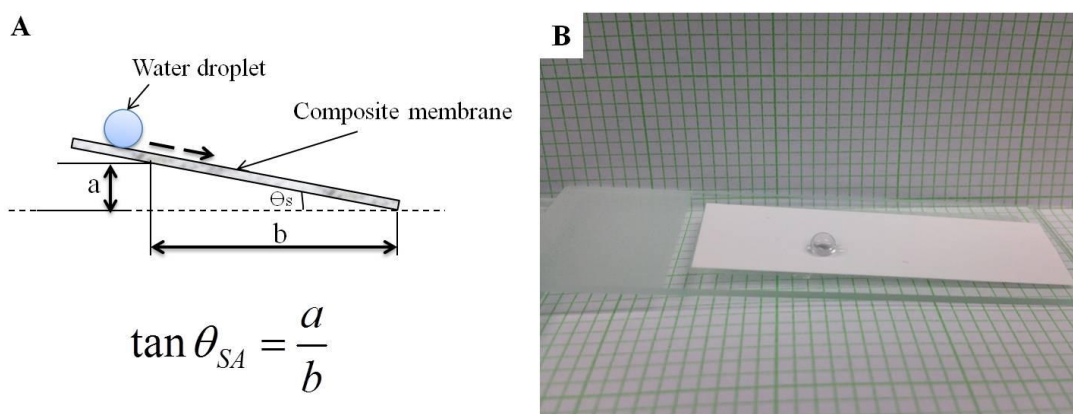


Figure 5-3. The sliding angle test configuration: (A) sliding angle calculation; (B) image of sliding angle testing

Other characterizations have been illustrated in section 3.2.4 and section 4.2.4. The MD performance was tested in the same DCMD setup described before (section 3.2.5).

5.3. Results and discussion

In order to prepare a robust superhydrophobic surface, the silica nanoparticles were first modified by perfluoropolyether (FS10), which made them hydrophobic to easily disperse in the second PVDF dope solution and able to stick to the PVDF ‘islands’ on the substrate, allowing the top surface to be more durable (Wang, Li et al. 2011). The chemical structure of the modifying agent, FS10, and the possible modification reaction pathway on the SiO₂ surface are given in **Figure 5-4**, which are demonstrated by XPS analysis.

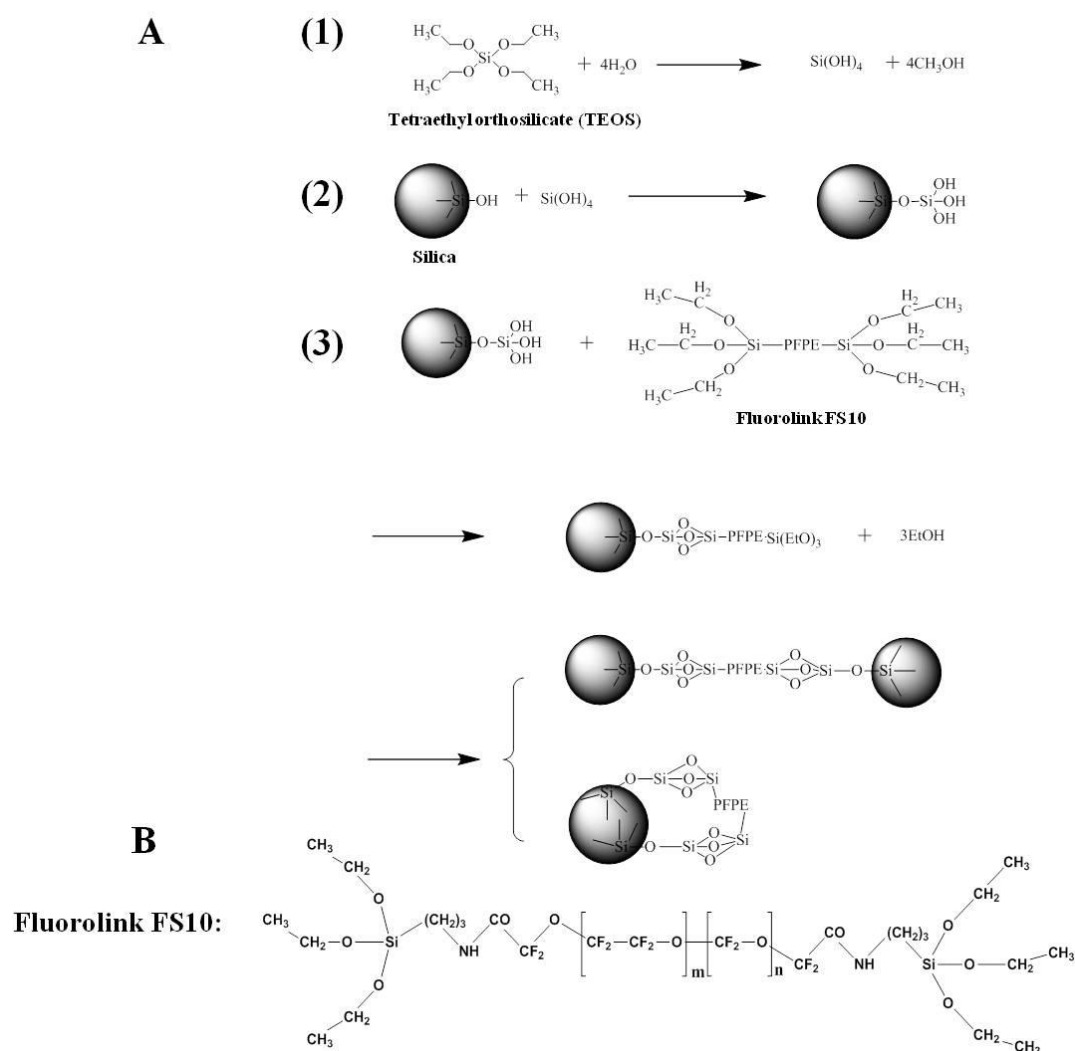


Figure 5-4. Schematic diagram of the mechanism of modification reaction on SiO₂ nanoparticle surface (A) and chemical structure of Fluorolink FS10 (B)

To examine the surface enrichment of fluorocarbon chains on the modified silica, an XPS analysis was carried out on unmodified and modified SiO₂ surfaces, as shown in **Figure 5-5**. It confirmed that the silica surface was successfully covered by the FS10, which shifted the hydrophilic silica nano-particles with OH groups to hydrophobic fluorinated nano-particles. As shown in **Figures 5-5A** and **5-5C**, compared with the original silica particles which only have silica and oxygen elements on the surface, the FS10 grafted silica particles (FS10-SiO₂) possess

additional carbon, nitrogen and fluoride elements. According to the chemical structure of FS10 shown in **Figure 5-4**, these additional elements are from the hydrophobic chemical FS10 reacted on the silica surface. The surface content of silica atoms was significantly lower than that of corresponding bulk concentration, indicating that a strong surface enrichment of organic phase such as carbon and fluoride elements was produced after the modification reaction.

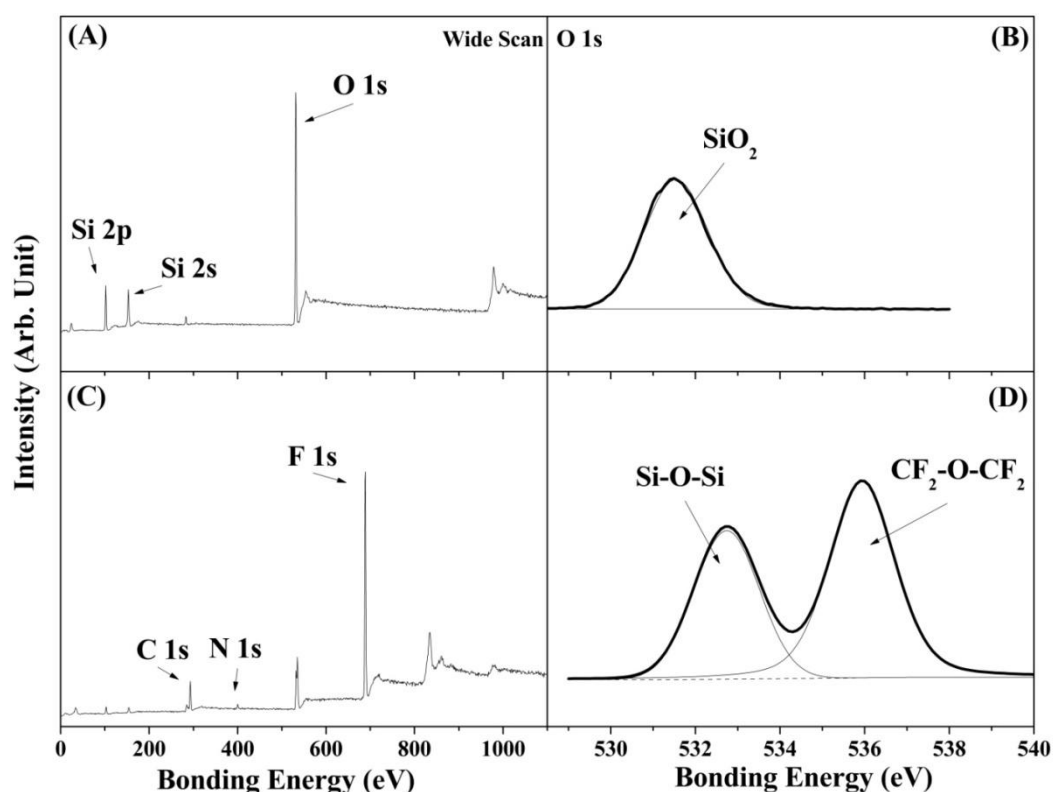


Figure 5-5. The XPS wide-scan and O 1s core-level spectra of (A and B) original SiO₂ nanoparticles and (C and D) modified SiO₂ surface.

Furthermore, the high-resolution of XPS O1s core-level spectra of control silica (**Figure 5-5B**) and fluorinated silica (**Figure 5-5D**) were curve-resolved into peaks to derive more information on the fluorinated segments segregation at the surface. As shown in **Figure 5-5B**, the binding energy oxygen peak at 531.8 eV corresponds to the chemical bonds in SiO₂ (Egerton, Parfitt et al. 1983). Concerning the O1s core-level spectra of modified silica, a figure with double peaks is clearly

observed in **Figure 5-5D**. While the oxygen components attributed to the PFPE segments ($\text{CF}_2\text{-O-CF}_2$) were centered at a higher binding energy around 536.3 eV, oxygen atoms linked to silica (Si-O-Si) which assisted the reaction between silica surface and FS10 are associated with the less pronounced peak at around 533.1 eV (Fabbri, Messori et al. 2006). The minor extent of oxygen double bonded to carbon present in FS10 also gives a small contribution to the second peak. By evaluating the chemical composition on silica surfaces before and after modification reaction, it is confirmed that the FS10 successfully covered the silica surface, which shifted the hydrophilic nanoparticles with OH groups on the surface to be fluorinated hydrophobic nanoparticles.

To further demonstrate that the superhydrophobic membrane surface contains modified silica particles and the modified silica was covered and protected by thin PVDF layers, independent evaluations of the surface characteristics of the original PVDF nanofiber and silica-PVDF composite membranes were conducted by XPS. As shown in **Figure 5-6A**, the C 1s core-level spectrum of the PVDF nanofiber membrane can be simply curve-fitted with two peak components, one at a binding energy (BE) of 285.0 eV for the carbon bonded to hydrogen (C-H_x) and the other at BE of 290 eV for a single carbon bonded to fluorine (C-F_2), which is typical of the C1s core level spectrum for PVDF (Moussaif, Pagnouille et al. 2000). As shown in **Figure 5-6B**, small amounts of hydrocarbon and fluoride carbon were also present on FS10-SiO₂ due to the chemical structure of FS10, and the prominent CF envelope can be fitted with two peaks that correspond to $\text{O-CF}_2\text{-O}$ and $\text{O-C}_2\text{F}_4\text{-O}$ at 294.9 eV and 293.5 eV, respectively (Toselli, Gardella et al. 2003). Beside these peaks, there are two other peaks that are attributed to the $\text{O-CH}_2\text{-C}$ (286.6 eV) and -CO-N- (287.9 eV) chemical bonds of the FS10 structure (Sastry 1997). According to the parameters determined from the curve fitting of the superhydrophobic silica-PVDF composite membrane (**Figure 5-6C**), the C1s

envelope identifies the primary presence of $-\underline{\text{CH}}_2-$ and $-\underline{\text{CF}}_2-$, which means the surface layer (within 10 nm) was mainly bound and covered by PVDF material.

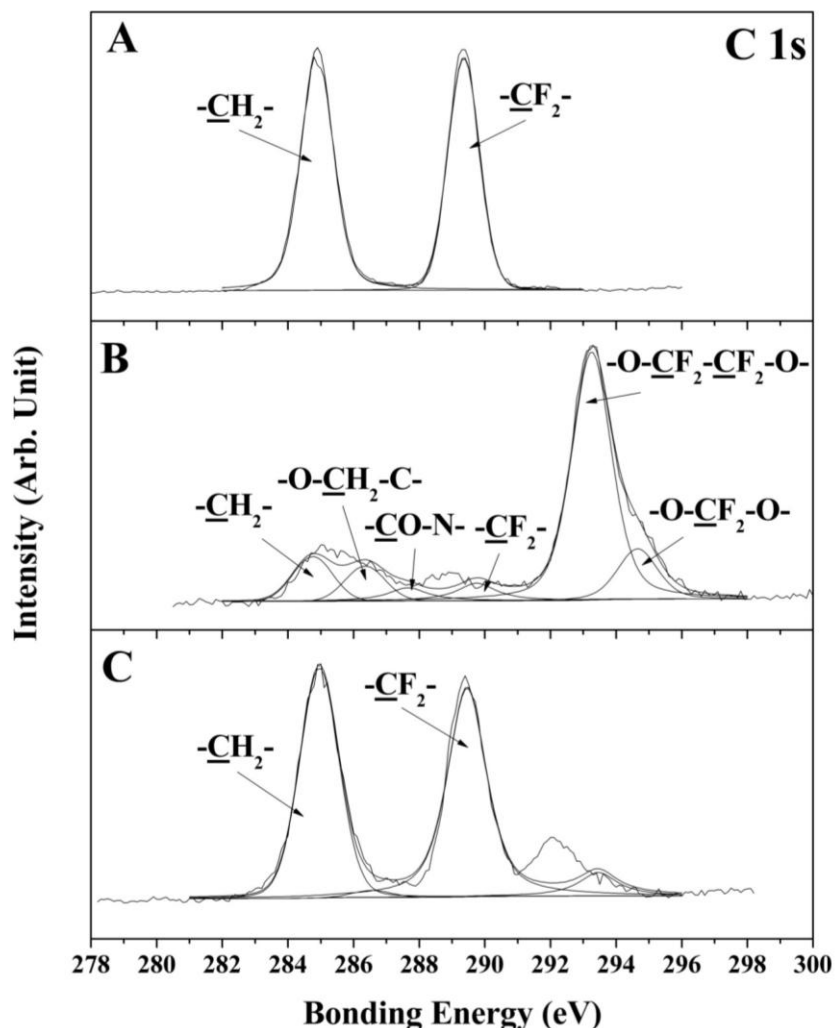


Figure 5-6. The XPS C 1s core-level spectra of (A) PVDF nanofiber membrane, (B) modified silica and (C) modified SiO₂-PVDF composite membrane

Optical photographs of the PVDF nanofiber membrane which was fabricated by 8 wt% PVDF dissolved in DMF and the superhydrophobic silica-PVDF composite membrane are shown in **Figures 5-7A** and **5-7B**, respectively. As shown in the FE-SEM image inserted in **Figure 5-7A**, the PVDF nanofiber membrane surface presents a continuous arrangement of nanofibers with an average

diameter of 170 nm. The nanofiber PVDF membrane possesses a contact angle of 142.8° , which is much higher than other PVDF membranes prepared by non-solvent induced phase separation (Chen, Yang et al. 2013). However, the PVDF nanofiber membrane also shows a high contact angle hysteresis. For example, it is observed that a water droplet cannot roll off from its surface even when the membrane is turned upside down as shown in small inserted pictures in **Figure 5-7C**. This is the so-called petal effect or Cassie impregnating wetting state (Feng, Zhang et al. 2008). Water droplets tend to penetrate into the larger-scaled grooves between the nanofibers and remain spherical above the nanofiber membrane. It is evident that the water sealed in the micro-sized grooves would assist water droplets in adhering to the membrane surface due to the surface tension force.

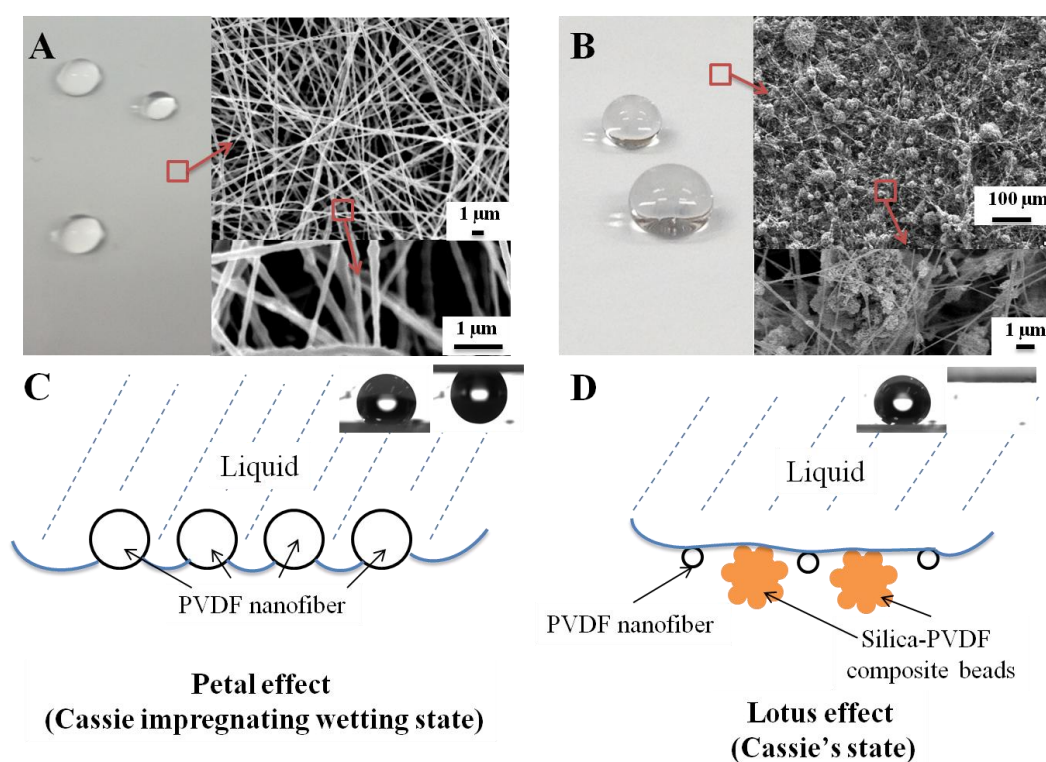


Figure 5-7. Photo images, FE-SEM surface morphologies of PVDF nanofiber membrane (A) and superhydrophobic silica-PVDF composite membrane (B) and corresponding schematic illustrations of nanofiber and superhydrophobic composite membrane (C and D)

On the other hand, after the modified SiO₂-PVDF blended dope (10 wt% SiO₂ and 5 wt% PVDF were mixed in DMF solvent homogeneously) was sprayed via electrospinning onto the nanofiber membrane surface, the nanofibers and nano-beads structure could be formed on the composite membrane surface as shown in **Figure 5-7B**. The nanofiber diameter was around 90 nm. The thinner diameter of the modified PVDF nanofibers was probably due to the lower polymer concentration used compared with the pure PVDF dope used for preparing the substrate (Liao, Wang et al. 2013). The water contact angle of the composite membrane is 156.3°. Additionally, the composite membranes possess excellent water repellence property as shown in **Figure 5-7D**. Similar to lotus leaf, the composite silica-PVDF membranes have a microstructure consisting of modified silica-PVDF mixed islands and a nanostructure comprising PVDF-bound silica nanoparticles on the islands surface. This hierarchical structure prevents water from intruding into the microstructural spaces. The triple contact lines between the solid and liquid or the solid and air on the randomly rough surface are expected to be contorted and unstable, which makes the water droplets easily moved (Bhushan and Jung 2011).

The deposition of modified silica-PVDF mixture on the PVDF nanofiber support by electrospinning is the critical step to shift the membrane from hydrophobic to superhydrophobic. The effects of the modified silica particle sizes which are 0.2- 0.3 µm and 10 - 15 nm, respectively, and spinning layers on water contact angle and sliding contact angle were investigated as shown in **Figure 5-8**.

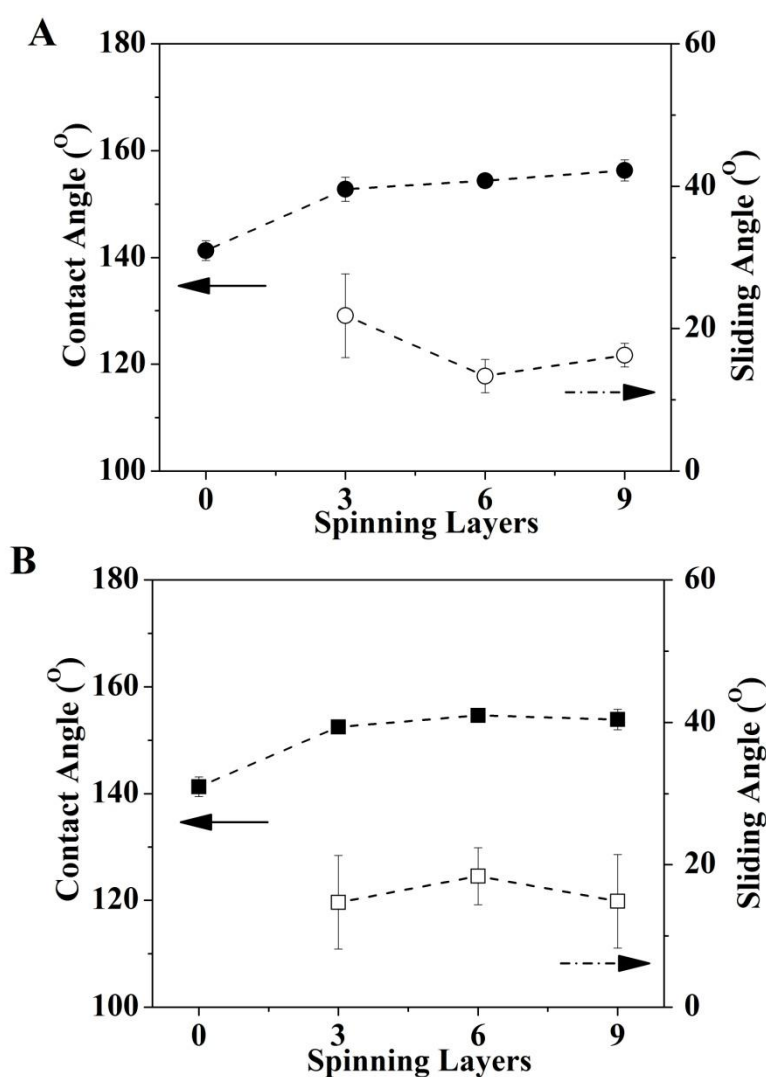


Figure 5-8. Variation of contact angle and sliding angles of composite membranes with different nano-particle sizes and various electrospinning times: (A) membrane fabricated by PVDF/ small FS10-SiO₂ mixture; (B) membrane fabricated by PVDF/ large FS10-SiO₂ mixture

It can be seen from **Figure 5-8** that the diameter of the modified silica particles has no obvious impact on water contact and sliding angles of as-prepared membranes. After spinning 3 layers of the composite dope, the membranes have contact angles over 150° and exhibit water repellence properties due to the

formation of both microstructures and secondary nanostructures. With an increase in spinning layer number, the contact angle of the composite membranes increased progressively to a plateau and the sliding contact angle decreased slightly. This is probably due to the enhancement of hierarchical structures. Furthermore, the water sliding angle difference between the PVDF nanofiber membrane and the composite membrane is pronounced. The PVDF nanofiber membrane shows a strong adhesive force for water droplets so that they cannot move, while the composite membrane has a low sliding angle less than 20° . It is believed that the micro- and nano-roughness increased the presence of air pockets on the composite membrane surface significantly, which could effectively trap air between the liquid and solid surface, preventing the liquid from penetrating into the surface cavities. Thus the build-up of a discrete contact between the liquid and the solid leads to the drastic reduction of sliding contact angle (Chen, Fadeev et al. 1999). Since the composite membranes with 9 superhydrophobic layers have the highest contact angle and the lowest sliding angle, the S-PVDF and L-PVDF, which refer to the membranes with small and large modified silica nanoparticles, respectively, were chosen for further study.

Prior to using the superhydrophobic membranes for MD tests, their durability was examined by ultrasonic treatment. As shown in **Figure 5-9**, compared with the L-PVDF membrane, the water contact angle of S-PVDF membrane decreased slightly after ultrasonic treatment. The possible reason is that a small amount of the modified silica particles on the S-PVDF membrane might be removed during the ultrasonic treatment, while the big particles on the L-PVDF membrane have better inter-tangled force with the polymer chains, making them more stable on the membrane surface. Nevertheless, both the S-PVDF and L-PVDF membranes still possess high contact angles above 150° and excellent water repellent properties after ultrasonic treatment for 30 minutes. Under FE-SEM, the surface morphologies of the S-PVDF and L-PVDF membranes also show no obvious difference before and after 30 min ultrasonic-treatment.

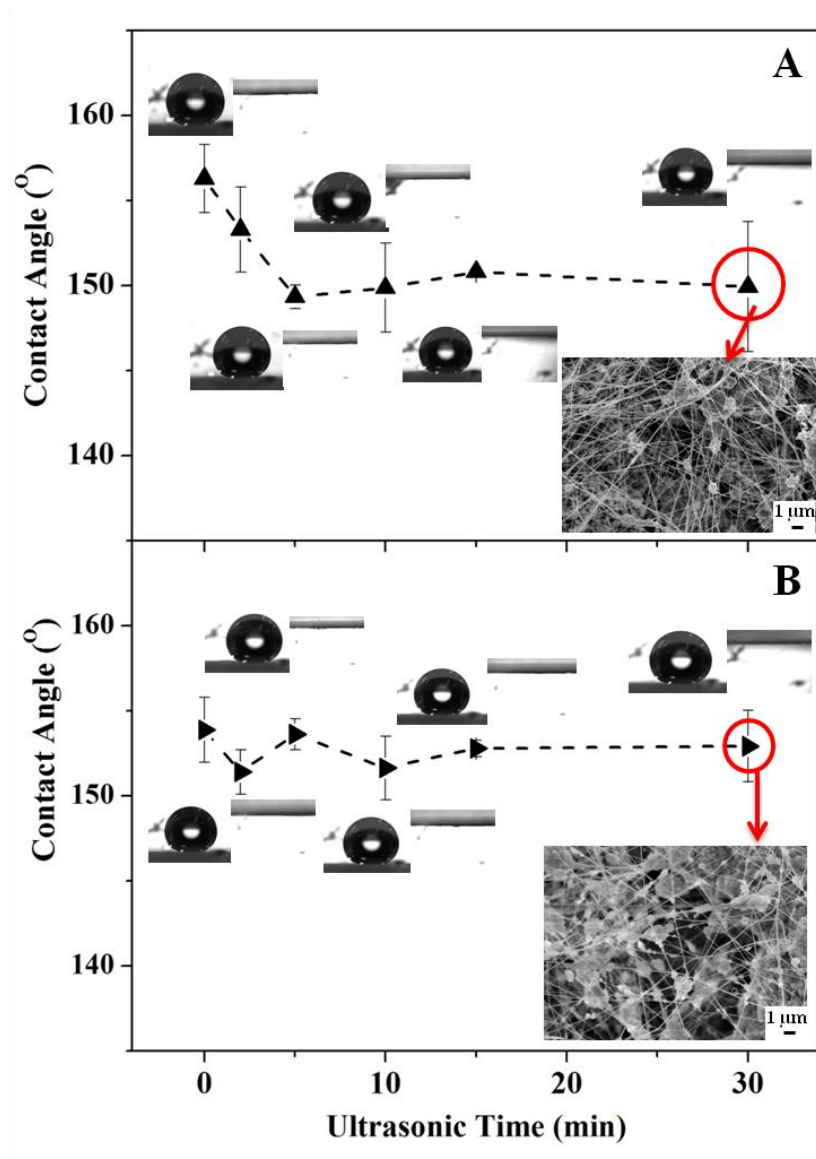


Figure 5-9. Behavior of the water droplets on the superhydrophobic surface of S-PVDF (A) and L-PVDF (B) after ultrasonic-treatment for different times

The MD performances of the PVDF nanofiber membrane, the composite membranes S-PVDF, L-PVDF and a commercial PVDF membrane (Durapore® Membrane filter, Millipore, Singapore) were tested in the DCMD configuration. As shown in **Table 5-2**, the PVDF nanofiber membrane has 142.8° water contact angle, 0.68 μm surface mean pore size and 1.27 μm max pore size. The composite membranes S-PVDF and L-PVDF have higher contact angles of 156.3° and 153.9°;

respectively, with similar surface pore sizes that are much larger than the commercial Millipore hydrophobic membranes. In addition, the three electro-spun membranes exhibit higher porosity, around 83%, than the commercial membrane. For a fair comparison, all the membranes used in the DCMD tests have a similar thickness between 100 to 130 μm . Due to the surface superhydrophobicity, the S-PVDF and L-PVDF membranes present a higher LEPw than the PVDF nanofiber membrane. The commercial PVDF has the highest LEPw due to its smaller pore size. Other membrane properties are also included in **Table 5-2**.

Table 5-2. Characteristic properties of PVDF nanofiber, S-PVDF, L-PVDF composite and commercial PVDF membranes

Membrane ID	PVDF	S-PVDF	L-PVDF	Commercial PVDF
Contact angle (°)	142.8 ± 1.4	156.3 ± 2.0	153.9 ± 1.9	135.0 ± 1.3
Surface mean pore size (μm)	0.68 ± 0.03	0.69 ± 0.02	0.77 ± 0.02	0.28 ± 0.01
Surface max pore size (μm)	1.27 ± 0.02	1.23 ± 0.01	1.22 ± 0.01	0.46 ± 0.01
Thickness (μm)	115 ± 8	102 ± 15	129 ± 8	111 ± 1
Bulk porosity (%)	85 ± 1	82 ± 2	83 ± 1	62 ± 1
LEPw(bar)	1.13 ± 0.08	1.75 ± 0.05	1.79 ± 0.07	2.25 ± 0.17
Tensile modulus Et (Mpa)	42 ± 5	35 ± 2	33 ± 2	10 ± 2
Tensile at break σ_B (Mpa)	9.6 ± 0.9	3.7 ± 0.6	4.2 ± 0.6	4.7 ± 1.8
Strain at break δ (%)	160 ± 3	99 ± 7	87 ± 22	19 ± 11

The MD tests were performed using a 3.5 wt% NaCl solution as the feed solution under a temperature of 60°C and the permeate side was set at 20°C. As shown in **Figure 5-10**, the permeate flux of the composite membranes S-PVDF and L-PVDF were 18.1 $\text{kg/m}^2\text{h}$ and 18.9 $\text{kg/m}^2\text{h}$, respectively, while the PVDF nanofiber membrane had a flux around 12.3 $\text{kg/m}^2\text{h}$ and the commercial PVDF flux was about 10 $\text{kg/m}^2\text{h}$. The composite membranes showed a stable performance over

50 hours of testing time and produced high quality water with conductivity below 5.0 $\mu\text{S}/\text{cm}$. However, the conductivity of the product water from the PVDF nanofiber membrane generally increased during 45 hours usage.

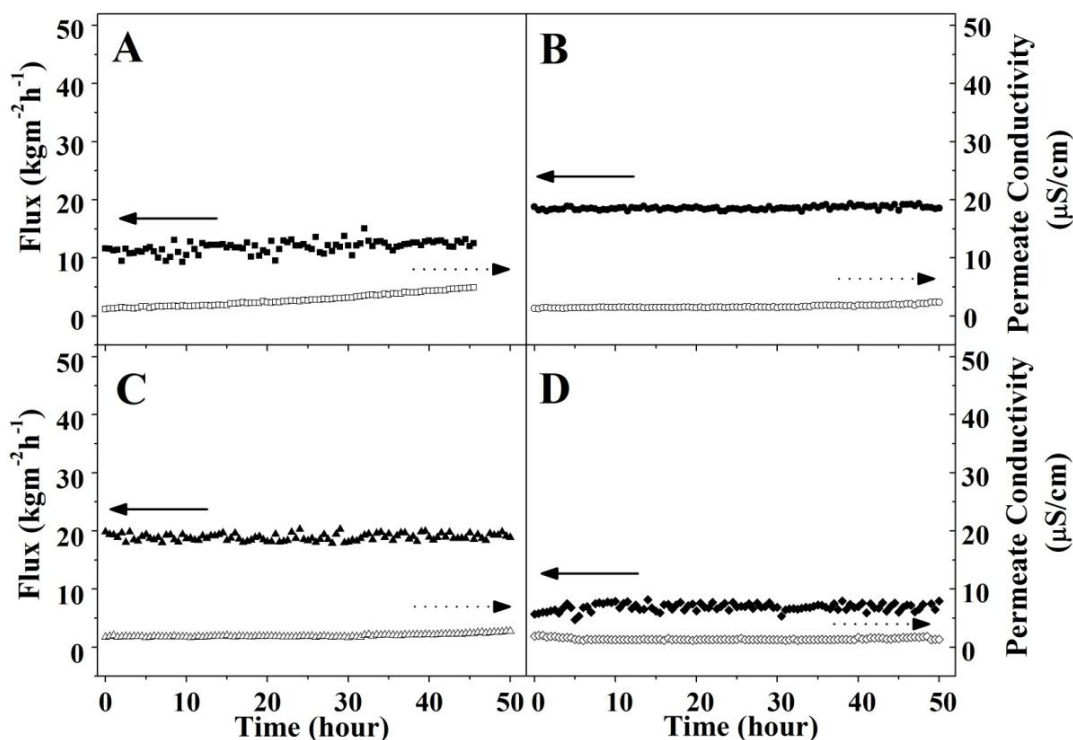


Figure 5-10. Continuous DCMD tests of the original electrospun PVDF membrane (A), S-PVDF (B), L-PVDF composite membranes (C) and commercial PVDF (D) (3.5 wt% NaCl solution as feed, $T_f=333\text{ K}$, $T_p=293\text{ K}$)

The more stable performances of the composite membranes are attributed to their greater hydrophobicity and the better water repellence of the membrane surface. There are several possible explanations for the higher water flux of the composite membranes compared with the PVDF nanofiber membrane. Firstly, when the hot salt solution on the feed side was flowing across the fresh nanofiber membrane surface during the test, water droplets might have gradually entered into the nanofiber sheet and accumulated between the nanofiber layers due to their loose overlap, which would reduce the temperature difference between the feed and

permeation sides and thus decrease water flux significantly (Liao, Wang et al. 2013). The FE-SEM images in **Figures 5-11A** and **5-11B** illustrate that a large gap appeared between the nanofiber layers due to the feed water accumulation, although no obvious feature changes can be observed on tested membrane surface.

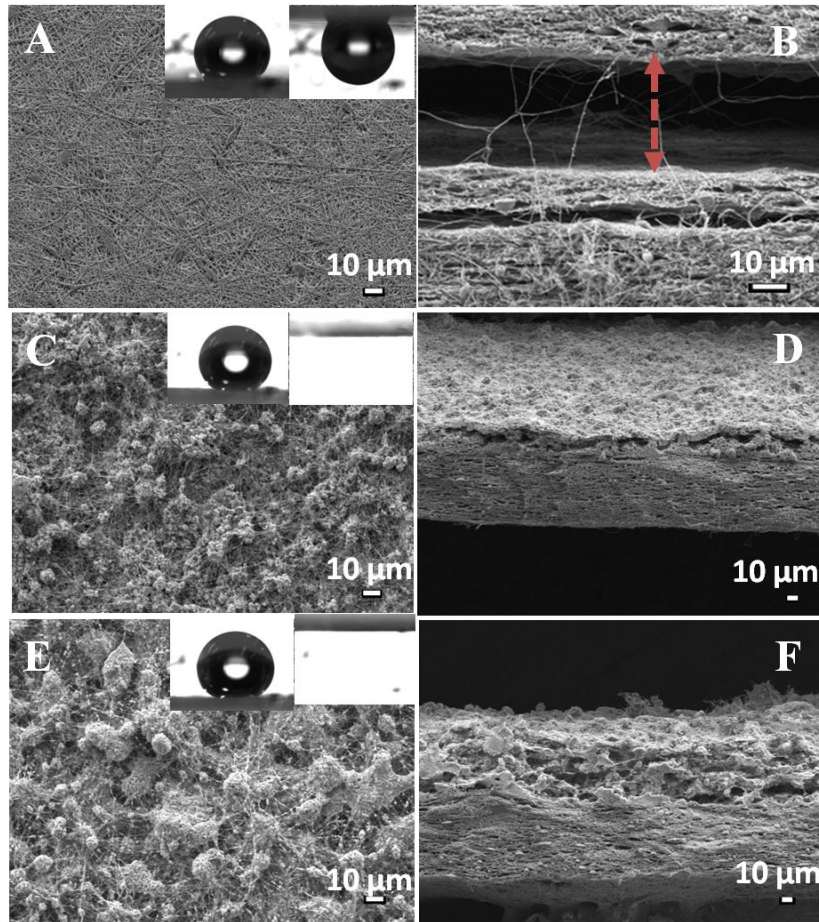


Figure 5-11. Surface and cross-section morphologies of fabricated electrospun membranes after continuous DCMD testing: (A and B) PVDF nanofiber membrane; (C and D) S-PVDF and (E and F) L-PVDF. Inserted images are the water contact pictures of corresponding used nanofibrous membranes

Secondly, the superhydrophobic composite PVDF membranes have higher effective surface porosity which offers more boundaries for phase transition from water in aqueous salt solution to vapour, than the nanofiber membrane. As depicted

in **Figure 5-12**, the meniscus at the membrane surface represents the effective liquid evaporation area. Compared with the nanofiber membrane in which the feed solution is entrapped between nanofibers due to the Petal effect, the superhydrophobic composite membranes have larger effective liquid evaporation areas because of the Lotus effect. As described previously, the hierarchical structure with increased roughness on a superhydrophobic surface would provide numerous orifices to trap water vapour inside during the MD process, and this tends to reduce the contact area between the liquid and solid but increase the contact areas between the liquid and vapour. This type of structure not only provides the surface with superhydrophobic and self-cleaning properties, it also provides more effective liquid areas to evaporate the water vapour and enhance the permeation flux in the MD process. Additionally, the superhydrophobic composite membranes have thin regions of increased vapour and air entrapment, which could lower the effective thermal conductivity of the membranes and thus reduce conductive heat losses and provide more driving force for evaporative transfer in the MD process. In contrast, as shown in **Figure 5-10D**, the flux of commercial PVDF was around $10.0 \text{ kg/m}^2\text{hr}$. The newly developed superhydrophobic PVDF membranes are very competitive compared with the commercial flat-sheet PVDF membrane.

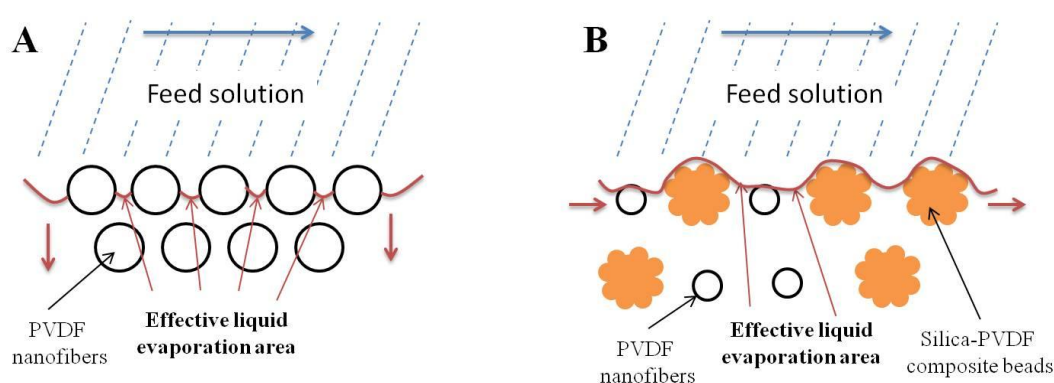


Figure 5-12. Schematic illustration of PVDF nanofiber membrane surface (A) and superhydrophobic PVDF membrane surface (B) used in the DCMD configuration

The stability of composite PVDF membranes in DCMD process was also investigated. According to the FE-SEM images shown in **Figure 5-11**, after being scoured by salt water for over 50 hours, the superhydrophobic S-PVDF and L-PVDF membranes still have the similar surface morphology as previously. The modified silica-blended PVDF beads could be observed on the composite membrane surface. Additionally, the S-PVDF and L-PVDF membranes still possess high water contact angle above 150° and excellent water repellence, while the surface of the PVDF nanofiber membrane maintains a strong adhesive force with water droplets, which demonstrates that the electrospun membranes are durable in the DCMD application.

5.4. Conclusions

The architecture of electrospun PVDF membranes in this study was designed in a highly controlled way to display specific structural features including various morphologies and topologies of composite skin and porous nanofibrous scaffold as well as to show unique superhydrophobic function. Developments have been achieved towards the exploitation of such composite membranes in DCMD application.

In order to prepare a robust superhydrophobic surface, the silica nanoparticles were modified to be hydrophobic, which could make the silica-PVDF composite layer more durable by sticking the modified silica to PVDF islands. The effects of silica diameter and silica-PVDF composite layer thickness on membrane contact angle, sliding angle and MD performance were investigated. It was found that the diameter of the modified silica particles has no obvious impact on water contact and sliding angles of as-prepared membranes. With increasing of composite layer thickness, the water contact angle of membrane increased progressively to a plateau and the sliding contact angle decreased slightly due to the enhancement of hierarchical structures. Furthermore, the durability of the superhydrophobic layer was examined by ultrasonic treatment. Both membranes prepared by small and large silica nanoparticles still possess high water contact angle above 150° and excellent water repellent properties after ultrasonic treatment for 30 min. when the feed and permeation temperature were 323K and 293K, the permeate flux of the composite membranes S-PVDF and L-PVDF were $18.1 \text{ kg/m}^2\text{h}$ and $18.9 \text{ kg/m}^2\text{h}$, respectively, which also exhibit more stable performance compared with PVDF nanofiber and commercial membranes. This should be attributed to their greater hydrophobicity and better water repellence. Moreover, it was observed that the modified silica-blended PVDF composite superhydrophobic layer is durable in continuous DCMD test.

CHAPTER 6

Electrospun superhydrophobic membranes with unique structures for membrane distillation

6.1. Introduction

Based on the prior studies, it is understood that in addition to the diameter of nanoparticles and the thickness of superhydrophobic layer, the concentration of nanoparticles in polymer dopes could have influences on the resultant membrane's properties as well, which will be investigated in this chapter.

Additionally, to further improve the wetting repellent property of superhydrophobic membrane, 3-dimensional (3D) superhydrophobic membranes are proposed to make as a possible solution. The 3D materials are distinct with maintenance of air at the surface as well as within the bulk of the materials, which could continuously create a new water-air-material interface as water penetrates into the materials. As a result, this type of structure has promising potential applications in the fields of chemical sensor, controlled release, delivery and separation systems (Li, Jia et al. 2007; Zhu, Li et al. 2008; Yohe, Herrera et al. 2012; Yohe, Freedman et al. 2013). Tunable 3D porous superhydrophobic copper films with various wall thickness and pore sizes exhibiting integrated microstructures and nanostructure were synthesized by gas bubble template-directed synthesis method (Li, Jia et al. 2007). 3D superhydrophobic dandelion-like microstructures were prepared by a self-assembly process from one dimensional nanofibers, driven by a combined interaction of hydrogen bonding, π - π stacking and hydrophobic interactions (Zhu, Li et al. 2008). Besides, 3D superhydrophobic electrospun meshes as reinforcement

materials have been fabricated for sustained local drug delivery against cancer cells, where air was used as a degradable component (Yohe, Herrera et al. 2012). The infiltration of water into the 3D superhydrophobic porous materials, the boundary conditions at which superhydrophobicity can occur, effects of addition of surfactant, critical surface tension measurement by solvents with various surface tensions, requisite pressure to cause water breakthrough have been investigated (Yohe, Freedman et al. 2013).

However, the 3D superhydrophobic membranes have not been designed and fabricated for MD process. Furthermore, due to the large bulk and surface porosity of the nanofibrous membrane, it may exhibit weak mechanical properties which have adverse impact on membrane packing in the module. Some investigations have been carried out to enhance the mechanical properties of MD membranes to satisfy the operational requirements. For example, clay particles have been added into dopes to improve tensile modulus of PVDF hollow fibers fabricated for DCMD (Wang, Foo et al. 2009). Multi-bore PVDF hollow fiber membranes with a lotus root-like geometry have also been designed to optimize the mechanical rigidity and elasticity of membranes (Wang and Chung 2012; Wang and Chung 2013). Nevertheless, no investigation has been carried out to improve the mechanical properties of MD nanofiber membranes to date.

Thus, in this work, we report two simple approaches to fabricate robust superhydrophobic membranes with high porosity and excellent mechanical property via electrospinning. The first approach involves electrospinning of an ultrathin 3D superhydrophobic selective skin prepared by different compositions with membranes fabricated in Chapter 5, on a porous PVDF nanofibrous support. The second approach is the electrospinning of 3D superhydrophobic PVDF-silica composite membrane onto a commercial non-woven support layer, which can provide outstanding mechanical properties to the composite membranes. The second approach is to electrospin thicker 3D superhydrophobic PVDF-silica

composite layers onto a commercial non-woven support, which not only assists PVDF-silica composite particles in shaping into a flat sheet but also provides outstanding mechanical properties to the composite membranes. The effects of dope compositions and membrane structures on water contact angle, water sliding angle, pore size and porosity, LEPw and mechanical properties of membranes were studied. MD tests were also carried out on selected membranes to examine their long-term performance. This study aims to compare the capabilities and performances of two different hierarchical-structure-designed membranes, and demonstrate that by carefully designing and manufacturing membranes to make them superhydrophobic and mechanically robust, the resultant membranes can achieve superb MD performance with high flux and long-term stability.

6.2. Materials and methods

6.2.1. Materials

The materials have been described in section 3.2.1 and section 5.2.1.

6.2.2. Fabrication of dual-layer superhydrophobic membranes

The process for modifications of silica has been illustrated in section 5.2.5.

The electrospinning parameters for various membranes were summarized in **Table 6-1**. For the electro-spinning of dual-layer membranes with nanofibrous support, a porous support layer was firstly fabricated using 8 wt% PVDF dope. A desired amount of LiCl (0.004 wt%) was added into the dope solution to improve the dope electrospinning ability, optimize the nanofiber membrane porosity, and control membrane pore sizes. On top of the electrospun PVDF support layer, a thin selective layer was electrospun using various PVDF dopes blended with hydrophobic-modified silica. The concentration of PVDF dopes varied from 3 to 5 wt% while the mass ratio of silica to PVDF was kept constant at 2:1. The as-prepared dual-layer membranes were coded as #3S-N, #4S-N, and #5S-N,

respectively. Another type of superhydrophobic dual-layer membranes #4S-W and #5S-W was prepared by electrospinning PVDF-silica dopes onto a non-woven support, as shown in Table 1. All fabricated membranes have a thickness of $72\ \mu\text{m} \pm 12\ \mu\text{m}$ (For the membranes with non-woven support, the thickness of the non-woven supports were excluded from the measurement).

6.2.3. Characterizations of PVDF nanofiber and composite membranes

The characterizations and DCMD test have been described in section 3.2.4, section 3.2.5, section 4.2.4 and section 5.2.4.

1 **Table 6-1** Operating parameters for superhydrophobic nanofiber membranes

Membrane ID	#3S-N	#4S-N	#5S-N	#4S-W	#5S-W
Dope composition of selective layer (wt%)	PVDF /SiO ₂ /DMF: 3/6/97	PVDF/SiO ₂ /DMF: 4/8/96	PVDF/SiO ₂ /DMF: 5/10/95	PVDF/SiO ₂ /DMF: 4/8/96	PVDF/SiO ₂ /DMF: 5/10/95
Dope composition of support layer (wt%)	PVDF/DMF: 8/92 (0.04 wt% LiCl as additive)			Non-woven scaffold	
Dope flow rate (selective/support layer) (mL min ⁻¹)	0.02 / 0.03			0.03 / -	
Travel Speed (mm sec ⁻¹)	0.1				
Travel Distance (cm)	7				
Distance (cm)	12				
Voltage (selective /support layer) (kV)	28 / 26			28 / -	
Loop Number (selective/support layer)	6 / 15	6 / 15	6 / 15	20 / -	

2

6.3. Results and discussion

6.3.1. Effects of dope concentration on stability of FS10-SiO₂ and PVDF dispersion

The stability of FS10-SiO₂-PVDF dispersion is significant for fabricating nano-composite membranes by electrospinning as the dope need to be homogenous during spinning. To observe the stability of dispersion, FS10-SiO₂-blended PVDF dopes with varying PVDF concentration (mass ratio of FS10-SiO₂ to PVDF was fixed at 2:1) were left to stand for several hours. The images of as prepared PVDF dopes after standing for different durations are shown in **Figure 6-1A**. At the beginning, all the dopes were homogenous. However, the dope with 2 wt% PVDF had separated into two phases after 30 min. After 4 h, the dope with 3 wt% PVDF was also observed to be separated. The observation suggests that homogenous dispersion lasts for a longer time in a more concentrated dope. This might be due to a better entanglement between PVDF macromolecular chains and FS10-SiO₂ particles, which prevents the particles from settling fast (**Figures 6-1B and 6-1C**).

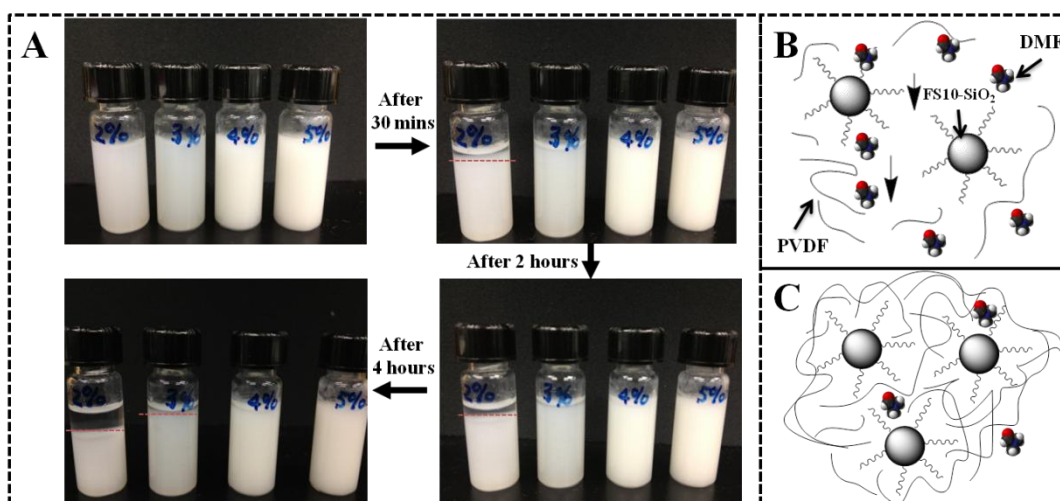


Figure 6-1. (A) Photographs of various FS10-SiO₂-blended PVDF dopes after hours and schematic illustrations of (B) unstable low concentrated dope and (C) stable high concentrated dope

Considering that the electrospinning of the superhydrophobic dual-layer membrane with non-woven support would take roughly 4 h, the dopes containing 4 wt% and 5 wt% PVDF were selected for the membrane preparation since they represent excellent stability after standing for 4 h. For the case of the superhydrophobic dual-layer membrane with nanofibrous support, the electrospinning of superhydrophobic selective layer could be completed within 1 h. Thus, the dope containing 3 wt% PVDF could also be utilized to prepare the membranes.

6.3.2. *Morphology of FS10-SiO₂-PVDF composite membranes*

Figure 6-2 shows the diagrams, surface, and cross-sectional morphology of superhydrophobic dual-layer composite membranes with nanofiber and non-woven supports. According to the designed hierarchical structure of the composite membrane with nanofibrous support as shown in **Figure 6-2A (1)**, the membrane constitutes of a porous PVDF nanofibrous support layer (**Figure 6-2A(2)**), and a FS10-SiO₂-PVDF superhydrophobic selective layer (**Figure 6-2A(3)**). The cross-section of this superhydrophobic dual-layer membrane is shown in **Figure 6-2A (4)**. The surface morphology of the membrane with nanofibrous support shows a structure with great amounts of protrusions and valleys, which provide micro-scaled and nano-scaled roughness for superhydrophobicity. According to **Figure 6-2A (4)**, no delamination between the support layer and the selective layer is observed, confirming a good adhesion at the interface. As shown in **Figure 6-2B (1)**, this superhydrophobic dual-layer membrane comprises a non-woven scaffold and a FS10-SiO₂-PVDF composite layer (**Figure 6-2B (2)**). In **Figure 6-2B (3)**, the surface morphology of the membrane with non-woven support is observed to be similar with that with nanofibrous support. The cross sectional morphology of the membrane is comprised of micro-beads and nano-beads (**Figure 6-2B (4)**). These micro- and nano-beads, which are formed due to the presence of the FS10-SiO₂ particles, make up the majority of the cross section and thus form a thicker “3-

dimensional roughness". This unique structure plays an important role in long-term performance of MD, as will be discussed in a later section.

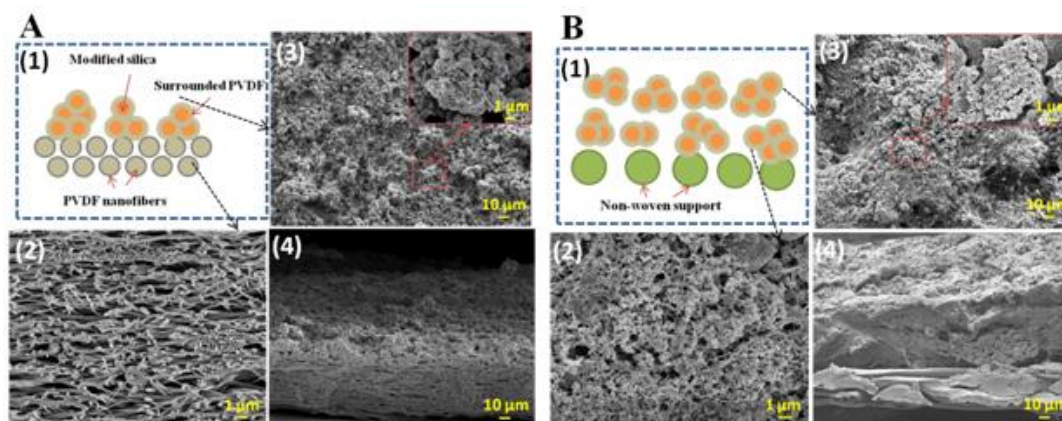


Figure 6-2. The diagrams and morphologies of superhydrophobic dual-layer membranes (A) #3S-N and (B) #5S-W: (1) schematic drawing; (2) enlarged cross section image of the middle layer; (3) surface morphology; (4) cross section morphology of prepared membranes

It is worth pointing out that in order to improve the integrity of both composite membranes, it is necessary to ensure strong adhesion at the interface between the composite skin layer and the nanofibrous support, and also guarantee robust combination between the composite layer and non-woven scaffold. Therefore, additive such as LiCl was not added into the composite FS10-SiO₂-PVDF dopes because the presence of such additive would reduce the fiber diameter, increase length-diameter ratio, and consequently accelerate the evaporation of solvent during electrospinning (Tang, Qiu et al. 2009). If the solvent evaporation is fast such that beads and fibers become completely dry when they are deposited on the support, poor adhesion between the composite layer and nanofibrous support or PET non-woven is likely to occur. In such case, the resultant membranes might not be robust enough to withstand changes in flow velocity, hydraulic pressure and back-flushing (Tang, Qiu et al. 2009). In contrast, in the case of fabricating highly

porous nanofibrous support, inorganic additive LiCl is necessary to accelerate solvent evaporation, fabricate dry nanofibers and get porous nanofibrous membranes. In this way, the dry nanofibers cannot be adhered to the PET non-woven scaffold.

6.3.3. Superhydrophobicity of FS10-SiO₂-PVDF composite membranes

The variations of water contact angle and sliding angle of different membranes are shown in **Figure 6-3**. Compared with commercial PVDF membrane GVHP possessing contact angle of $135^{\circ} \pm 6^{\circ}$, all as-prepared membranes show a higher water contact angle of more than 150° , indicating that these membranes are superhydrophobic. In addition, water droplet tends to adhere on the surface of the commercial PVDF membrane even after turning the membrane upside down, as shown in **Figure 6-3**. In contrast, all as-prepared superhydrophobic membranes exhibit a water sliding angle lower than 30° .

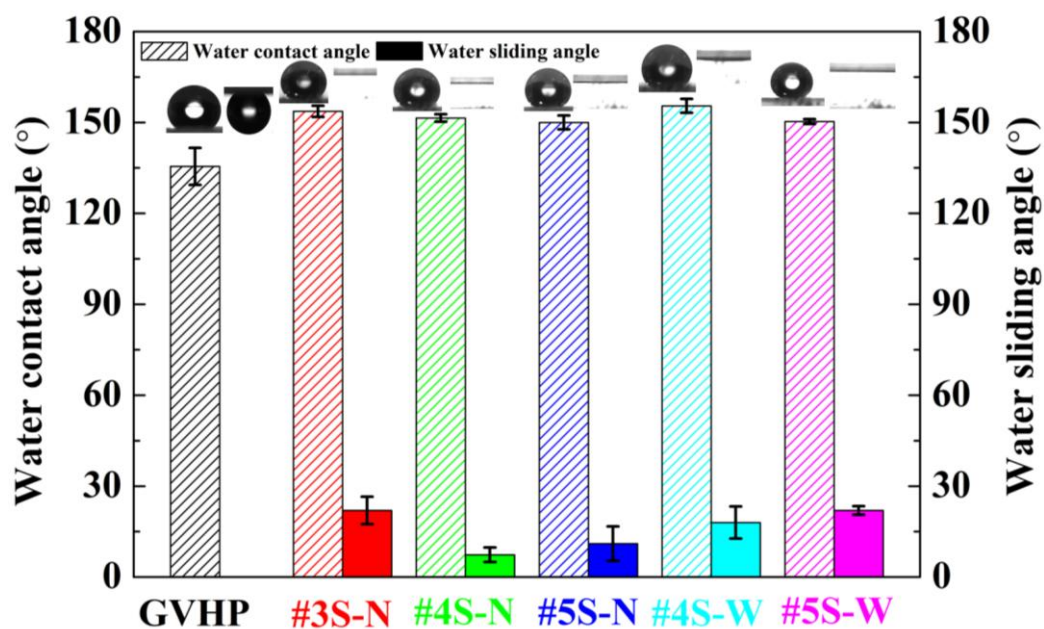


Figure 6-3. Variation of water contact angle and sliding angle as a function of different membrane fabrication dopes and structures

As further evidence to the superhydrophobicity, **Figure 6-4A** shows how a water droplet on a needle tip interacted with the surface of a superhydrophobic membrane when the needle was brought near to and away from the membrane. The water droplet did not show any tendency to spread on the superhydrophobic surface of the as-prepared membranes even when the water droplet on membrane surface was pushed by the needle. The membrane surface remained dry after moving away the needle. A key membrane characteristic that is responsible for the superhydrophobicity is the surface topography. Therefore, the surface topography of as-prepared superhydrophobic membranes was examined by AFM. As shown in **Figure 6-4B**, the membrane surface shows a structure with ridges and valleys, which are attributed to the formation of micro- and nano-beads comprising of FS10-SiO₂-PVDF composite. The FS10-SiO₂-PVDF composite small asperities are scattered on membrane surface, which are essential to enhance the roughness and achieve superhydrophobicity. The contact angle of a liquid on such a rough surface comprising solid (the ridges) and void (the valleys) can be described by the Cassie-Baxter equation as shown in equation 4-3. As illustrated in **Figure 6-4C**, air is trapped under the liquid droplet between the small hills shaped by silica-PVDF composites, which implies a decrease of f_{SL} and therefore superhydrophobicity. The liquid droplet is suspended on the top of the asperities and the air fraction present between the surface and liquid droplet makes its suspension much easier, which consequently enable the liquid roll off from membrane surface spontaneously after tilting a small angle. Due to the rough surface, the as-prepared membranes exhibit superhydrophobicity to not only water but also other liquids such as coffee and milk, as shown in **Figure 6-4C**.

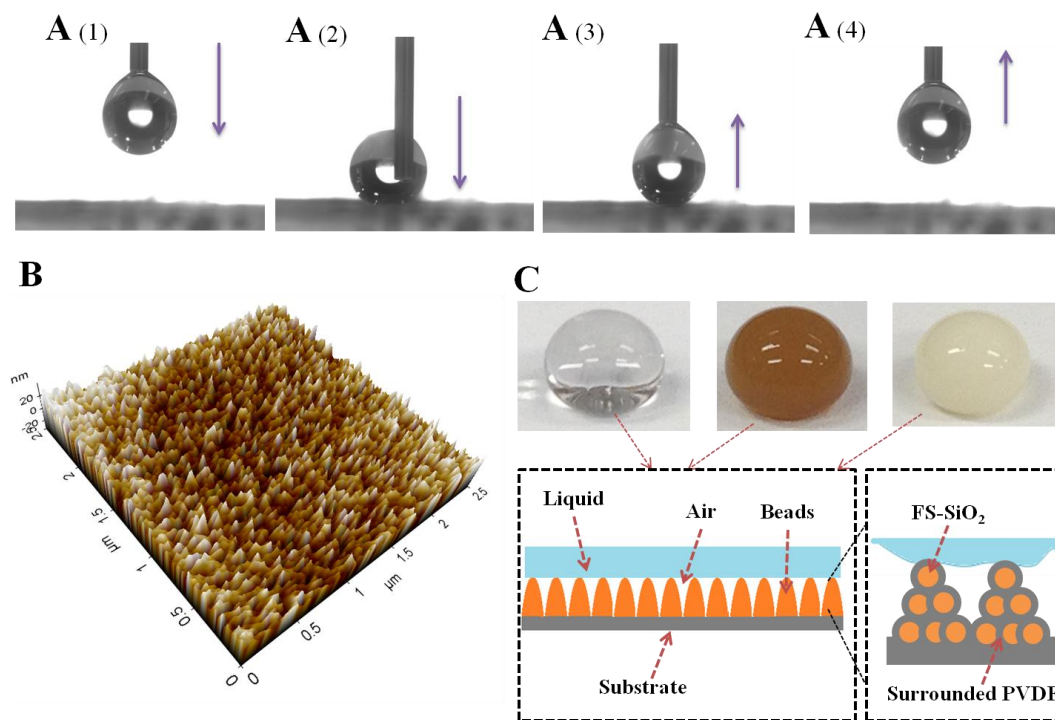


Figure 6-4. (A) Captured images of water droplet movement on the surface of superhydrophobic membrane #3S-N, (B) surface topography of superhydrophobic membrane #3S-N, (C) the liquid-membrane interface scheme on silica blended superhydrophobic membrane

6.3.4. Comparison of different PVDF membranes

The pore size and porosity of commercial PVDF and fabricated superhydrophobic PVDF membranes as well as their LEPw are summarized in **Figure 6-5**. Compared with the membranes fabricated in this work, because of sponge-like structure as shown in **Figure 6-6A**, the commercial PVDF membrane possesses the smallest maximum and mean pore sizes which are $0.59 \pm 0.01 \mu\text{m}$ and $0.41 \pm 0.01 \mu\text{m}$, respectively. For the superhydrophobic dual-layer membranes with nanofibrous support, it is found that the maximum pore size of #5S-N ($0.83 \pm 0.06 \mu\text{m}$) is larger than that of #3S-N and #4S-N, indicating that the pore size tends to increase when the dope was prepared with a higher concentration of PVDF and

FS-SiO₂. This might be attributed to the formation of larger beads with increasing dope concentration, as shown in **Figures 6-6B** and **6-6C**. The larger beads tend to exhibit a higher accumulated charge during electrospinning, thus creating a stronger repulsive force between each other. As a result, the membrane prepared using a dope with a higher concentration (i.e., #5S-N) exhibits a less compact structure and a larger pore size.

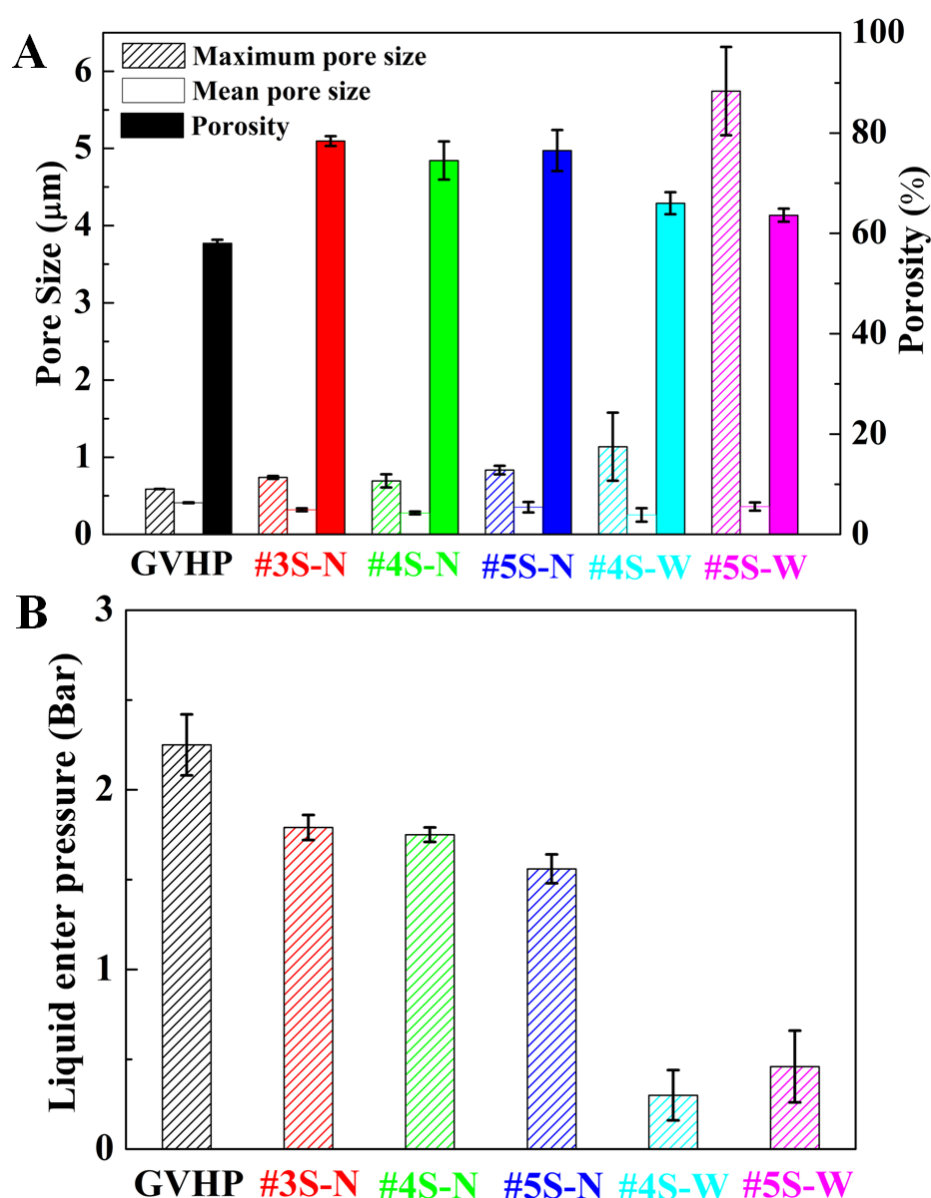


Figure 6-5. Comparisons of (A) pore sizes and porosity, and (B) LEPw of different PVDF membranes

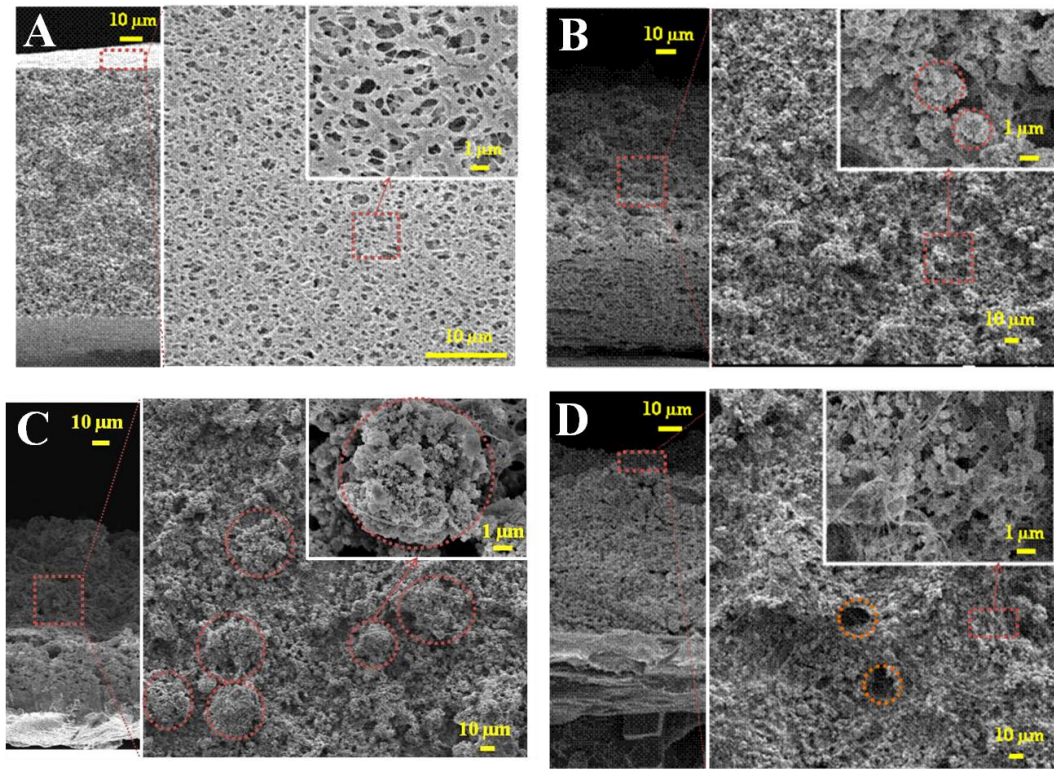


Figure 6-6. Cross section and surface morphologies of commercial PVDF membrane GVHP (A), #3S-N (B), #4S-N (C) and #5S-W (D)

On the other hand, the maximum pore size of the superhydrophobic dual-layer membrane with non-woven support #5S-W ($> 5.5 \mu\text{m}$) is observed to be significantly larger than all the other membranes. This make the membrane unsuitable for MD application since maximum pore sizes of most MD membranes are below $0.6 \mu\text{m}$ (Schneider, Hölz et al. 1988). Compared with the dual-layer membranes with nanofibrous scaffold, it seems that the dope composition has a more significant effect on pore size for membranes prepared mainly by PVDF and FS-SiO₂ composite dope. This might because, unlike the membranes that consist of only a thin layer of bead structure (the selective layer) and bulk structure of them is composed by overlapped nanofibers, the majority of the membranes with non-woven support are made up of micro- and nano-beads (as described in Section 6.3.2). Due to the repulsive force between the beads during electrospinning as

above-mentioned, it is possible to produce even bigger holes on the surface, as shown in **Figure 6-6D**. As a result, the maximum pore size of the non-woven-supported membranes is increased.

The overall porosity of the PVDF membranes is also presented in **Figure 6-5A**. It is observed that the commercial PVDF membrane has the lowest porosity of $58 \pm 1\%$ compared with the as-prepared membranes. In general, the non-woven-supported membranes exhibit a lower porosity than the nanofiber-supported membranes due to much compacter structure. Thanks to the porous nanofibrous support of the dual-layer membranes #3S-N, #4S-N, and #5S-N, they all exhibit a higher porosity around 80%, which could decrease mass transfer resistance in MD process.

As aforementioned, one of the critical membrane characteristics for MD application is the stability of membrane performance in long-term usage, which could be represented by LEPw. When the hydraulic pressure on membrane surface exceeds LEPw, water and salt in the feed side will overcome the surface tension and enter hydrophobic membrane pores. This consequently contaminates the permeate and reduces the flux significantly. According to the Laplace equation, the LEPw is directly proportional to the cosine of liquid-solid contact angle (θ), the liquid surface tension (γ_L), and the geometric factor (B), and is reversely proportional to the largest pore radius (r_{max}) as following (Lawson and Lloyd 1997):

$$P_{liquid}-P_{vapor} = \Delta P_{interface} = \frac{-2\gamma_L B \cos \theta}{r_{max}} < LEPw \quad (5-1)$$

A reduction of r_{max} and an enhancement of θ would increase the LEPw of a membrane. As can be seen in **Figure 6-5B**, the commercial membrane exhibits the largest LEPw of 2.25 ± 0.17 bar due to the smallest pore size. Although the nanofiber-supported dual-layer membranes have a larger pore size and a higher porosity, they still show competitive LEPw above 1.5 bar. This is attributed to the

enhanced contact angle due to the rough surface. On the other hand, the LEPw of the dual-layer superhydrophobic membranes with non-woven support are around 0.5 bar because of the presence of big pores.

The tensile stress-strain curves of commercial and electrospun PVDF membranes are shown in **Figure 6-7A**. Mechanical reinforcement can be achieved when the nanofiber and nanobeads are dispersed and attached on the non-woven support such that the external load is efficiently transferred between the composite layer and the non-woven support layer. When comparing the stress-strain curves for the non-woven-supported superhydrophobic membranes with that of the nanofiber-supported and commercial membranes, it is clear that the tensile modulus (slope of the initial, linear portion of stress-strain curve) of non-woven-supported membranes is improved. In addition, because of the excellent combination between the composite layer and the non-woven support layer, the prepared membranes possess better mechanical strength than the non-woven scaffold itself. The average tensile modulus and the ultimate tensile strength of the membranes are summarized in **Figure 6-7B**. The tensile modulus of #5S-W (170 ± 22 MPa) increased by 336% compared with dual-layer membrane #5S-N (39 ± 4 MPa). Meanwhile, the tensile strengths of the dual-layer membranes with non-woven support are also better than the ones with nanofibrous support.

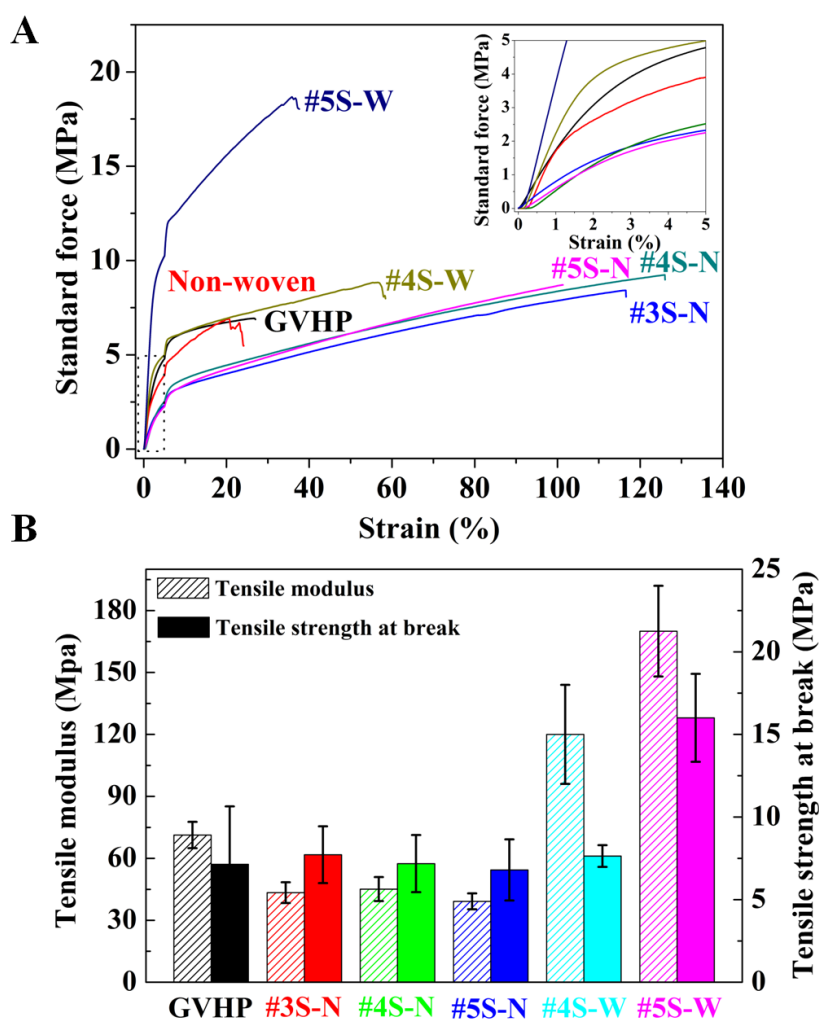


Figure 6-7. Tensile properties of different PVDF membranes

6.3.5. Continuous DCMD performance

The newly developed superhydrophobic membranes #3S-N and #5S-W are chosen to test in DCMD process as #3S-N possesses the highest porosity and #5S-W exhibits the best mechanical properties. As shown in **Figures 6-8A** and **6-8C**, the dual-layer membrane #3S-N has a permeate flux of $24.6 \pm 1.2 \text{ kg m}^{-2} \text{ h}^{-1}$, which is higher than that of #5S-W ($20.8 \pm 2.8 \text{ kg m}^{-2} \text{ h}^{-1}$). The flux of the as-prepared membranes are all higher than commercial GVHP membrane, which only have a flux of $10.6 \text{ kg m}^{-2} \text{ h}^{-1}$ under the same testing condition (Liao, Wang et al. 2013). As

shown in **Figures 6-8B** and **6-8D**, the surface morphology of as-developed membranes did not show obvious alteration after continuous MD process, indicating that the superhydrophobic surface is durable for long-term applications.

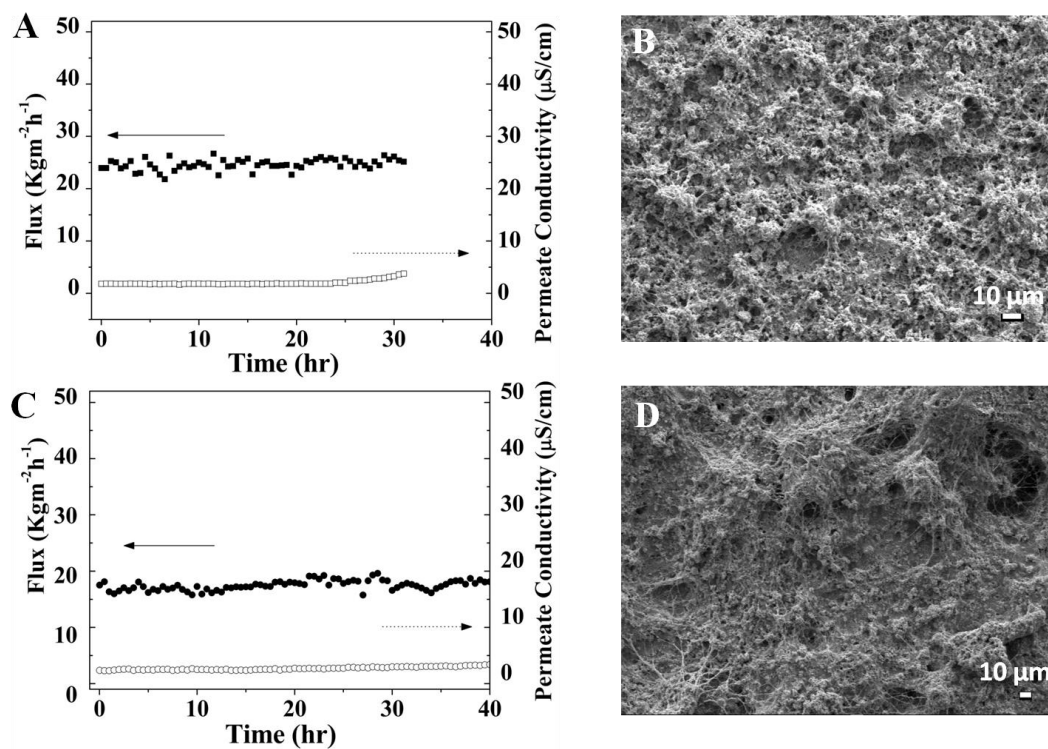


Figure 6-8. Continuous DCMD test and membrane surface morphology after the test of #3S-N (A and B) and #5S-W superhydrophobic membranes (C and D). (3.5 wt% NaCl solution as feed, $T_f=333$ K, $T_p=293$ K)

Compared with the nanofiber-supported superhydrophobic membrane #3S-N, the non-woven-supported superhydrophobic membrane #5S-W has a more stable performance over a testing duration of 40 h even though it has a lower LEPw and larger membrane pore size. This might be attributed to the better wetting resistance of the thicker 3D superhydrophobic structure of membrane #5S-W. **Figure 6-9** schematically demonstrates the wetting of the two different superhydrophobic dual-layer membranes, respectively. In the case of the nanofiber-supported membrane

(**Figure 6-9A**), there is only an ultrathin 3D superhydrophobic layer on the top of the membrane, thus the superhydrophobicity is metastable; once the air or vapor entrapped under the water–membrane interface is lost, wetting of the thin superhydrophobic layer occurs; water will then continuously penetrate the pores of the less hydrophobic PVDF support layer in a relatively fast manner, until completely wetting the membrane. In contrast, as shown in **Figure 6-9B**, due to the entire 3D superhydrophobic structure, another stable water–membrane interface with air or vapor entrapped underneath it is immediately created even after the wetting of the topmost layer, which makes #5S-W a better membrane for long-term MD application.

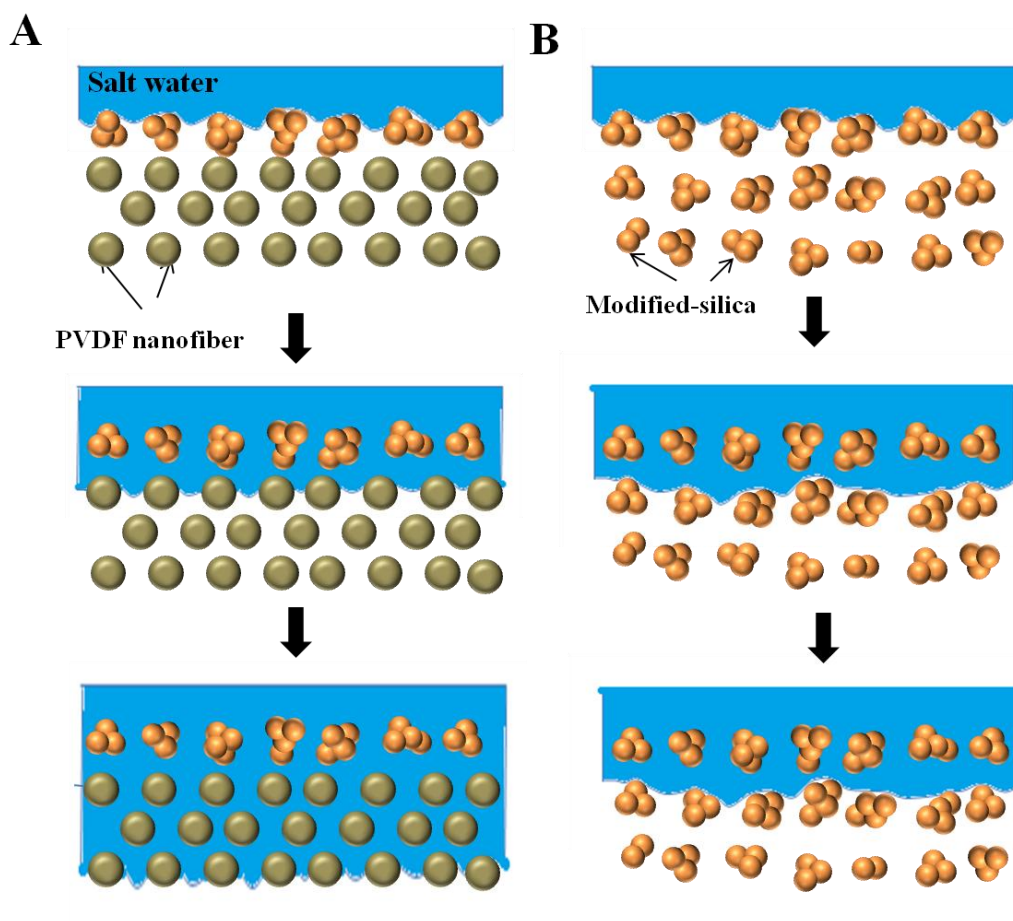


Figure 6-9. Possible membrane wetting processes of (A) #3S-W and (B) #5S-N superhydrophobic membranes

6.3.6. Comparison of properties and DCMD performance of different electrospun PVDF membranes

Table 6-2 shows a comparison of properties and DCMD performance of various PVDF nanofiber membranes between this work and the literature data. In addition to the high rejection over 99.99%, a flux enhancement of electrospun membrane #3S-N with longer stable performance has been achieved in this work, which is attributed to the porous nanofibrous support layer and superhydrophobic skin. The mechanical properties and long-term stability of the non-woven-supported superhydrophobic dual-layer membrane #5S-W reported in this study are much better than that of other fabricated PVDF nanofiber membrane (stable in continuous testing 40 h with rejection over 99.99%), which are due to the excellent combination with non-woven and the unique 3D superhydrophobic structure.

Table 6-2. Properties and DCMD performances of different electrospun PVDF membranes

Membrane		Mean pore size	Max pore size	Membrane thickness	Contact angle	Young's modulus	Tensile strength	Elongation at break	Feed solution property		Permeate solution property		Permeation flux	Rejection	Long-term performance
		μm	μm	μm	$^{\circ}$	Mpa	Mpa	%	Solution	$T_{f,in}$ ($^{\circ}\text{C}$)	Solution	$T_{p,in}$ ($^{\circ}\text{C}$)	($\text{kg m}^{-2} \text{h}^{-1}$)	%	
PVDF-Clay nanofiber membranes ³⁴	S1	0.58			128								6 ^a	98.27	wet in 8 h
	S2	0.60			134				3.5 wt% NaCl	80		17	6 ^a	99.95	
	S3	0.63	–	–	142	–	–	–					5 ^a	99.99	stable in 8 h
	S4	0.64			154								5 ^a	99.97	
PVDF-HFP nanofiber membrane ³⁵	10 PH-hot pressed 2 layer	0.26	0.77	110					1.0 wt% NaCl (18 mS cm^{-1})	65	tap water (110 $\mu\text{S cm}^{-1}$)	24	20-21	98 ^c	–
	15 PH-hot pressed 2 layer	0.51	1.04	170						50		24	8~9		
	EMN 1h		5.20 ^{a,b}	144	139	24	4.5	138					28 ^a	99.4 ^d	The change of permeation flux and conductivity was below 5% in 25 h
PVDF nanofiber membrane ³⁶	EMN 2 h		4.40 ^{a,b}	464	139	35	6.4	134	3.0 wt% NaCl	60	Distilled water	20	13 ^a	99.9 ^d	
	EMN 3 h	–	3.80 ^{a,b}	833	140	44	7.2	134					11 ^a	99.9 ^d	
	EMN 4 h		2.90 ^{a,b}	1529	139	75	10.2	130					7 ^a	99.9 ^d	
PVDF nanofiber membrane ²	M-9-LS-LM-Heat	0.18	0.36		138								11	>99.99 ^d	stable in 10 h
	M-9-LS-LM-Heat	0.21	0.33	–	136	–	–	–	3.5 wt% NaCl (60 mS cm^{-1})	60	Distilled water (< 5 $\mu\text{S cm}^{-1}$)	20	21	>99.99 ^d	stable in 15 h
This work	#3S-N	0.32	0.74	72	154	68	7.9	94		60		20	25	>99.99 ^d	stable in 25 h
	#5S-W	0.36	5.74	76	150	369	16.9	34					21	>99.99 ^d	stable in 40 h

6.4. Conclusions

In summary, the structural features of two novel designed superhydrophobic membranes are superb for membrane desalination for the following reasons: (1) the membranes possess contact angles higher than 150° , which means they exhibit superhydrophobicity towards various kinds of liquid such as milk, coffee, juice and oil-water mixture. This superhydrophobic nature of the membranes makes them suitable for not only water desalination but also concentrating other solutions; (2) the higher hydrophobicity allows membranes with larger pore sizes to be used in MD process while still maintaining a stable performance in long-term MD process; (3) the superhydrophobic nanofiber-supported dual-layer membranes have higher porosity that enhances MD flux while the superhydrophobic non-woven-supported dual-layer membranes exhibit excellent mechanical durability preventing breakage and also better water resistance as a result of a thicker 3D micro- and nano-superhydrophobic structure; (4) these superhydrophobic layers are robust and durable in continue MD operations.

CHAPTER 7

Conclusions and recommendations

7.1. Overall conclusions

Electrospinning is an effective and useful method for fabricating a wide range of one-dimensional and functional nanofibers. The unique characters of nanofiber membranes such as high surface-to-volume ratio, high porosity of up to 90% and the easy incorporation of nanoparticles or nanotubes into the structure make them highly attractive for many applications, including membrane distillation (MD).

This thesis presents the design and fabrication of novel superhydrophobic membranes by electrospinning for DCMD application. The current MD membranes are subjected to a lower than expected flux due to the lower porosity and mass transfer efficiency, and unsatisfied wetting resistance because of insufficient hydrophobicity. Therefore, nanofiber PVDF membranes with adjustable thickness, high hydrophobicity, and high porosity have been fabricated by electrospinning in Chapter 3. The effects of a series of factors including polymer dope compositions, spinning parameters and heat-press post-treatment on the structures and properties of resultant membranes were examined. In Chapter 4, superhydrophobic nanofiber membranes have been successfully achieved by modifications to optimize the surface morphology and roughness. The modifications were carried out on entire nanofibers or only on membrane surface. To make the membrane robust and superhydrophobic, the newly developed membrane consists of a superhydrophobic silica-PVDF composite selective skin formed on PVDF porous nanofiber scaffold via electrospinning as shown in Chapter 5. This fabrication method could be easily scaled up due to its simple preparing procedures. And to further improve the

mechanical properties of electrospun superhydrophobic membranes and investigate the effect of 3D superhydrophobic structure on membrane properties, the superhydrophobic dual-layer membranes were designed, constructed and compared in Chapter 6. All the membranes were characterized by the standard protocols in term of structure and morphology, chemical groups on surface, pore size and pore size distribution, water contact angle, mechanical properties and DCMD performance, *etc.*

The major findings and conclusions are summarized as follows:

- 1) By means of controlling polymer concentration and adding suitable additives in the dope solution, the nanofibers with a small diameter could be fabricated and membranes formed by the nanofibers possess small pore sizes as described in Chapter 3;
- 2) The membranes with small pore sizes could be prepared by slowing down the sprayer moving speed and reducing the moisture in the spinning chamber;
- 3) Surface contact angle measurements confirmed that all the electrospun PVDF membranes exhibited a rougher surface with high hydrophobicity;
- 4) Heat-press post-treatment was considered as a necessary step to improve fresh nanofiber membrane integrity, enhance water permeation flux and help prevent membrane pores from wetting in DCMD operation;
- 5) The modification method illustrated in Chapter 4 is an effective way to make the PVDF nanofiber membrane superhydrophobic;
- 6) The hierarchical or nanostructured surface morphology and topology of modified PVDF nanofiber membranes contributed to the superhydrophobic property;
- 7) Compared with unmodified membrane, the modified I-PVDF nanofiber membrane exhibited stable performance in DCMD process attributed to the superhydrophobic surface property. The high adhesive force with water

make the pristine nanofiber membrane being wetted easily while the superhydrophobicity of modified I-PVDF nanofiber membrane would enhance membrane anti-wetting property;

- 8) Inspired by the unique structure of lotus leaf, a strategy to construct superhydrophobic composite nanofiber membranes with robust superhydrophobicity and high porosity is described in Chapter 5;
- 9) The effects of silica diameter on membrane contact angle, sliding angle and MD performance were investigated;
- 10) DCMD tests demonstrated that the newly developed membranes were able to present stable high performance over 50 h of testing time, and the superhydrophobic selective layer exhibited excellent durability in ultrasonic treatment and continuous DCMD test;
- 11) As shown in Chapter 6, the resultant dual-layer membranes prepared via electrospinning exhibit superhydrophobicity towards various kinds of liquid such as milk, coffee, juice and oil-water mixture. This superhydrophobic nature of the membranes makes them suitable for not only water desalination but also concentrating of other solutions;
- 12) The higher hydrophobicity allows membranes with larger pore size to be used in MD process while still maintaining a stable performance in long-term MD process;
- 13) The nanofiber-supported dual-layer membranes had higher porosity that enhances MD flux while the non-woven-supported dual-layer membranes exhibited excellent mechanical rigidity and better water resistance as a result of a thicker 3D micro- and nano-hierarchical superhydrophobic structure combined with non-woven support.

7.2. Recommendations for future research

To facilitate the commercialization of the electrospun membranes for water industries in large scale, more research are needed with respect to controlling membrane maximum pore size, stabilizing membrane long-term performance, enhancing fouling resistance, exploiting the large surface area of nanofibrous membranes for treating waste water, *etc.*

Most unmodified nanofibrous membranes fabricated by electrospinning possess maximum surface pore size larger than 1 μm and exhibit fiber diameter ranging from 100 nm to 1000 nm. In order to decrease the maximum pore size, transitions from micro-sized pores to nano-sized pores and from nanofiber with diameter above 100 nm to several nanometers are necessary. The anti-wetting property of nanofiber membrane could be enhanced by using nanofibrous membranes with smaller fiber diameters while the permeation flux could be maintained due to the high porosity of the ultrafine nanofibrous layer. Meanwhile, the ultrafine nanofibers allow the grafted or polymerized skin layer to be captured and supported at the surface other than deeply penetrating inside the membrane under high pressure or continuous scouring, which may extend the membrane applications in high pressure-driven water treatment processes. The potential approach to steadily produce a mass amount of nanofibers with a diameter smaller than 100 nm is to optimize conductivity, surface tension and viscosity of electrospun polymer dopes, which require further research.

Additionally, one of major problems in membrane processes is the reduction of the flux to far below the theoretical capacity of the membrane due to membrane fouling. Nanofiber membranes also suffer a rapid decay of flux due to irreversible fouling in some membrane processes. Secondary treatments including chemical clean, further optimization of membrane hydrophilicity, functionalization of nanofibrous membranes could be carried out to enhance membrane performance.

Furthermore, surface-to-volume ratio of nanofibers can be up to 10^3 times of microfibers, which could be exploited in water research as water absorbent fibers. The structure and chemical groups on nanofiber surface could be changed by chemical modification to reject bacteria, salt ions, organic compounds, heavy metals, *etc.*

Moreover, engineering approaches could also be explored for nanofiber membrane application. For instances, drying the membrane during MD process may be an alternative choice to prolong the membrane life with the supply of a pressurized gas in the permeate side, which could push the feed solution out of membrane pores so that the membrane can be used for another cycle.

The past several years have witnessed significant progress in research activities regarding electrospun membrane fabrication for water treatments and also figured out crucial challenges. The continuous efforts on exploration of nanofibrous membranes with highly controlled nanostructures will address the challenges and facilitate rapid developments of electrospun membrane fabrication technology for water treatment.

References

- Adnan, S., M. Hoang, et al. (2012). "Commercial PTFE membranes for membrane distillation application: Effect of microstructure and support material." Desalination **284**(0): 297-308.
- Agarwal, S., A. Greiner, et al. (2013). "Functional materials by electrospinning of polymers." Progress in Polymer Science **38**(6): 963-991.
- Alves, V. D. and I. M. Coelho (2006). "Orange juice concentration by osmotic evaporation and membrane distillation: A comparative study." Journal of Food Engineering **74**(1): 125-133.
- Bédafi-Bakó, K. and B. Koroknai (2006). "Enhanced water flux in fruit juice concentration: Coupled operation of osmotic evaporation and membrane distillation." Journal of Membrane Science **269**(1-2): 187-193.
- Bagger-Jørgensen, R., A. S. Meyer, et al. (2004). "Recovery of volatile aroma compounds from black currant juice by vacuum membrane distillation." Food Engineering **64**(1): 23-31.
- Banat, F., N. Jwaied, et al. (2007). "Performance evaluation of the “large SMADES” autonomous desalination solar-driven membrane distillation plant in Aqaba, Jordan." Desalination **217**(1-3): 17-28.
- Banat, F. A., F. Abu Al-Rub, et al. (1999). "Modeling of dilute ethanol–water mixture separation by membrane distillation." Separation and Purification Technology **16**(2): 119-131.
- Banat, F. A. and M. Al-Shannag (2000). "Recovery of dilute acetone–butanol–ethanol (ABE) solvents from aqueous solutions via membrane distillation." Bioprocess & Biosystems Engineering **23**(6): 643.

- Barakat, N. A. M., M. A. Kanjwal, et al. (2009). "Spider-net within the N6, PVA and PU electrospun nanofiber mats using salt addition: Novel strategy in the electrospinning process." Polymer **50**(18): 4389-4396.
- Barbe, A. M., J. P. Bartley, et al. (1998). "Retention of volatile organic flavour/fragrance components in the concentration of liquid foods by osmotic distillation." Journal of Membrane Science **145**(1): 67-75.
- Barthlott, W. and C. Neinhuis (1997). "Purity of the sacred lotus, or escape from contamination in biological surfaces." Planta **202**(1): 1-8.
- Bharat, B. and J. Yong Chae (2008). "Wetting, adhesion and friction of superhydrophobic and hydrophilic leaves and fabricated micro/nanopatterned surfaces." Journal of Physics: Condensed Matter **20**(22): 225010.
- Bhardwaj, N. and S. C. Kundu (2010). "Electrospinning: A fascinating fiber fabrication technique." Biotechnology Advances **28**(3): 325-347.
- Bhattacharai, N., D. Edmondson, et al. (2005). "Electrospun chitosan-based nanofibers and their cellular compatibility." Biomaterials **26**(31): 6176-6184.
- Bhattacharai, S. R., N. Bhattacharai, et al. (2004). "Novel biodegradable electrospun membrane: scaffold for tissue engineering." Biomaterials **25**(13): 2595-2602.
- Bhushan, B. (2008). "Nanotribology and Nanomechanics in Nano/Biotechnology." Philosophical Transactions: Mathematical, Physical and Engineering Sciences **366**(1870): 1499-1537.
- Bhushan, B. and Y. C. Jung (2011). "Natural and biomimetic artificial surfaces for superhydrophobicity, self-cleaning, low adhesion, and drag reduction." Progress in Materials Science **56**(1): 1-108.
- Bonyadi, S. and T.-S. Chung (2009). "Highly porous and macrovoid-free PVDF hollow fiber membranes for membrane distillation by a solvent-dope solution co-extrusion approach." Journal of Membrane Science **331**(1-2): 66-74.

- Bonyadi, S. and T. S. Chung (2007). "Flux enhancement in membrane distillation by fabrication of dual layer hydrophilic–hydrophobic hollow fiber membranes." Journal of Membrane Science **306**(1–2): 134-146.
- Bottino, A., G. Capannelli, et al. (2005). "Novel porous poly (vinylidene fluoride) membranes for membrane distillation." Desalination **183**(1-3): 375-382.
- Bouguecha, S. and M. Dhahbi (2003). "Fluidised bed crystalliser and air gap membrane distillation as a solution to geothermal water desalination." Desalination **152**(1-3): 237-244.
- Burton, Z. and B. Bhushan (2006). "Surface characterization and adhesion and friction properties of hydrophobic leaf surfaces." Ultramicroscopy **106**(8–9): 709-719.
- Cassano, A., E. Drioli, et al. (2003). "Clarification and concentration of citrus and carrot juices by integrated membrane processes." Journal of Food Engineering **57**(2): 153-163.
- Cassie, A. B. D. and S. Baxter (1944). "Wettability of porous surfaces." Transactions of the Faraday Society **40**: 546-551.
- Chang, H., G.-B. Wang, et al. (2010). "Modeling and optimization of a solar driven membrane distillation desalination system." Renewable Energy **35**(12): 2714-2722.
- Charfi, K., M. Khayet, et al. (2010). "Numerical simulation and experimental studies on heat and mass transfer using sweeping gas membrane distillation." Desalination **259**(1-3): 84-96.
- Chen, C., K. Liu, et al. (2013). "Morphology and performances of electrospun polyethylene glycol/poly (dl-lactide) phase change ultrafine fibers for thermal energy storage." Solar Energy Materials and Solar Cells **117**(0): 372-381.
- Chen, G., X. Yang, et al. (2013). "Performance enhancement and scaling control with gas bubbling in direct contact membrane distillation." Desalination **308**(0): 47-55.

- Chen, W., A. Y. Fadeev, et al. (1999). "Ultrahydrophobic and Ultralyophobic Surfaces: Some Comments and Examples." Langmuir **15**(10): 3395-3399.
- Couffin, N., C. Cabassud, et al. (1998). "A new process to remove halogenated VOCs for drinking water production: vacuum membrane distillation." Desalination **117**(1-3): 233-245.
- Deitzel, J. M., J. Kleinmeyer, et al. (2001). "The effect of processing variables on the morphology of electrospun nanofibers and textiles." Polymer **42**(1): 261-272.
- Deitzel, J. M., J. D. Kleinmeyer, et al. (2001). "Controlled deposition of electrospun poly(ethylene oxide) fibers." Polymer **42**(19): 8163-8170.
- Demir, M. M., I. Yilgor, et al. (2002). "Electrospinning of polyurethane fibers." Polymer **43**(11): 3303-3309.
- Diban, N., O. C. Voinea, et al. (2009). "Vacuum membrane distillation of the main pear aroma compound: Experimental study and mass transfer modeling." Journal of Membrane Science **326**(1): 64-75.
- Ding, B., C. Li, et al. (2006). "Formation of novel 2D polymer nanowebs via electrospinning." Nanotechnology **17**(15): 3685.
- Dosunmu, O. O., G. G. Chase, et al. (2006). "Electrospinning of polymer nanofibres from multiple jets on a porous tubular surface." Nanotechnology **17**(4): 1123.
- Dumée, L., V. Germain, et al. (2011). "Enhanced durability and hydrophobicity of carbon nanotube bucky paper membranes in membrane distillation." Journal of Membrane Science **376**(1-2): 241-246.
- Edwie, F., M. M. Teoh, et al. (2012). "Effects of additives on dual-layer hydrophobic-hydrophilic PVDF hollow fiber membranes for membrane distillation and continuous performance." Chemical Engineering Science **68**(1): 567-578.
- Egerton, T. A., G. D. Parfitt, et al. (1983). "XPS analysis of uncoated and silica-coated titanium dioxide powders." Colloids and Surfaces **7**(4): 311-323.

- El Amali, A., S. Bouguecha, et al. (2004). "Experimental study of air gap and direct contact membrane distillation configurations: application to geothermal and seawater desalination." Desalination **168**(0): 357.
- Essalhi, M. and M. Khayet (2013). "Self-sustained webs of polyvinylidene fluoride electrospun nanofibers at different electrospinning times: 1. Desalination by direct contact membrane distillation." Journal of Membrane Science **433**(0): 167-179.
- Fabbri, P., M. Messori, et al. (2006). "Perfluoropolyether-based organic–inorganic hybrid coatings." Polymer **47**(4): 1055-1062.
- Feng, C., K. C. Khulbe, et al. (2008). "Production of drinking water from saline water by air-gap membrane distillation using polyvinylidene fluoride nanofiber membrane." Journal of Membrane Science **311**(1–2): 1-6.
- Feng, L., Y. Zhang, et al. (2008). "Petal Effect: A Superhydrophobic State with High Adhesive Force." Langmuir **24**(8): 4114-4119.
- Fong, H., I. Chun, et al. (1999). "Beaded nanofibers formed during electrospinning." Polymer **40**(16): 4585-4592.
- Fong, H. and H. Reneker Darrell (2000). Electrospinning and the formation of nanofibers. Cincinnati, Ohio, Hanser.
- Formhals, A. (1934). Process and apparatus for preparing artificial threads. US. **1975504**.
- Fujii, Y., S. Kigoshi, et al. (1992). "Selectivity and characteristics of direct contact membrane distillation type experiment. II. Membrane treatment and selectivity increase." Journal of Membrane Science **72**(1): 73-89.
- García-Payo, M. C., M. Essalhi, et al. (2010). "Effects of PVDF-HFP concentration on membrane distillation performance and structural morphology of hollow fiber membranes." Journal of Membrane Science **347**(1–2): 209-219.

García-Payo, M. C., M. A. Izquierdo-Gil, et al. (2000). "Air gap membrane distillation of aqueous alcohol solutions." Journal of Membrane Science **169**(1): 61-80.

Gleick, P. H. (2003). "Global Freshwater Resources: Soft-Path Solutions for the 21st Century." Science **302**(5650): 1524-1528.

Gopal, R., S. Kaur, et al. (2006). "Electrospun nanofibrous filtration membrane." Journal of Membrane Science **281**(1–2): 581-586.

Gryta, M. and M. Barancewicz (2010). "Influence of morphology of PVDF capillary membranes on the performance of direct contact membrane distillation." Journal of Membrane Science **358**(1–2): 158-167.

Gryta, M., J. Grzechulska-Damszel, et al. (2009). "The influence of polypropylene degradation on the membrane wettability during membrane distillation." Journal of Membrane Science **326**(2): 493-502.

Guillén-Burrieza, E., J. Blanco, et al. (2011). "Experimental analysis of an air gap membrane distillation solar desalination pilot system." Journal of Membrane Science **379**(1-2): 386-396.

Gunko, S., S. Verbych, et al. (2006). "Concentration of apple juice using direct contact membrane distillation." Desalination **190**(1-3): 117-124.

Han, T., D. H. Reneker, et al. (2007). "Buckling of jets in electrospinning." Polymer **48**(20): 6064-6076.

He, J.-H., Y. Wu, et al. (2005). "Critical length of straight jet in electrospinning." Polymer **46**(26): 12637-12640.

Hill, N. P., A. E. McIntyre, et al. (1986). "Behaviour of chlorophenoxy herbicides during the activated sludge treatment of municipal waste water." Water Research **20**(1): 45-52.

- Hou, D., J. Wang, et al. (2009). "Fabrication and characterization of hydrophobic PVDF hollow fiber membranes for desalination through direct contact membrane distillation." Separation and Purification Technology **69**(1): 78-86.
- Hou, D., J. Wang, et al. (2012). "Preparation and properties of PVDF composite hollow fiber membranes for desalination through direct contact membrane distillation." Journal of Membrane Science **405–406**(0): 185-200.
- Hu, J., X. Wang, et al. (2011). "One-step Electro-spinning/netting Technique for Controllably Preparing Polyurethane Nano-fiber/net." Macromolecular Rapid Communications **32**(21): 1729-1734.
- Huang, Q.-l., C.-f. Xiao, et al. (2011). "Study on the effects and properties of hydrophobic poly(tetrafluoroethylene) membrane." Desalination **277**(1–3): 187-192.
- Huang, Z.-M., Y. Z. Zhang, et al. (2003). "A review on polymer nanofibers by electrospinning and their applications in nanocomposites." Composites Science and Technology **63**(15): 2223-2253.
- Huebner, A. L. and H. N. Chu (1971). "Instability and breakup of charged liquid jets." Journal of Fluid Mechanics **49**(02): 361-372.
- Huo, R., Z. Gu, et al. (2009). "Preparation and properties of PVDF-fabric composite membrane for membrane distillation." Desalination **249**(3): 910-913.
- Hwang, H. J., K. He, et al. (2011). "Direct contact membrane distillation (DCMD): Experimental study on the commercial PTFE membrane and modeling." Journal of Membrane Science **371**(1-2): 90-98.
- Iwamoto, S., A. N. Nakagaito, et al. (2007). "Nano-fibrillation of pulp fibers for the processing of transparent nanocomposites." Applied Physics A: Materials Science & Processing **89**(2): 461-466.
- Jensen, M. B., K. V. Christensen, et al. (2011). "A model of direct contact membrane distillation for black currant juice." Journal of Food Engineering **107**(3-4): 405-414.

- Jiao, B., A. Cassano, et al. (2004). "Recent advances on membrane processes for the concentration of fruit juices: a review." Journal of Food Engineering **63**(3): 303-324.
- Kameoka, J., R. Orth, et al. (2003). "A scanning tip electrospinning source for deposition of oriented nanofibres." Nanotechnology **14**(10): 1124.
- Karagiannis, I. C. and P. G. Soldatos (2008). "Water desalination cost literature: review and assessment." Desalination **223**(1-3): 448-456.
- Katti, D. S., K. W. Robinson, et al. (2004). "Bioresorbable nanofiber-based systems for wound healing and drug delivery: Optimization of fabrication parameters." Journal of Biomedical Materials Research Part B: Applied Biomaterials **70B**(2): 286-296.
- Khayet, M. (2011). "Membranes and theoretical modeling of membrane distillation: A review." Advances in Colloid and Interface Science **164**(1-2): 56-88.
- Khayet, M., C. Y. Feng, et al. (2002). "Preparation and characterization of polyvinylidene fluoride hollow fiber membranes for ultrafiltration." Polymer **43**(14): 3879-3890.
- Khayet, M., P. Godino, et al. (2000). "Theory and experiments on sweeping gas membrane distillation." Journal of Membrane Science **165**(2): 261-272.
- Khayet, M., A. O. Imdakm, et al. (2010). "Monte Carlo simulation and experimental heat and mass transfer in direct contact membrane distillation." International Journal of Heat and Mass Transfer **53**(7-8): 1249-1259.
- Khayet, M. and T. Matsuura (2011). Chapter 5 - Thermally Induced Phase Separation for MD Membrane Formation. Membrane Distillation. Amsterdam, Elsevier: 89-120.
- Kidoaki, S., I. K. Kwon, et al. (2005). "Mesoscopic spatial designs of nano- and microfiber meshes for tissue-engineering matrix and scaffold based on newly devised multilayering and mixing electrospinning techniques." Biomaterials **26**(1): 37-46.

- Koschikowski, J., M. Wieghaus, et al. (2003). "Solar thermal-driven desalination plants based on membrane distillation." Desalination **156**(1-3): 295-304.
- Laganà F., G. Barbieri, et al. (2000). "Direct contact membrane distillation: modelling and concentration experiments." Journal of Membrane Science **166**(1): 1-11.
- Lai, C.-L., R.-M. Liou, et al. (2011). "Preparation and characterization of plasma-modified PTFE membrane and its application in direct contact membrane distillation." Desalination **267**(2-3): 184-192.
- Lalia, B. S., E. Guillen-Burrieza, et al. (2013). "Fabrication and characterization of polyvinylidene fluoride-co-hexafluoropropylene (PVDF-HFP) electrospun membranes for direct contact membrane distillation." Journal of Membrane Science **428**(0): 104-115.
- Lalia, B. S., V. Kochkodan, et al. (2013). "A review on membrane fabrication: Structure, properties and performance relationship." Desalination **326**(0): 77-95.
- Larsen, G., R. Spretz, et al. (2004). "Use of Coaxial Gas Jackets to Stabilize Taylor Cones of Volatile Solutions and to Induce Particle-to-Fiber Transitions." Advanced Materials **16**(2): 166-169.
- Lawson, K. W. and D. R. Lloyd (1996). "Membrane distillation. II. Direct contact MD." Journal of Membrane Science **120**(1): 123-133.
- Lawson, K. W. and D. R. Lloyd (1997). "Membrane distillation." Journal of Membrane Science **124**(1): 1-25.
- Lee, C. H. and W. H. Hong (2001). "Effect of operating variables on the flux and selectivity in sweep gas membrane distillation for dilute aqueous isopropanol." Journal of Membrane Science **188**(1): 79-86.
- Lee, H., S. M. Dellatore, et al. (2007). "Mussel-Inspired Surface Chemistry for Multifunctional Coatings." Science **318**(5849): 426-430.

- Lee, H. J., J. Won, et al. (2002). "Solution properties of poly(amic acid)–NMP containing LiCl and their effects on membrane morphologies." Journal of Membrane Science **196**(2): 267-277.
- Lee, K. H., H. Y. Kim, et al. (2003). "The change of bead morphology formed on electrospun polystyrene fibers." Polymer **44**(14): 4029-4034.
- Li, D., J. T. McCann, et al. (2006). "Electrospinning: A Simple and Versatile Technique for Producing Ceramic Nanofibers and Nanotubes." Journal of the American Ceramic Society **89**(6): 1861-1869.
- Li, D. and Y. Xia (2004). "Direct Fabrication of Composite and Ceramic Hollow Nanofibers by Electrospinning." Nano Letters **4**(5): 933-938.
- Li, D. and Y. Xia (2004). "Electrospinning of Nanofibers: Reinventing the Wheel?" Advanced Materials **16**(14): 1151-1170.
- Li, J.-M., Z.-K. Xu, et al. (2003). "Microporous polypropylene and polyethylene hollow fiber membranes. Part 3. Experimental studies on membrane distillation for desalination." Desalination **155**(2): 153-156.
- Li, Q., S. Mahendra, et al. (2008). "Antimicrobial nanomaterials for water disinfection and microbial control: Potential applications and implications." Water Research **42**(18): 4591-4602.
- Li, Y., W.-Z. Jia, et al. (2007). "Superhydrophobicity of 3D Porous Copper Films Prepared Using the Hydrogen Bubble Dynamic Template." Chemistry of Materials **19**(23): 5758-5764.
- Liao, Y., B. Cao, et al. (2009). "A facile method for preparing highly conductive and reflective surface-silvered polyimide films." Applied Surface Science **255**(19): 8207-8212.
- Liao, Y., R. Wang, et al. (2013). "Engineering superhydrophobic surface on poly(vinylidene fluoride) nanofiber membranes for direct contact membrane distillation." Journal of Membrane Science **440**(0): 77-87.

- Liao, Y., R. Wang, et al. (2013). "Fabrication of polyvinylidene fluoride (PVDF) nanofiber membranes by electro-spinning for direct contact membrane distillation." Journal of Membrane Science **425–426**(0): 30-39.
- Lin, T., H. Wang, et al. (2004). "The charge effect of cationic surfactants on the elimination of fibre beads in the electrospinning of polystyrene." Nanotechnology **15**(9): 1375.
- Lin, T., H. Wang, et al. (2005). "Self-Crimping Bicomponent Nanofibers Electrospun from Polyacrylonitrile and Elastomeric Polyurethane." Advanced Materials **17**(22): 2699-2703.
- Lin, Y., Y. Yao, et al. (2008). "Preparation of poly(ether sulfone) nanofibers by gas-jet/electrospinning." Journal of Applied Polymer Science **107**(2): 909-917.
- Lukanin, O. S., S. M. Gunko, et al. (2003). "The effect of content of apple juice biopolymers on the concentration by membrane distillation." Journal of Food Engineering **60**(3): 275-280.
- Luo, C. J., M. Nangrejo, et al. (2010). "A novel method of selecting solvents for polymer electrospinning." Polymer **51**(7): 1654-1662.
- M, T. (1996). "Preparation and properties of flat-sheet membranes from poly(vinylidene fluoride) for membrane distillation." Desalination **104**(1-2): 1-11.
- Ma, M., Y. Mao, et al. (2005). "Superhydrophobic Fabrics Produced by Electrospinning and Chemical Vapor Deposition." Macromolecules **38**(23): 9742-9748.
- Ma, Z., Y. Hong, et al. (2009). "Superhydrophobic Membranes with Ordered Arrays of Nanospiked Microchannels for Water Desalination." Langmuir **25**(10): 5446-5450.
- Marcel, M. (1990). Basic principles of membrane technology. London, Kluwer Academic Publisher.

- Marek, G. (2007). "Influence of polypropylene membrane surface porosity on the performance of membrane distillation process." Journal of Membrane Science **287**(1): 67-78.
- Mariah, L., C. A. Buckley, et al. (2006). "Membrane distillation of concentrated brines—Role of water activities in the evaluation of driving force." Journal of Membrane Science **280**(1–2): 937-947.
- Martínez, L. and J. M. Rodríguez-Maroto (2008). "Membrane thickness reduction effects on direct contact membrane distillation performance." Journal of Membrane Science **312**(1–2): 143-156.
- Mattoso, L. H. C., R. D. Offeman, et al. (2008). "Effect of relative humidity on the morphology of electrospun polymer fibers." Canadian Journal of Chemistry **86**(6): 590-599.
- Morton, W. J. (1902). Method of dispersing fluids. US **706691**.
- Moussaif, N., C. Pagnouille, et al. (2000). "XPS analysis of the PC/PVDF interface modified by PMMA. Location of the PMMA at the interface." Polymer **41**(9): 3391-3394.
- Na, H., Y. Zhao, et al. (2008). "Effect of hot-press on electrospun poly(vinylidene fluoride) membranes." Polymer Engineering and Science **48**(5): 934-940.
- Neinhuis, C. and W. Barthlott (1997). "Characterization and Distribution of Water-repellent, Self-cleaning Plant Surfaces." Annals of Botany **79**(6): 667-677.
- Nicolaisen, B. (2003). "Developments in membrane technology for water treatment." Desalination **153**(1–3): 355-360.
- Nosonovsky, M. and B. Bhushan (2007). "Hierarchical roughness optimization for biomimetic superhydrophobic surfaces." Ultramicroscopy **107**(10–11): 969-979.
- Oki, T. and S. Kanae (2006). "Global Hydrological Cycles and World Water Resources." Science **313**(5790): 1068-1072.

Park, S., K. Park, et al. (2007). "Apparatus for preparing electrospun nanofibers: designing an electrospinning process for nanofiber fabrication." Polymer International **56**(11): 1361-1366.

Phattaranawik, J., R. Jiratananon, et al. (2003). "Effect of pore size distribution and air flux on mass transport in direct contact membrane distillation." Journal of Membrane Science **215**(1-2): 75-85.

Phattaranawik, J., R. Jiratananon, et al. (2003). "Heat transport and membrane distillation coefficients in direct contact membrane distillation." Journal of Membrane Science **212**(1-2): 177-193.

Prince, J. A., G. Singh, et al. (2012). "Preparation and characterization of highly hydrophobic poly(vinylidene fluoride) – Clay nanocomposite nanofiber membranes (PVDF–clay NNMs) for desalination using direct contact membrane distillation." Journal of Membrane Science **397–398**(0): 80-86.

Qtaishat, M., T. Matsuura, et al. (2008). "Heat and mass transfer analysis in direct contact membrane distillation." Desalination **219**(1-3): 272-292.

Ramakrishna, S., K. Fujihara, et al. (2006). "Electrospun nanofibers: solving global issues." Materials Today **9**(3): 40-50.

Rao, M., X. Geng, et al. (2012). "Preparation and performance of gel polymer electrolyte based on electrospun polymer membrane and ionic liquid for lithium ion battery." Journal of Membrane Science **399–400**(0): 37-42.

Razmjou, A., E. Arifin, et al. (2012). "Superhydrophobic modification of TiO₂ nanocomposite PVDF membranes for applications in membrane distillation." Journal of Membrane Science **415–416**(0): 850-863.

Reneker Darrell, H. and H. Fong (2006). Polymeric Nanofibers: Introduction. Polymeric Nanofibers, American Chemical Society. **918**: 1-6.

Reneker, D. H. and I. Chun (1996). "Nanometre diameter fibres of polymer, produced by electrospinning." Nanotechnology **7**(3): 216.

Reneker, D. H., W. Kataphinan, et al. (2002). "Nanofiber garlands of polycaprolactone by electrospinning." Polymer **43**(25): 6785-6794.

Reneker, D. H. and A. L. Yarin (2008). "Electrospinning jets and polymer nanofibers." Polymer **49**(10): 2387-2425.

Reneker, D. H., A. L. Yarin, et al. (2000). "Bending instability of electrically charged liquid jets of polymer solutions in electrospinning." Journal of Applied Physics **87**(9): 4531.

Rutledge, G. C. and S. V. Fridrikh (2007). "Formation of fibers by electrospinning." Advanced Drug Delivery Reviews **59**(14): 1384-1391.

Ryu, Y. J., H. Y. Kim, et al. (2003). "Transport properties of electrospun nylon 6 nonwoven mats." European Polymer Journal **39**(9): 1883-1889.

Sarti, G. C., C. Gostoli, et al. (1993). "Extraction of organic components from aqueous streams by vacuum membrane distillation." Journal of Membrane Science **80**(1): 21-33.

Sastry, M. (1997). "Correlation of C 1s binding energies in organic molecules with atomic charge calculated using a modified Sanderson formalism." Journal of Electron Spectroscopy and Related Phenomena **85**(1-2): 167-174.

Schneider, K., W. Hütz, et al. (1988). "Membranes and modules for transmembrane distillation." Journal of Membrane Science **39**(1): 25-42.

Schofield, R. W., A. G. Fane, et al. (1990). "Factors affecting flux in membrane distillation." Desalination **77**(0): 279-294.

Shin, Y. M., M. M. Hohman, et al. (2001). "Electrospinning: A whipping fluid jet generates submicron polymer fibers." Applied Physics Letters **78**(8): 1149.

Shin, Y. M., M. M. Hohman, et al. (2001). "Experimental characterization of electrospinning: the electrically forced jet and instabilities." Polymer **42**(25): 09955-09967.

- Sill, T. J. and H. A. von Recum (2008). "Electrospinning: Applications in drug delivery and tissue engineering." Biomaterials **29**(13): 1989-2006.
- Smit, E., U. Büttner, et al. (2005). "Continuous yarns from electrospun fibers." Polymer **46**(8): 2419-2423.
- Su, M., M. M. Teoh, et al. (2010). "Effect of inner-layer thermal conductivity on flux enhancement of dual-layer hollow fiber membranes in direct contact membrane distillation." Journal of Membrane Science **364**(1–2): 278-289.
- Subbiah, T., G. S. Bhat, et al. (2005). "Electrospinning of nanofibers." Journal of Applied Polymer Science **96**(2): 557-569.
- Subramanian, A., D. Vu, et al. (2005). "Preparation and evaluation of the electrospun chitosan/PEO fibers for potential applications in cartilage tissue engineering." J Biomater Sci Polym Ed **16**(7): 861-873.
- Sun, B., Y. Z. Long, et al. "Advances in three-dimensional nanofibrous macrostructures via electrospinning." Progress in Polymer Science(0).
- Talwar, S., A. S. Krishnan, et al. (2010). "Electrospun Nanofibers with Associative Polymer–Surfactant Systems." Macromolecules **43**(18): 7650-7656.
- Tang, N., Q. Jia, et al. (2010). "Preparation and morphological characterization of narrow pore size distributed polypropylene hydrophobic membranes for vacuum membrane distillation via thermally induced phase separation." Desalination **256**(1–3): 27-36.
- Tang, N., Q. Jia, et al. (2010). "Preparation and morphological characterization of narrow pore size distributed polypropylene hydrophobic membranes for vacuum membrane distillation via thermally induced phase separation." Desalination **256**(1–3): 27-36.
- Tang, Y., N. Li, et al. (2012). "Effect of spinning conditions on the structure and performance of hydrophobic PVDF hollow fiber membranes for membrane distillation." Desalination **287**(0): 326-339.

Tang, Z., C. Qiu, et al. (2009). "Design and fabrication of electrospun polyethersulfone nanofibrous scaffold for high-flux nanofiltration membranes." Journal of Polymer Science Part B: Polymer Physics **47**(22): 2288-2300.

Tasuku, O., D. Bin, et al. (2007). "Super-hydrophobic surfaces of layer-by-layer structured film-coated electrospun nanofibrous membranes." Nanotechnology **18**(16): 165607.

Taylor, G. (1964). "Disintegration of Water Drops in an Electric Field." Proceedings of the Royal Society of London. Series A, Mathematical and Physical Sciences **280**(1382): 383-397.

Taylor, G. (1969). "Electrically Driven Jets." Proceedings of the Royal Society of London. Series A, Mathematical and Physical Sciences **313**(1515): 453-475.

Teo, W. E. and S. Ramakrishna (2005). "Electrospun fibre bundle made of aligned nanofibres over two fixed points." Nanotechnology **16**(9): 1878.

Teo, W. E. and S. Ramakrishna (2006). "A review on electrospinning design and nanofibre assemblies." Nanotechnology **17**(14): R89.

Teoh, M. M. and T.-S. Chung (2009). "Membrane distillation with hydrophobic macrovoid-free PVDF-PTFE hollow fiber membranes." Separation and Purification Technology **66**(2): 229-236.

Teoh, M. M., T.-S. Chung, et al. (2011). "Dual-layer PVDF/PTFE composite hollow fibers with a thin macrovoid-free selective layer for water production via membrane distillation." Chemical Engineering Journal **171**(2): 684-691.

Teoh, M. M., N. Peng, et al. (2011). "Development of Novel Multichannel Rectangular Membranes with Grooved Outer Selective Surface for Membrane Distillation." Industrial & Engineering Chemistry Research **50**(24): 14046-14054.

Theron, A., E. Zussman, et al. (2001). "Electrostatic field-assisted alignment of electrospun nanofibres." Nanotechnology **12**(3): 384.

- Thompson, C. J., G. G. Chase, et al. (2007). "Effects of parameters on nanofiber diameter determined from electrospinning model." Polymer **48**(23): 6913-6922.
- Toselli, M., J. A. Gardella, et al. (2003). "Surface chemical analysis of poly(ϵ -caprolactone)–perfluoropolyether–poly(ϵ -caprolactone) triblock copolymers by X-ray photoelectron spectroscopy." Polymer International **52**(8): 1262-1274.
- Tun, C. M., A. G. Fane, et al. (2005). "Membrane distillation crystallization of concentrated salts—flux and crystal formation." Journal of Membrane Science **257**(1–2): 144-155.
- Vahedi, A. and B. Gorczyca (2012). "Predicting the settling velocity of flocs formed in water treatment using multiple fractal dimensions." Water Research **46**(13): 4188-4194.
- Valdés, H., J. Romero, et al. (2009). "Concentration of noni juice by means of osmotic distillation." Journal of Membrane Science **330**(1-2): 205-213.
- Wagner, P., R. Fürstner, et al. (2003). "Quantitative assessment to the structural basis of water repellency in natural and technical surfaces." Journal of Experimental Botany **54**(385): 1295-1303.
- Wang, K. Y., S. W. Foo, et al. (2009). "Mixed Matrix PVDF Hollow Fiber Membranes with Nanoscale Pores for Desalination through Direct Contact Membrane Distillation." Industrial & Engineering Chemistry Research **48**(9): 4474-4483.
- Wang, N., X. Wang, et al. (2012). "Tunable fabrication of three-dimensional polyamide-66 nano-fiber/nets for high efficiency fine particulate filtration." Journal of Materials Chemistry **22**(4): 1445-1452.
- Wang, P. and T.-S. Chung (2012). "Design and fabrication of lotus-root-like multi-bore hollow fiber membrane for direct contact membrane distillation." Journal of Membrane Science **421–422**(0): 361-374.

Wang, P. and T.-S. Chung (2013). "A New-Generation Asymmetric Multi-Bore Hollow Fiber Membrane for Sustainable Water Production via Vacuum Membrane Distillation." Environmental Science & Technology **47**(12): 6272-6278.

Wang, P., M. M. Teoh, et al. (2011). "Morphological architecture of dual-layer hollow fiber for membrane distillation with higher desalination performance." Water Research **45**(17): 5489-5500.

Wang, S., Y. Li, et al. (2011). "Preparation of a durable superhydrophobic membrane by electrospinning poly (vinylidene fluoride) (PVDF) mixed with epoxy-siloxane modified SiO₂ nanoparticles: A possible route to superhydrophobic surfaces with low water sliding angle and high water contact angle." Journal of Colloid and Interface Science **359**(2): 380-388.

Wang, W., Y. Jiang, et al. (2011). "Fabrication of silver-coated silica microspheres through mussel-inspired surface functionalization." Journal of Colloid and Interface Science **358**(2): 567-574.

Wang, X., B. Ding, et al. (2013). "Electro-spinning/netting: A strategy for the fabrication of three-dimensional polymer nano-fiber/nets." Progress in Materials Science **58**(8): 1173-1243.

Wang, X., B. Ding, et al. (2011). "Electro-netting: Fabrication of two-dimensional nano-nets for highly sensitive trimethylamine sensing." Nanoscale **3**(3): 911-915.

Wang, X., B. Ding, et al. (2010). "A highly sensitive humidity sensor based on a nanofibrous membrane coated quartz crystal microbalance." Nanotechnology **21**(5): 055502.

Wang, X., B. Ding, et al. (2011). "Large-scale fabrication of two-dimensional spider-web-like gelatin nano-nets via electro-netting." Colloids and Surfaces B: Biointerfaces **86**(2): 345-352.

Wenzel, R. N. (1936). "RESISTANCE OF SOLID SURFACES TO WETTING BY WATER." Industrial & Engineering Chemistry **28**(8): 988-994.

- Wu, B., X. Tan, et al. (2006). "Removal of 1,1,1-trichloroethane from water using a polyvinylidene fluoride hollow fiber membrane module: Vacuum membrane distillation operation." Separation and Purification Technology **52**(2): 301-309.
- Wu, Y., Y. Kong, et al. (1991). "An experimental study on membrane distillation-crystallization for treating waste water in taurine production." Desalination **80**(2-3): 235-242.
- Yang, S., X. Wang, et al. (2011). "Controllable fabrication of soap-bubble-like structured polyacrylic acid nano-nets via electro-netting." Nanoscale **3**(2): 564-568.
- Yang, X., R. Wang, et al. (2011). "Performance improvement of PVDF hollow fiber-based membrane distillation process." Journal of Membrane Science **369**(1-2): 437-447.
- Yang, X., R. Wang, et al. (2011). "Performance improvement of PVDF hollow fiber-based membrane distillation process." Journal of Membrane Science **369**(1-2): 437-447.
- Yarin, A. L., S. Koombhongse, et al. (2001). "Bending instability in electrospinning of nanofibers." Journal of Applied Physics **89**(5): 3018.
- Yohe, S. T., J. D. Freedman, et al. (2013). "A Mechanistic Study of Wetting Superhydrophobic Porous 3D Meshes." Advanced Functional Materials **23**(29): 3628-3637.
- Yohe, S. T., V. L. M. Herrera, et al. (2012). "3D superhydrophobic electrospun meshes as reinforcement materials for sustained local drug delivery against colorectal cancer cells." Journal of Controlled Release **162**(1): 92-101.
- Zhang, D. and J. Chang (2008). "Electrospinning of Three-Dimensional Nanofibrous Tubes with Controllable Architectures." Nano Letters **8**(10): 3283-3287.
- Zhang, J., N. Dow, et al. (2010). "Identification of material and physical features of membrane distillation membranes for high performance desalination." Journal of Membrane Science **349**(1-2): 295-303.

Zhang, X., M. R. Reagan, et al. (2009). "Electrospun silk biomaterial scaffolds for regenerative medicine." Advanced Drug Delivery Reviews **61**(12): 988-1006.

Zhao, Z.-P., C.-Y. Zhu, et al. (2011). "Concentration of ginseng extracts aqueous solution by vacuum membrane distillation 2. Theory analysis of critical operating conditions and experimental confirmation." Desalination **267**(2-3): 147-153.

Zhaohui, T., Q. Changquan, et al. (2009). "Design and fabrication of electrospun polyethersulfone nanofibrous scaffold for high-flux nanofiltration membranes." Journal of Polymer Science Part B: Polymer Physics **47**.

Zhu, Y., J. Li, et al. (2008). "Superhydrophobic 3D Microstructures Assembled From 1D Nanofibers of Polyaniline." Macromolecular Rapid Communications **29**(3): 239-243.

Zong, X., K. Kim, et al. (2002). "Structure and process relationship of electrospun bioabsorbable nanofiber membranes." Polymer **43**(16): 4403-4412.